Gold nanoparticles as a platform for small molecule SELEX

by

McKenzie Smith
BSc (Hon), Carleton University 2014

A thesis submitted to the Faculty of Graduate and Postdoctoral Affairs in partial fulfillment of the requirements for the degree of

Master of Science

in

Chemistry

Carleton University
Ottawa, Ontario

The undersigned hereby recommends to the

Department of Chemistry

acceptance of the thesis

Gold nanoparticles as a platform for small molecule SELEX

Submitted by:

McKenzie Smith

In partial fulfillment of the requirements of the degree of

Master of Science in Chemistry

Dr. Maria C. DeRosa

(Supervisor)

Abstract

Both naturally occurring and synthetic small molecules play a significant role in a variety of applications. For example, small molecule food contaminants that occur in-field or postharvest are of importance, both agriculturally and economically. Mycotoxins are toxic secondary metabolites produced by filamentous fungi that can potentially contaminate a variety of foodstuffs. Detection of these small molecules is required as mycotoxins pose multiple health-risks and proceed past processing and food safety. Current detection methods are expensive, time consuming and unavailable for on-site detection leaving an unmet need for alternative methods of detection.

Aptamers are single stranded oligonucleotides that can bind to specific target molecules with high selectivity and affinity. Emerging as molecular recognition agents, aptamers can be used in a number of novel detection methods for small molecule quantification and analysis. Aptamers are selected through an in vitro process known as Systematic Evolution of Ligands by Exponential Enrichment (SELEX). Aptamers can be adsorbed onto the surface of citrate-capped AuNPs to serve as the molecular recognition element of a rapid colourimetric biosensor assay. Based on this interaction, AuNPs could potentially serve as a novel platform for small molecule SELEX. Although molecular recognition of small molecules is of great interest, selection of aptamers for small molecules has proven to be a challenge. Furthermore, not all of these reported small molecule aptamers can be easily incorporated in the AuNP bioassay. Selecting for aptamers in a manner that will mimic established AuNP biosensor conditions provides a number of advantages compared to traditional SELEX. As a first step towards establishing a AuNP SELEX platform, we evaluated the partitioning of mycotoxin

aptamers that remain on the AuNP surface from aptamers-target complexes in solution. Having uncovered several challenges associated with AuNPs as a SELEX partitioning strategy, we next synthesized, optimized, and characterized core-shell gold coated magnetic nanoparticles (Fe_3O_4-AuNPs), which were phase-transferred aqueous solution. We demonstrated that Fe_3O_4-AuNPs could function as an improved AuNP SELEX platform and provide a novel method to study ssDNA aptamer-AuNP non-specific interactions. Finally, our studies on the adsorption and separation of ssDNA aptamers using Fe_3O_4-AuNPs highlight future opportunities for novel aptamer biomedical applications and other biosensor development.

Acknowledgements

First and foremost, I would like to thank my supervisor, Dr. Maria DeRosa. As an undergraduate student, you gave me the opportunity to work in your research lab and realize my potential. Your passion for science and your innovative research inspired me to pursue a graduate degree. From the first day I joined the lab, you have welcomed and encouraged me as a member of your research group! You challenge me to solve problems independently, yet you are always there to offer advice and support! Your enthusiasm and optimism, even during the challenges of my project, encouraged me to persevere. Without a doubt, I wouldn't be where I am today without you- Thank you, Maria!

My fellow DeRosa Lab members (past and present), I am grateful to have had the opportunity to work alongside such amazing scientists and people. Maureen- Since my second year until probably a few hours ago, you have been there to encourage me! Your support and guidance has often been the advice I needed to advance my research project, my career and myself. Thank you for the time and knowledge you dedicated to this project! EM, EM and KH- thank you for welcoming me into the lab, teaching me what you know and for supporting me at every step along the way! Erin- thank you for the cat leggings and answering my ridiculous questions. Emily- thank you for being hilarious and for listening to me rant about nothing. Dan- thank you for going through this degree alongside me! Chris- thank you for being the rational organic chemist that you are and helping me with the Schlenk line. Dr. Velu- thank you for your guidance, encouragement and positivity! To NF, AR, EH, PT and AK- Thank you for your support and for being an amazing group of intelligent women who share their snacks with me.

I would like to thank the wonderful faculty, staff and students of the chemistry department at Carleton University. Elena- Thank you for always being organized and there to answer my many questions, but most of all thank you for always looking out for me as one of your TAs and being the listening ear I needed during times of stress. To Dr. Anatoli Ianoul and his research group- thank you for sharing your vast nanoparticle knowledge to help me further understand the platform of my research project. I would also like to thank Dr. Sean Barry and his group for allowing me to crash group events, for equipment I've borrowed (and returned ☺) and for their guidance and support. Dr. Miller- Thank you for taking the time to give me career advice and for the immense knowledge and experience I gained from taking your graduate toxicology course. Dr. Robert Burk- Thank you for inspiring others with your passion for science and teaching! Chantelle- Thank you for your continuous support and for your guidance when I was applying for a Masters degree. I would also like to thank JJ for the many laughs and encouraging words during his assistance with TEM analysis.

To my friends who I know don't care about the title of my thesis but ask me anyways, thank you for your interest in my work. To my cats, Rosie and Franklin, thank you for being cute and bringing me your toy mice when I'm stressed. I would like to especially thank my parents, Brad and Sharon Smith. I cannot thank you enough for your continuous love, support and encouragement. Dad- Thank you for being dependable and for encouraging me to shoot for the stars! Mom- Thank you for keeping me humble, and for reminding me to look at life from a different perspective. Finally to Matthew, your unfailing support and delicious food kept me going! Thank you for believing in me, even when I didn't believe in myself. You make me a better scientist and a better person!

Table of Contents

List of Tables

List of Figures

List of Abbreviations

6-FAM: 6-carboxyfluorescein phosphoramidite

A: adenine

AuNP: gold nanoparticle

C: cytosine

Cit: citrate

CPG: controlled pore glass

DMAP: 4-di(methylamino)pyridine

DNA: deoxyribonucleic acid

DON: deoxynivalenol

dsDNA: double stranded DNA

DNase I: deoxyribonuclease I

ELISA: enzyme-linked immunosorbent assay

EU: European union

FAM: fluorescein phosphoramidite

FB_1: Fumonisin B1

Fe_3O_4 NP: iron oxide nanoparticle

Fe_3O_4-AuNPs: core-shell gold coated magnetic nanoparticles

G: guanine

HPLC: high performance liquid chromatography

HRTEM: high resolution transmission electron microscopy

HSAB: hard-soft acid-base

K_a: association constant

K_d: dissociation constant

k: rate constant

LC-MS: liquid chromatography mass spectrometry

LFD: lateral flow device

LOD: limit of detection

NPs: nanoparticles

nt: nucleotide

OTA: ochratoxin A

PAGE: polyacrylamide gel electrophoresis

PCR: polymerase chain reaction

RNA: ribonucleic acid

SELEX: systematic evolution of ligands by ligands by exponential enrichment

SEM: scanning electron microscopy

SPR: surface plasmon resonance

ssDNA: single stranded DNA

T: thymine

TBE: tris(hydroxymethyl)aminomethane/borate/ethylenediaminetetraacetic acid buffer

TEMED: N, N, N', N'- tetramethylethylenediamine

TLC: thin layer chromatography

UV-Vis: ultraviolet-visible spectrophotometry

Chapter 1: Introduction

1.1 Small molecule targets

Small molecule targets are chemical compounds (< 900 Da) that require detection. There has been a growing demand for the detection of various small molecule targets including; toxins, antibiotics, drugs, heavy metals, etc.[1] These small molecule targets play an important role in a number of biological and chemical processes. Given their importance in agriculture, medicine and the environment, the detection and quantification of these small molecules is of great interest.[2] From a medical standpoint, both harmful and beneficial small molecules are able to diffuse across cell membranes.[3] Similarly, small molecule food contaminants that occur in-field or postharvest are detrimental both agriculturally and economically. However, small molecules can also play a helpful role in agriculture, serving as pesticides or by offering opportunities for energy storage.[4] Although detection of small molecules is challenging compared to other target types, their impact cannot be ignored.[2]

1.1.1 Mycotoxins: *An example small molecule target*

Mycotoxins are secondary metabolites produced by filamentous fungi, primarily *Aspergillus, Penicillium, Alternaria, Fusarium and Claviceps* genera.[5] In 1962, thousands of turkey poults died in England after the consumption of imported peanuts from Brazil and Africa. This mass fatality of livestock was investigated and ingestion of a secondary metabolite produced by *Aspergillus flavus* within the imported food product was found as the cause of death.[6] Detection of these small molecules is required as mycotoxins can

contaminate a variety of foodstuffs, are stable past the food processing, and pose multiple health-risks.[6]

The adverse health effects associated with each mycotoxin must be considered when attempting to understand its toxicity and regulation. However, mycotoxin exposure and its effects in humans are not as well studied or understood in comparison to an animal model. Depending on the mycotoxin, research suggests that exposure (ingestion, absorption or inhalation) may lead to possible carcinogenic, mutagenic, estrogenic, hemorrhagic, nephrotoxic, teratogenic, hepatotoxic, neurotoxic and/or immunosuppressive effects.[7] These effects often depend upon the extent and length of exposure.

Mycotoxins are more commonly found in hot and humid climates that favour the growth of the secondary metabolite-producing fungi. However, mycotoxins have been found in temperate conditions as well.[8,9] This is because each fungal species has its own optimal growing conditions. Therefore, different climates can favour the production of certain mycotoxins. Improper harvest, storage and handling can mistakenly provide these conditions, resulting in the growth of various fungal species.[6] These conditions also favour the growth of various foodstuffs, which results in the association of specific mycotoxins with certain food products. Although human exposure is largely due to consumption of contaminated plant products, derived food products such as milk, cheese or other animal products can be a source of contamination.[6] In general, mycotoxins are found to contaminate a variety of foodstuffs including wheat and other grains, fruit/dried fruit, coffee, wine and nuts. Although the effects of mycotoxins on humans are not completely understood, many countries have developed strict regulations for food and

feed to control contamination.[6] The following table summarizes known mycotoxins into 6 main categories[7]; Aflatoxins, Fumonisins, Ochratoxins, Patulin, Trichothecenes, and Zearalenone (Table 1.1). The chemical structure, the fungal species responsible[9], contaminated food product(s)[6], potential health effects[5], and a EU regulation limit range in food[10] of each mycotoxin group is described.

Table 1.1 Categories of mycotoxins with an example chemical structure, the producing species, contaminated food products, possible adverse health effects and regulation.

Mycotoxin	Sample chemical structure	Producing species	Food product(s)	Potential health effects	Regulation limit (in Food)
Aflatoxins B1 (AFB1)	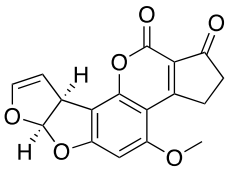	*A. flavus*, *A. parasiticus*	Cereals, Spices, Seeds and Nuts	Liver lesions, cirrhosis, primary hepatocellular carcinoma, Kwashiorkor, Reye's syndrome	0-20 µg/kg
Fumonisins B1 (FB1)	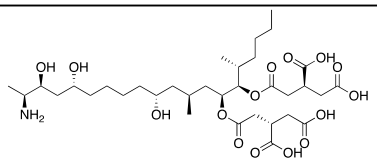	*F. verticillioides*, *F. proliferatum*	Corn	Esophageal carcinoma	200-4000 µg/kg
Ochratoxin A (OTA)	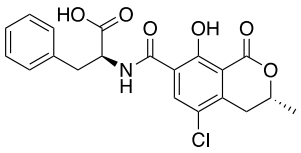	*A. ochraceus*, *P. verrucosum*, *A. carbonarius*	Oats, Barley, Wheat, Cereals, Coffee, Fruit, and Nuts	Endemic nephropathy, urothelial tumours	0.5- 80 µg/kg
Patulin	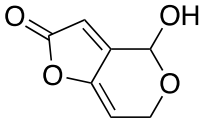	*Penicillim expansum*	Apples, Pears, Cherries and other Fruits	Damage to gastrointestinal, respiratory systems, DNA, many enzymes	10- 50 µg/kg
Deoxynivalenol	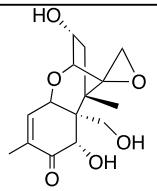	*F. graminearum*, *F. culmorum*	Grain, Corn	Nausea, vomiting, abdominal pain, diarrhea, dizziness, headache	200-1000 µg/kg
Zearalenone	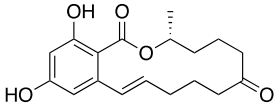	*F. graminearum*, *F. culmorum*	Oats, Rye, Barley, corn and wheat	Premature puberty in girls, cervical cancer	20-400 µg/kg

1.1.1.1 Current detection methods

As mycotoxins pose various adverse health effects, the detection of these small molecules food contaminants is of global interest. However, many factors present challenges for reliable mycotoxin detection and regulation. In some cases, contamination does not result in physical damage to the crop or contaminate the crop in a homogenous manner.[11] For example, one area of a crop may be affected while another area is not contaminated, thus a large sample weighing approximately 5-10 lbs must be collected and tested.[12] Methods such as thin layer chromatography (TLC), enzyme-linked immunosorbent assay (ELISA), high performance liquid chromatography (HPLC) with fluorescence (FLD), diode array detector (DAD) and liquid chromatography mass spectrometry (LC-MS) have been used to detect mycotoxins.[13] Although sensitive and reliable, these methods present a number of limitations. LC-MS and HPLC-MS/MS are very expensive and time consuming as these methods require transportation of the sample to a laboratory, expensive equipment, and a knowledgeable laboratory technician.[14] ELISA has been reported as an alternative detection method, however the high occurrence of false positives or false negative results can make the method unreliable.[15] Furthermore, antibodies are included in ELISA as the molecular recognition agent of the assay.[13] Therefore, the limitations associated with antibodies (section 1.2) become limitations of ELISA as a detection method.

1.2 Aptamers

Aptamers are single stranded deoxyribonucleic acid (DNA) or ribonucleic acid (RNA) molecules that can bind to specific target molecules with high selectivity and affinity. Aptamers are selected through an *in vitro* process known as Systematic Evolution of Ligands by Exponential Enrichment (SELEX) (discussed further in section 1.2.1).[16] Aptamers can be used in a number of novel detection methods for small molecule quantification and analysis and have been reported to detect a wide range of target molecules, ranging from whole cells and viruses to small molecules.[17–19] The single-stranded DNA or RNA molecules can fold into three-dimensional structures including hairpins, stems, loops, triplexes and quadruplexes.[2] For example, many published aptamers fold into a G-quadruplex aptamer conformation to bind to the target molecule.[20–22] The aptamer can interact with a specific target molecule through hydrogen bonding, electrostatic interactions, π- bond stacking and the hydrophobic effect.[19]

Aptamers have been referred to as 'chemical antibodies'. This is because aptamers are similar in function to antibodies, but are chemically synthesized *in vitro*. In comparison to antibodies, which are obtained using an *in vivo* process, aptamers provide a number of advantages over their counterparts. Since aptamers are chemically synthesized, their production is less expensive. Aptamers can be chemically labeled with a number of different modifications, providing opportunities in sensing and imaging. In comparison to antibodies, aptamers are more chemically stable with longer shelf lives, withstanding greater changes in pH and temperature. Although antibodies have long been the gold standard for molecular recognition and sensing, aptamers are emerging as a new, advantageous alternative.[2,23–25]

1.2.1 Systematic Evolution of Ligands by EXponential enrichment (SELEX)

Aptamers are selected through an *in vitro* process known as Systematic Evolution of Ligands by EXponential enrichment (SELEX). Although *in vitro* evolution was first reported in the 1960s, the potential of this process was not realized until modern biotechnological advances.[26] Fairly recently, in 1990, a number of research groups reported the use of *in vitro* evolution to select functional nucleic acids.[27] Tuerk and Gold called this process 'SELEX', while Ellington and Szostak named the selected functional nucleic acids 'Aptamers'.[16,28] In general, the SELEX process involves adsorption, partitioning, recovery and amplification of the selected sequences (Figure 1.1). Starting with an initial library of 10^{13}- 10^{15} different sequences, this process is repeated multiple times.[29] Typically, a SELEX library is made up of 30-80 nucleotide bases that are flanked by primer binding sites used for amplification through polymerase chain reaction (PCR).[30] The initial library is introduced to the target molecule (often tethered to a solid support) and washing steps are used to ensure the removal of non-functional sequences. Since the interactions between the nucleic acids and the target molecule are non-covalent, mild conditions can be used to elute the binding sequences.[19] These select nucleic acid sequences are amplified with PCR and used as the pool for subsequent selection. Each cycle is referred to as a SELEX round. Approximately 5-15 SELEX rounds yield a reduced number of sequences with affinity for the target molecule.[31] To select aptamer sequences that bind specifically to the target molecule, a negative and counter selection are employed. The selected sequences are introduced to the solid support matrix, other competing target molecules or other molecules in a sample matrix. To improve

specificity, sequences with an affinity for the negative or counter control are removed from the pool.[32]

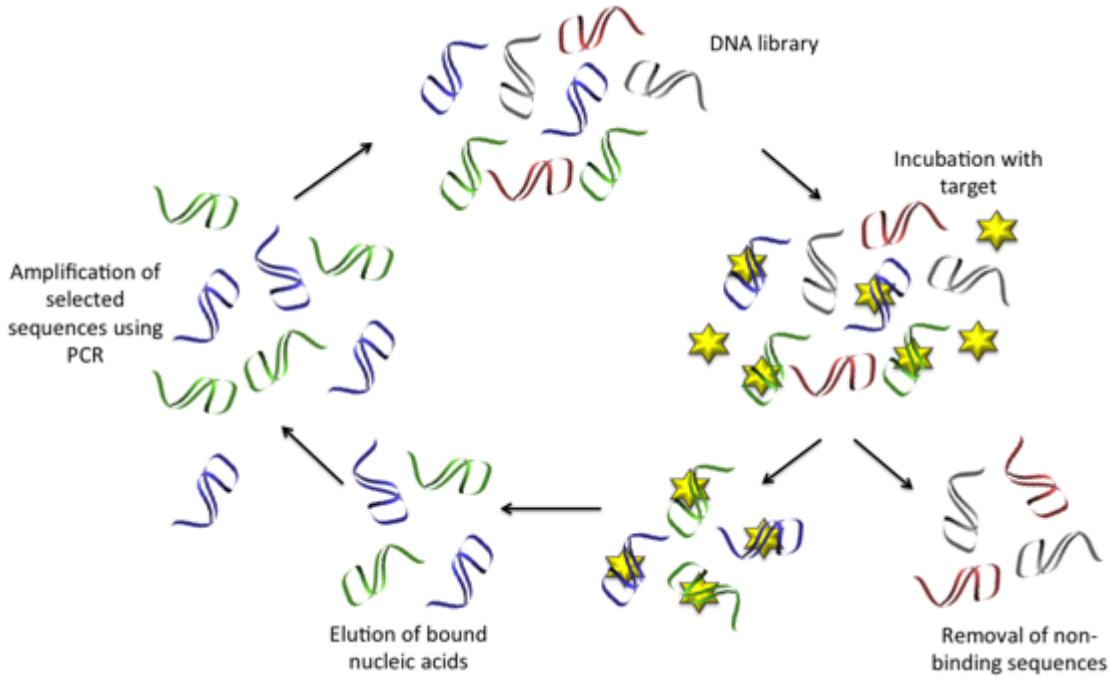

Figure 1.1 The Systematic Evolution of Ligands by EXponential enrichment (SELEX) process. Starting with a DNA library, the sequences are incubated with target (yellow star). Selected sequences with affinity for the target (green and blue ribbons) are separated from non-binding sequences (red and grey ribbons). The binding sequences are eluted from the target molecule and amplified through polymerase chain reaction (PCR). These sequences are the enriched DNA library for the next selection round.

1.2.1.1 Current SELEX modifications and partitioning methods

The previously described SELEX process has been modified to yield a number of SELEX variations to improve selected aptamers or simplify the process. Generic SELEX refers to methods that do not require any additional equipment or modifications to the

original SELEX process, whereas the other categories are some variation of this general process.[16,28,33,34] Changes to the nucleic acid library[35–38], target immobilization[39,40], selection stringency[32], amplification, and monitoring enrichment[40] have been reported. In addition, the SELEX process has been automated.[41–43] As an example, FluMag-SELEX immobilizes the target to a magnetic bead for partitioning and sequences are fluorescein labeled to monitor amplification.[40] More recently, capture SELEX is advantageous as the small molecule target can be free in solution. Complementarity between the primer region and the capture probe allow for immobilization of the DNA library before target incubation.[44] All adaptions aim to generate improved aptamers or simplify the SELEX process.[2]

SELEX requires a reliable partitioning method to separate the sequences that bind the target molecule from the non-binding sequences. For example, FluMag-SELEX works by immobilizing a target molecule on the surface of a magnetic bead.[40] This method would be suitable for a small molecule target, however a virus or whole cell would be considered inappropriate. Modifications to the SELEX partitioning step must consider the target type. Specifically these modifications aim to model future application conditions, or attempt to increase specificity (reducing non-specific binding, etc) of the selected sequences. The following table outlines and describes the various partitioning methods to date (Table 1.2).[45]

Table 1.2 List of described SELEX partitioning methods

Partitioning Method	Description
Affinity chromatography	A solid support matrix (e.g.: column chromatography) is used to separate binding sequences from sequences without affinity for the target
Affinity chromatography (Magnetic Beads)	A sub-category of affinity chromatography. Functionalized magnetic beads serve as the solid support matrix during selection. The target molecule is immobilized to the bead surface. By physical magnetic separation, the binding sequences are separated from non-binding sequences which are left in the supernatant solution.
Capillary electrophoresis	Electrokinetic separation of binding sequences
Cell washing	Through a washing step, the non-binding sequences are removed from the cell and separated from binding sequences
Centrifugation	Non-binding sequences can be separated via centrifugation from aptamer-target complexes based on a difference in weight
Filtration	The size difference between an aptamer-target complex and non-binding aptamer sequences allows for filtration. Alternatively, affinity of the target for the filter itself can separate non-binding sequences
Gel electrophoresis	A difference in size results in a difference in gel migration, allowing the non-binding sequences to be separated from the aptamer-target complex
Not required	A SELEX that does not require a separation technique

These partitioning methods all aim to separate the sequences with affinity for the target molecule from non-binding sequences. Some modified partitioning methods have shown general improvements. For example, affinity chromatography using magnetic beads reduces non-specific binding with the solid support matrix due to the highly cross-linked coating.[32] However, most of these developed separation methods are advantageous for specific targets and conditions.[45] Importantly, the affinity of selected aptamers can be influenced by the selection process. Therefore, the end use and application of the selected aptamer needs to be considered when choosing a SELEX method and partitioning

technique. For example, affinity chromatography requires that the target be immobilized to a solid support matrix and does not reflect binding in solution.[2,24,32] This is a practical example of why the selection process should mimic the further testing conditions or application of the selected sequence.

1.2.1.2 Challenges and opportunities for small molecule aptamer selection

In comparison to proteins, selecting aptamers for small molecule targets is a challenging task. This is evident when considering the number of aptamers for other target types in comparison to aptamers selected for small molecule targets. Specifically, only 25% of all aptamers selected between 1990 and 2013 are for small molecule targets (Figure 1.2).[45]

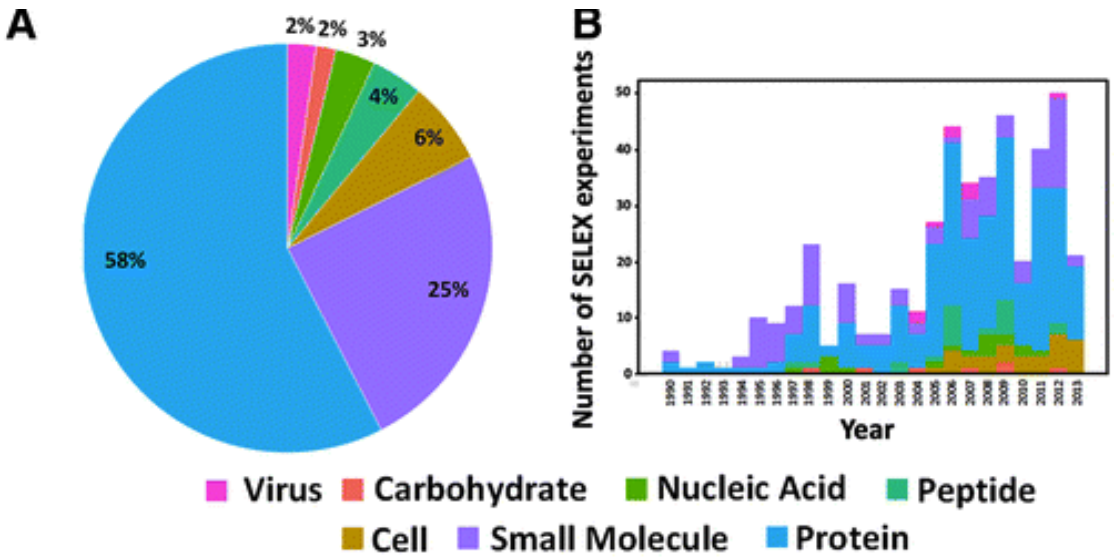

Figure 1.2 Percentage of aptamers selected for various target types

Carothers and co-workers confirmed that the affinity of an aptamer for its target molecule is inversely proportional to the size of the target.[46,47] Although the size of the

target influences aptamer affinity, there have been several aptamers selected for small molecule targets with K_d values in the low nanomolar range.[48] Target immobilization, partitioning and binding affinity measurements are technical challenges for small molecule SELEX.[2] An unaltered form of the target molecule is ideal for selection. For this reason, partitioning methods that do not require target immobilization are advantageous. However, methods that rely on a dramatic change in the size of the aptamer-target complex are not usually possible for small molecule targets due to their size.[2] Immobilization of the target molecule results in fewer available functional groups and an increase in non-specific binding to the solid support matrix.[2,49]

1.2.2 Assay dependent differences in small molecule aptamer evaluations

To assess the affinity of an aptamer for its target molecule, the equilibrium between the individual components (aptamer and target) and the formed aptamer-target conjugate (complex) must be considered. The described equilibrium is as follows:

$$Aptamer + Target \rightleftharpoons Complex \qquad \textbf{Equation 1}$$

The dissociation constant (K_d) is the equilibrium constant in the reverse reaction. The K_d measures the larger complex's tendency to separate or dissociate reversibly into individual components. The K_d can be calculated by the concentration of the products over the concentration of the reagents:

$$K_d = \frac{[Aptamer][Target]}{[Complex]} \qquad \textbf{Equation 2}$$

Therefore, the K_d is inversely proportional to the affinity of the aptamer for the target molecule. Since this value is an equilibrium constant, the K_d can also be described as a ratio between the forward and reverse reaction rates:

$$K_d = \frac{k_{off}}{k_{on}} \quad \textbf{Equation 3}$$

Therefore, the K_d is measured to determine the affinity of the aptamer for its target molecule. Apparent K_d values can be experimentally calculated using various methods based on conformational changes, fluorescence/absorbance, mass-sensitive surface detection, separation or other techniques. As previously mentioned, the binding of an aptamer to a small molecule target does not result in a large change in mass. Therefore, methods such as SPR, atomic force microscopy, or equilibrium dialysis are made difficult for small molecule targets.[2] Often, small molecule target binding affinity methods require either immobilization of the target or aptamer in solution (magnetic bead assay), or fluorescence of the target molecule (fluorescence polarization).[2]

Recently, our research suggests that the experimental K_d value is dependent on the method of analysis and binding conditions.[50] Furthermore, differences in the binding and selection conditions of a specific aptamer influence binding and the apparent K_d of the sequence. Our work compares the apparent K_d values determined via various binding affinity methods. These inconsistencies are summarized for each of the seven OTA aptamers. Specifically, only some of the aptamers found to have an affinity for the target molecule are able to detect OTA via a AuNP assay (assay described further in section 2.1.3) (Table 1.3).[50]

Table 1.3 Characterization of ochratoxin A (OTA) aptamers through various quantitative and qualitative binding affinity methods

OTA aptamer	KD values (nM)							Qual. binding
	Equilibrium dialysis	Ultra-filtration	Affinity chrom.	Flu. Polarization	SPR	DNAse assay	SYBR Green	AuNP assay
1.12.2	287±56	255±89	374 ± 255	125±23	163±15	NB	146±43	Yes
T22	160 ± 21	250 ± 49	n/a	77 ± 9	63 ± 12	n/a	31 ± 9	Yes
A08	NB	NB	286 ± 149	NB	NB	200±155	108±61	Yes
A08m	n/a	n/a	406 ± 166	n/a	NB	NB	169±52	Yes
B08	n/a	n/a	114 ± 49	n/a	NB	670±330	17±5	No
H8	NB	NB	29 ± 16	NB	NB	54±23	NB	No
H12	NB	NB	40 ± 14	NB	NB	270±201	NB	No

Similarly, studying the binding of these aptamers to OTA through various in-solution binding parameter, we are able to recommend which sequences are best suited for these solution-based assays and applications.[51] Interestingly, 1.12.2, A08, A08m H8 and H12 obtain similar binding affinities, yet H8 and H12 did not respond in the AuNP assay or SYBR Green (SG) assay. Confirmed with ultrafiltration and equilibrium dialysis, H8 and H12 were considered unsuited for in-solution assays.[51]

1.3 Aptamer-based gold nanoparticle biosensors

Nanoparticles have gained significant interest with a notable increase in nanoparticle biosensor research. The unique physiochemical properties and high surface area to volume ratio of nanoparticles are useful elements for many sensor applications.[52,53] Among these, gold nanoparticles (AuNPs) are commonly used due to their interesting and tunable optical properties.[54] The stability and biocompatibility of AuNPs provide an attractive and versatile platform for various biosensing applications.[52,54] AuNPs have conductive properties and, depending on size, can quench fluorescence.[52,55] This makes AuNPs attractive as an electrochemical[56] or fluorescent-based[57–59] biosensor platform. The properties of AuNP are not only used for sensing purposes, but are also used for drug delivery, diagnostic and photothermal applications.[54,60] Sensing with AuNPs is divided into the following categories: colourimetric, fluorescent-based, electrical and electrochemical, and AuNP-based surface plasmon resonance (SPR) sensors.[53] As one example, the optical properties of AuNPs allow naked eye colourimetric detection. Salt-induced AuNP aggregation results in a colour change from wine-red to blue, which can be used in signal detection.[61]

Aptamers can be incorporated into a AuNP-based sensor as the molecular recognition element. Thiol modified aptamers can be covalently bound to AuNPs[62,63] through the thiol sulfur and gold surface, or unmodified aptamers can be adsorbed[64–67] onto the surface of the nanoparticle. Based on the covalent or non-specific interaction between aptamers and AuNPs, a number of different aptamer based AuNP sensors have been developed for a variety of targets, including small molecules.[57,58,67–74]

1.3.1 On-site lateral flow device (LFD)

A lateral flow device (LFD) is a AuNP-based sensor that can easily and quickly detect a target molecule in solution. Functionally similar to a pregnancy test, this LFD is easy-to-use, inexpensive and quick. This device, like other immunochromatographic devices, relies on the migration of the sensing conjugate along the membrane. The LFD is made up of four components: the wicking pad, the conjugation pad, the nitrocellulose membrane and the adsorption pad. The buffer or solvent is added to the wicking pad, which commences migration. The conjugation pad is made of a glass fiber and contains the labeled recognition probes. Migration of the solvent occurs over the nitrocellulose pad, where there is a control and test line applied. In our developed LFD, the control line is made up of poly(diallyldimethylammonium chloride) (PDDA) and the test like is composed of streptavidin. Finally, in terms of the solvent front, there is an absorption pad, which acts as a 'basin' at the end of the device. Single-stranded DNA aptamers can be adsorbed onto the surface of AuNPs (Section 2.1.3). These aptamers are modified with biotin on the 5' end of the sequence. The control line (made of PDDA) is positively charged and is capable to stopping particles that pass the test line. The test line contains streptavidin, which will interact with the biotin modification of the ssDNA aptamer. Based on these interactions, the detection of a target in solution is made possible. The solution being tested is added to the wicking pad. If the solution is contaminated with the target molecule of interest, the aptamer will leave the AuNP surface and preferentially bind the target molecule. Therefore, when target is present, the aptamer will be displaced from the AuNP surface and leads to the loss of AuNPs at the test line. This is easily observed as there is a disappearance of the characteristic wine- red colour spot at the test

line. This mechanism is used to signal target detection in an easy-to-use, colourimetric LFD.[75] For example, it is reported that OTA and AFB_1 can be detected with an aptamer-based LFD.[76,77] Figure 1.3 illustrates this biosensor and its mechanism.

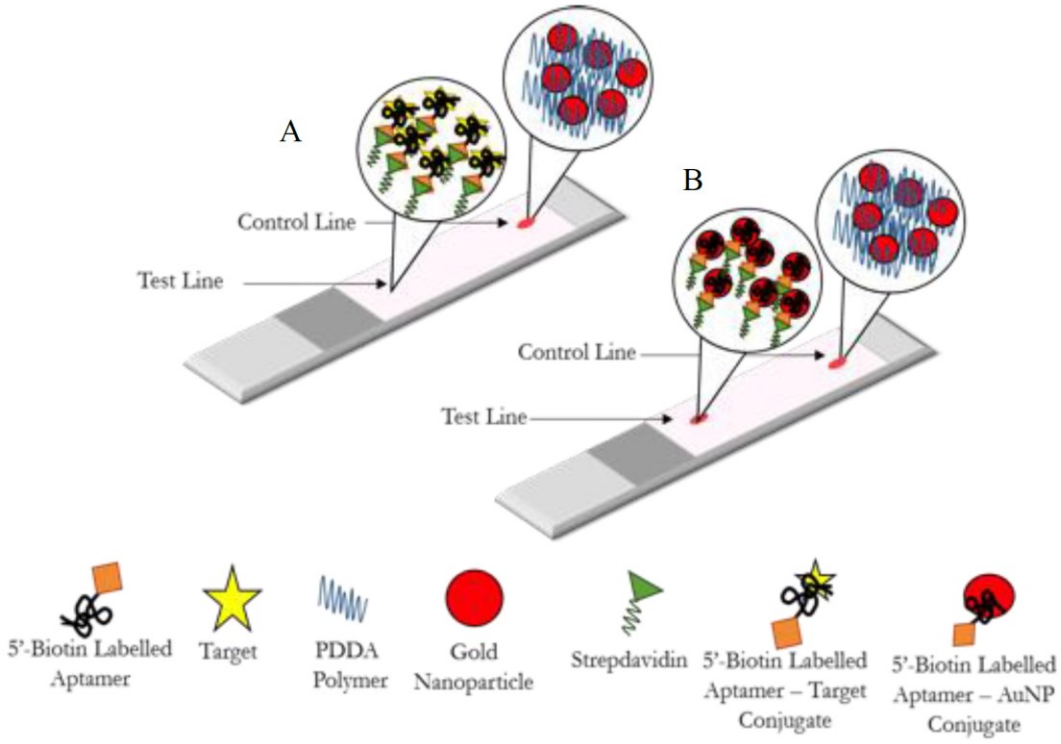

Figure 1.3 Illustration of the gold nanoparticle (AuNP) based lateral flow device (LFD) process. To begin, biotin labeled aptamers (black line with organic diamond) are adsorbed onto the AuNP (red circle). The control line is made up of PDDA polymer (blue line) and the test line is made up of streptavidin (green triangle). When target (yellow star) is present in solution, the AuNP is displaced when the aptamer binds its target (A) and only one red spot is seen. Without target (yellow star), the aptamer remains on the AuNP surface (B), leading to two red spots on the LFD.

1.3.2 Current challenges with aptamer-based gold nanoparticle assays

Considering the vast opportunities of aptamer based AuNP sensors, it is of interest to address their current challenges. The interaction between aptamers and AuNPs is required to develop a sensing platform.[64–67] However, this interaction cannot be stronger than the interaction within the aptamer-target complex as the sensor relies upon the aptamer leaving the AuNP surface to preferentially bind its target molecule in solution. As the interaction between the aptamer and the AuNP is non-covalent, the relative strength of this interaction relative to the interaction within the aptamer-target complex determines the success of the sensor. The sequence and length of an aptamer can influence the interaction between the aptamer and AuNP surface. Similarly, the affinity of the aptamer for its target can vary depending on the binding conditions.[50,51] In a collaborative study, our research group reported that not all aptamers with affinity for a small molecule target (OTA) were capable of detecting the target through the AuNP assay. Optimization of the sensor parameters is often required when applying the sensor platform to a new aptamer sequence and target molecule. For each target and aptamer, the conditions (including reaction time and the concentration of aptamer, target and salt) vary significantly. In some cases, the selected aptamer is unable to function as the molecular recognition element in the AuNP biosensor altogether.[50] Therefore, although this alternative method of detection offers a number of advantages, these inconsistences limit the versatility of the sensor. Other challenges may arise from an interaction between the target molecule itself and the AuNP platform. Since the mechanism of the sensor is designed to use the target molecule in solution to remove the aptamer from the AuNP surface, an interaction between the target and the AuNP is unfavorable.[19,50] These

limitations hinder the versatility and reliability of the sensor. Future development of the AuNP sensor should focus on overcoming these challenges and selecting aptamers with these future binding conditions in mind.

1.4 A novel SELEX approach

As previously mentioned, SELEX can be modified to improve aptamer selection.[16,28,33–44] Selecting for aptamers in a manner that will mimic established AuNP biosensor conditions provides a number of advantages compared to traditional SELEX.[50] As the molecular recognition element of the developed AuNP sensor, the selected aptamers will have affinity for the target under these specific testing conditions. Using AuNPs as a SELEX platform will generate sequences that can be removed from the AuNP surface when target is introduced. This selection process will eliminate sequences that do not adsorb onto the AuNP surface before target introduction, as well as partition sequences without affinity for the target molecule. Therefore, AuNP SELEX functions as a multi-purpose selection process by generating sequences that adsorb onto the AuNP surface but leave this surface when the target molecule is present.

In this novel SELEX approach, AuNPs are incorporated as the solid support matrix or platform during selection. The initial library of sequences is adsorbed onto the AuNP surface. This ssDNA-AuNP complex is isolated from the sequences that did not adsorb onto the AuNPs. We hypothesize that target incubation will result in the removal of sequences surface with affinity for the target from the AuNP surface. In solution, these binding sequences can be separated from the sequences that remain on the AuNP surface. Eluted from the target molecule, the selected sequences can be amplified through PCR

amplification and used as the pool for the next SELEX round. After a number of rounds, sequences with affinity for the target molecule under these conditions will be selected. Figure 1.4 illustrates the developed mechanism. The developed SELEX method can potentially address previously mentioned limitations of the aptamer based AuNP sensor and ensure that the selected aptamer can be used as the molecular recognition element of this assay.

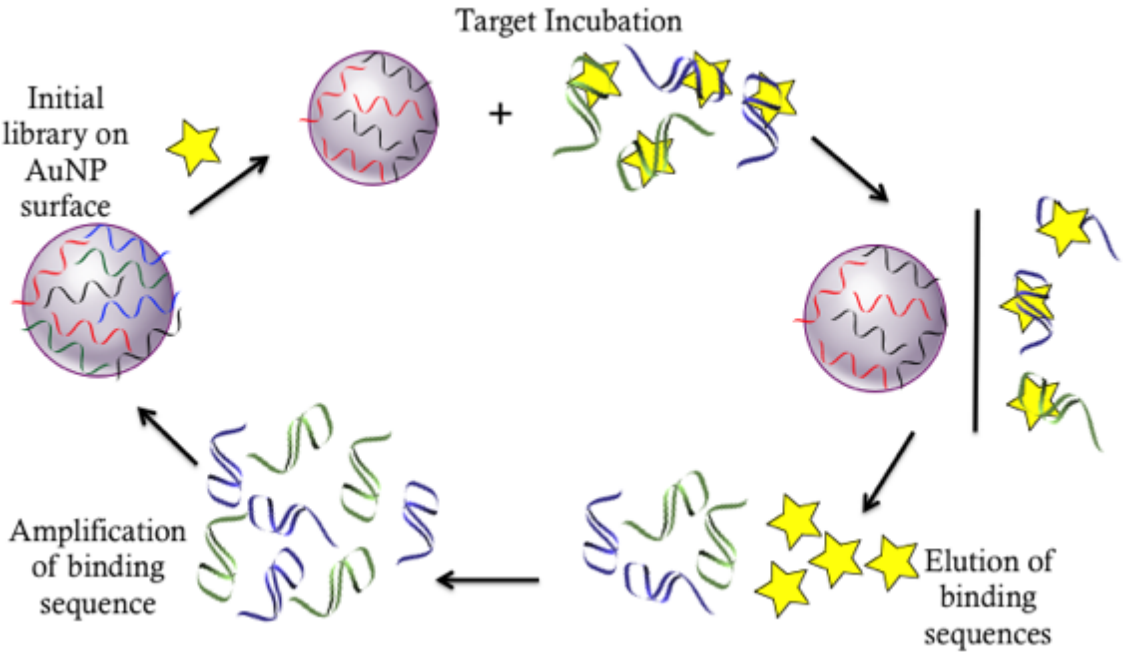

Figure 1.4 Gold nanoparticle (AuNP) based Systematic Evolution of Ligands by Exponential enrichment (SELEX) process. The initial library is adsorbed onto the AuNP surface. After target (yellow star) incubation, the binding sequences (blue and green ribbons) are partitioned from the non-binding sequences (red and black ribbons) left on the AuNP surface. The selected sequences are eluted from the target and amplified through PCR amplification. These amplified sequences are the pool of the next SELEX round.

1.5 Thesis Objective

In this study, we aim to investigate AuNPs as a platform for small molecule SELEX and outline the possible challenges and opportunities of this method. First, various partitioning methods will be compared and optimized for our AuNP SELEX application. Second, the capacity of AuNPs for adsorbed ssDNA aptamers will be considered for these partitioning methods. Finally, the developed method will be tested through a proof-of-concept SELEX experiment to determine the specificity and overall potential of the developed method.

Chapter 2: Investigating gold nanoparticles as a platform for small molecule SELEX

2.1 Introduction

2.1.1 Centrifugation as a partitioning method for AuNP-based SELEX

Centrifugation is one possible SELEX partitioning method, which relies upon a difference in mass/density between the complex and the individual components in solution.[24] Since centrifugation does not require immobilization onto a solid support matrix, the aptamer and target remain free in solution. This is an ideal situation since it more closely mimics the final application conditions of the target (*i.e.,* free in solution). However, to-date this method has been inaccessible to small molecule aptamer selection, since the difference in the aptamer mass vs. the aptamer-small molecule mass is too small.

As one potential alternative, the difference in size and mass between AuNPs and ssDNA may be exploited to separate AuNP-ssDNA conjugates from free ssDNA in solution via centrifugation. In this approach, the initial library of random DNA sequences could be adsorbed onto the surface of AuNPs. Using centrifugation to pellet the AuNPs out of solution, the supernatant containing free DNA sequences can be easily aspirated and removed. Next, the target molecule (for which an aptamer is desired) could be added in solution to the isolated AuNPs with adsorbed putative aptamer sequences. The putative aptamers with affinity for the target molecule will be released from the AuNP surface to bind to the target molecule. Centrifugation can be used again to partition the aptamer-

target complex from the aptamers that remain on the AuNP surface. The workflow of this new approach is shown in Figure 2.1.

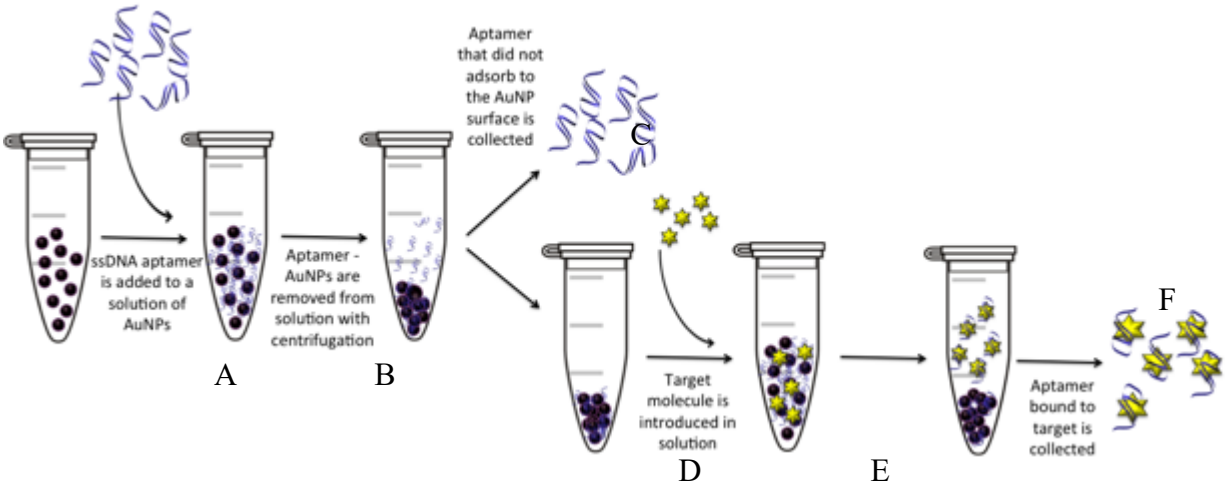

Figure 2.1 Partitioning via centrifugation for AuNP based SELEX. After ssDNA (blue ribbons) are adsorbed onto the AuNP surface (purple circles) (A), the AuNPs can be separated from solution through centrifugation (B). The supernatant containing the sequences not adsorbed to the AuNPs in solution can removed (C). After target (yellow star) incubation (D), the non-binding sequences that remain on the AuNP surface can be separated (E). The binding sequences interact with the target in solution and can be collected (F).

2.1.2 Interactions between gold nanoparticles and DNA aptamers

The adsorption mechanism of DNA and citrate capped AuNPs is not completely understood, this is evidenced by several inconsistencies in the literature. Early work by Li and Rothberg theorizes that single stranded DNA (ssDNA) is electrostatically adsorbed to the surface of negatively charged citrate capped AuNPs.[59] Specifically, the Derjaguin-Landau-Verwey- Overbeek (DLVO) theory is used to explain the adsorption of ssDNA onto citrate capped AuNPs. Compared to dsDNA, the free bases of ssDNA distance the negative charge of the phosphate backbone from the citrate capped AuNP surface, which allows for adsorption. Whereas, the negative charge of both phosphate backbones of

dsDNA prevents adsorption due to repulsive forces between the citrate capped AuNP and dsDNA (Figure 2.2).

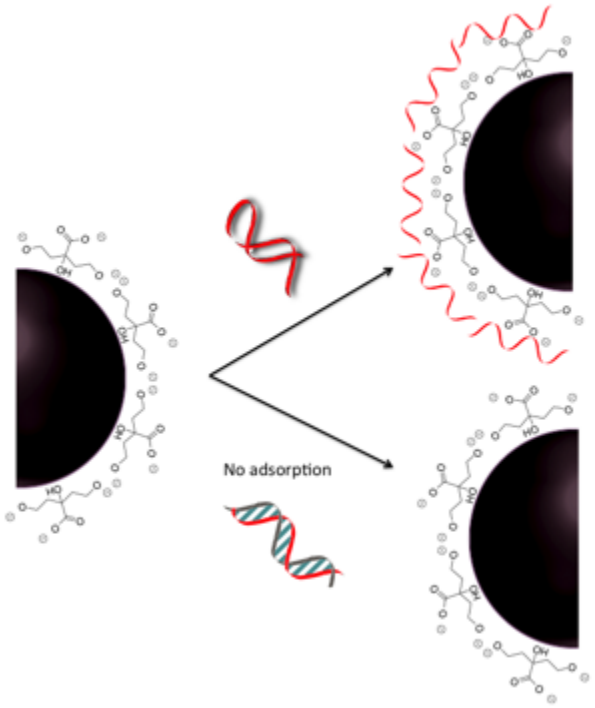

Figure 2.2 Adsorption of ssDNA (red ribbon) onto the surface of citrate capped gold nanoparticles (AuNPs). dsDNA (blue and red double helix) does not adsorb.

The DLVO theory was challenged, as this mechanism does not explain the base, sequence dependent variations in adsorption.[78] Furthermore, the difference in linear charge density between ssDNA and dsDNA was not large enough to justify the differences in adsorption. Nelson and Rothberg proposed that ssDNA displace citrate ions on the surface of AuNPs.[78] Although this mechanism was experimentally founded, the proposed interactions (hydrogen bonding and the hydrophobic effect) were not founded as the main contributing factor for DNA adsorption. Recently, the most accepted hypothesized adsorption mechanism is the displacement of citrate ions with ssDNA

through specific chemical interactions between the available bases of ssDNA and the AuNP surface (Figure 2.3).[79,80] Observed base dependent adsorption is supported with this adsorption mechanism.

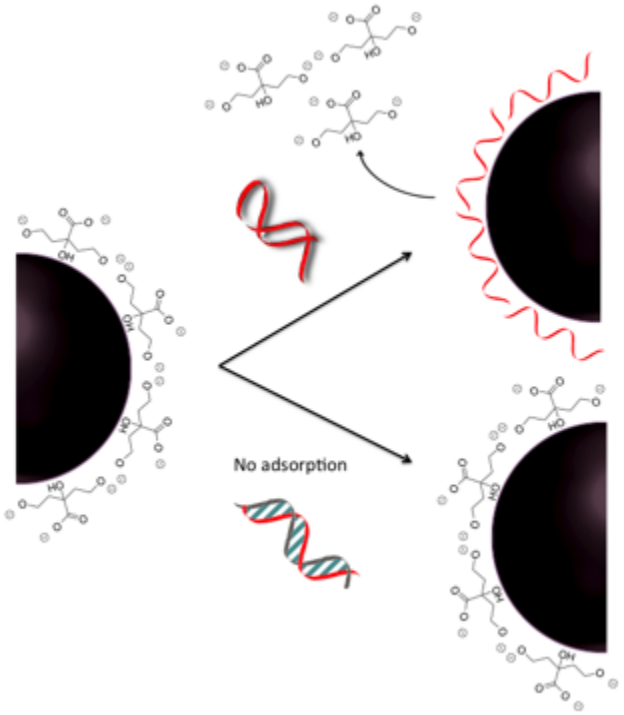

Figure 2.3 Adsorption of ssDNA (red ribbon) onto AuNPs by displacing the citrate ions on the AuNP surface. dsDNA (blue and red double helix) does not adsorb.

In particular, Pong et al. report that the base pairs interact differently with the AuNP surface, and therefore, exhibit dissimilarities in adsorption.[81] Through computational analysis, their findings support the idea that ssDNA interacts with AuNPs through the available purine/pyrimidine rings. Specifically, dT binds to AuNPs more weakly compared to the other bases (dA, dC and dG). This difference is attributed to the available primary amines on dA, dC and dG (Figure 2.4).[81] However, recent studies use

surface enhanced Raman spectroscopy (SERS) to determine that the nitrogen sites are the main interaction points with AuNP surface.[80]

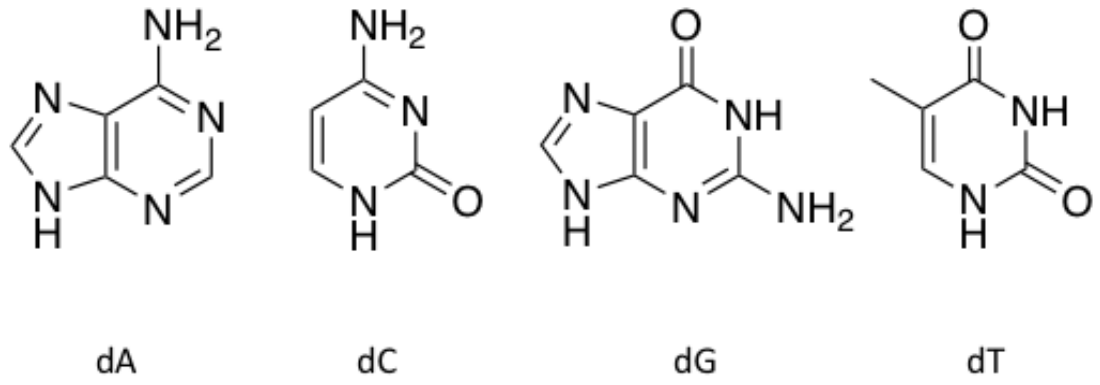

Figure 2.4 Chemical structure of nucleobases, adenine (dA), cytosine (dC), guanine (dG) and thymine (dT)

The adsorption of ssDNA onto the surface of AuNPs can also be explained with the Langmuir adsorption model.[79,82] This theory describes adsorption in terms of the adsorbant and the available sites for the adsorption: in our case, ssDNA and the AuNP surface. Using this model, the adsorbate (ssDNA) and available sites for adsorption on the AuNP surface (AuNP) are in equilibrium with the formed complex (AuNP-ssDNA) when adsorption occurs:

$$ssDNA + AuNP \rightleftharpoons ssDNA \cdot AuNP \qquad \textbf{Equation 4}$$

The equilibrium between the individual components (ssDNA and AuNPs) and the adsorption of ssDNA onto AuNPs (ssDNA-AuNPs) is described. If the rate constant of adsorption in the forward reaction is k_1 and the rate of desorption in the reverse reaction is k_2, then the rate equations are as follows:

$$rate = k_1[AuNP][ssDNA] \qquad \textbf{Equation 5}$$

$$rate = k_2[AuNP - ssDNA] \quad \textbf{Equation 6}$$

Since the rate of adsorption and desorption are equal at equilibrium, the dissociation equilibrium constant (K_d) can be represented by the following:

$$k_a[AuNPs][ssDNA] = k_d[AuNPs - ssDNA] \quad \textbf{Equation 7}$$

$$K_d = \frac{k_2}{k_1} = \frac{[AuNP][ssDNA]}{[AuNP - ssDNA]} \quad \textbf{Equation 8}$$

For a single adsorbate (one ssDNA aptamer sequence), the rate of adsoption is equal to the rate of desorption. Therefore, the fraction of the surface sites covered at equilibrium can be represented with the following equation:

$$\theta = \frac{KC}{(1 + KC)} \quad \textbf{Equation 9}$$

where θ is the adsorbed DNA, C is the concentration of ssDNA aptamer and K is the Langmuir constant. Assuming monolayer coverage, θ is restricted between 0 and 1. Therefore, θ can be used to determine the amount of ssDNA adsorbed to the AuNP surface. Adsorption is proportional to the value of θ, as the value of θ increases with the amount of ssDNA adsorbed to the AuNP surface.[79,82]

2.1.3 Salt induced aggregation assay for colourimetric detection

Six years ago, Zheng et al. (2011) reported one of the first aptamer-based colourimetric biosensor for the detection of a small molecule target.[64] In comparison to other detection methods such as electrochemistry or high performance liquid chromatography (HPLC), colourimetric sensors are advantageous for their simple, quick and on-site detection.[2] The optical properties of AuNP are exploited, as aggregation

results in a visible colour change.[61] In this study, a DNA aptamer previously selected for dopamine was adsorbed onto the surface of citrate capped AuNPs. This adsorption protected the AuNPs from salt-induced aggregation. However, when the specific target molecule was introduced in solution, the aptamer was released from the AuNP surface to preferentially bind its target, dopamine. Therefore, the presence of dopamine resulted in salt-induced aggregation, which is used for colourimetric detection (Figure 2.5).[64] Similarly, several other reports employing aptamers in the AuNP biosensor have been published.[55,59,64–66] However, for each target and aptamer, the conditions (including reaction time and the concentration of aptamer, target and salt) vary significantly.[50]

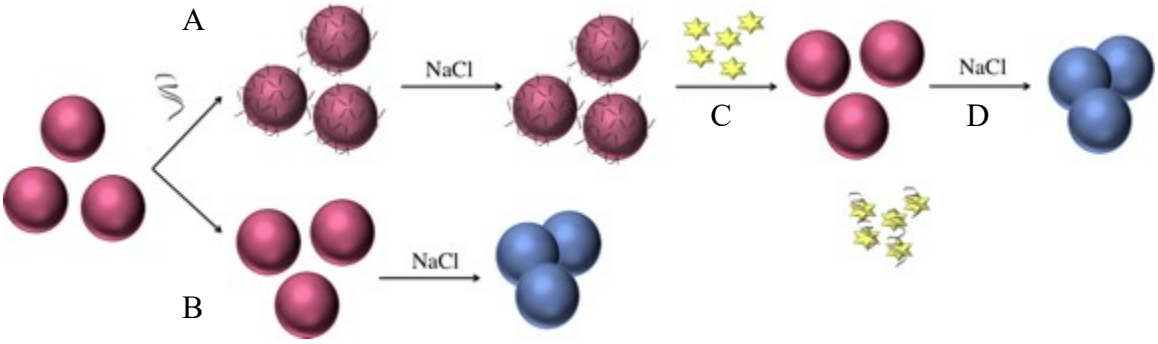

Figure 2.5 Illustration of the salt-induced AuNP aggregation assay. ssDNA aptamers (black ribbon) are adsorbed onto the surface of AuNPs (red spheres) protecting the AuNPs from salt induced aggregation with sodium chloride (NaCl) (A). Without the adsorption of ssDNA aptamer, the AuNPs are subject to salt-induced aggregation (blue spheres) (B). When target (yellow stars) is present in solution, the aptamer will leave the AuNP surface to preferentially bind the target molecule (C) and leave the AuNPs exposed to salt-induced aggregation (D).

2.1.4 Chapter objectives

To leverage AuNPs as a platform for small molecule SELEX, first a reliable partitioning method must be established. This chapter describes our investigation of rationally-selected partitioning methods (including filtration, gel electrophoresis and centrifugation) to assess which technique is sufficiently reliable for separating ssDNA in solution from ssDNA adsorbed onto AuNPs. The best separation method was employed to examine AuNP capacity for ssDNA aptamers, structure and length adsorption bias between aptamer sequences, and the mechanism of adsorption. Through the successful and reliable separation of adsorbed ssDNA aptamers from sequences in solution, this work provides insight into the non-covalent interaction between ssDNA aptamers and AuNPs.

2.2 Experimental

2.2.1 Materials

Phosphoramidites and 1000 Å pore size controlled glass pore (CGP) columns were purchased from Glen Research. Ochratoxin A (OTA), Gold (III) chloride trihydrate ($HAuCl_4 \bullet 3H_2O$), and Sodium citrate dehydrate ($HOC(COONa)(CH_2COONa)_2 \cdot 2H_2O$) were purchased from Sigma-Aldrich.

2.2.2 DNA aptamer preparation, purification and quantification

All aptamers and primers were synthesized on a BioAutomation Mermade 6 oligonucleotide synthesizer (Plano, Texas). The unmodified aptamer sequences were synthesized using standard phosphoramidite chemistry on a 1μmol controlled glass pore

(CGP) columns with a 1000 Å pore size. Sequences were modified with 5'- fluorescein phosphoramidite (Glen Research). To cleave the sequences from the column after synthesis, the beads were placed in a 1.5 mL eppendorf tube with 1 mL of ammonium hydroxide (NH_4OH) and allowed to incubate overnight at 55 °C. The tubes were removed from heat and allowed to cool for at least 30 mins. The solution was centrifuged to pellet the beads and the supernatant containing the sequences was removed and placed in a clean 2 mL eppendorf tube. The beads were washed with 1 mL of deionized water and centrifuged to pellet the beads. The supernatant was removed and added to the same 2 mL eppendorf tube. The tubes were placed on Savant AES2010 SpeedVac overnight or until dry.

Synthesized aptamers were purified using polyacrylamide gel electrophoresis (PAGE). A 12% denaturing gel solution was prepared by combining 31.5 g of urea, 23.5 mL acrylamide (acrylamide/ bis-acrylamide 40% solution), 15 mL of 5x Tris/ borate/ EDTA (TBE) buffer and 14 mL of deionized water in a 250 mL beaker. The solution was heated with stirring to 37 °C. The hot solution was filtered by gravity using Whatman No. 1 filter paper and allowed to cool to room temperature. 450 µL of 10% ammonium persulfate and 35 µL of TEMED (N, N, N', N'- tetramethylethylenediamine) were quickly added to the solution immediately before pouring the gels. The solution was swirled and poured between two glass gel plates with a plastic comb, and the gel was allowed to polymerize for 30 mins. After polymerization, the gels were equilibrated on a SE Chroma Standard Dual gel electrophoresis unit at 300 V for 15 mins. The DNA samples were prepared by adding 300 µL of deionized water and 300 µL of formamide to the 2 mL eppendorf tube containing the dried sequences. This solution was vortexed and

heated to 90°C for 5 mins. All 600 µL of sample was loaded onto a gel and run at 300 V for approximately 2 hours. The gel was imaged using the epiUV and fluorescence features of an Alpha Imager Multi Light Cabinet (Alpha Innotech). The fluorescent band in the gel was cut out of the gel, broken in a 50 mL tube and incubated for 2-3 days in approximately 25mL of water at 37°C in a New Brunswick Scientific Innova 40 incubation shaker at 160 rpm. The gel was then filtered through 0.22 µm cellulose acetate syringe filters into a new 50 mL tube. The filtered solution was dried on a Labconco freezone lyophilizer. When dry, the sequences were re-dissolved in a minimum amount of deionized water. Using Desalting Amicon-Ultra 0.5 mL 3 kDa centrifuge tubes, the sequences were desalted and rinsed. The DNA was quantified using a Cary 300 Bio UV-Vis Spectrometer (Varian, USA) at 260 nm.

2.2.3 Synthesis of gold nanoparticles (AuNPs)

All glassware used for the AuNP synthesis was washed with aqua regia (3:1 mixture concentrated HCl/HNO_3) and rinsed thoroughly with deionized water. In a 250 mL Erlenmeyer flask, 2 mL of 50 mM $HAuCl_4 \bullet 3H_2O$ was added to 98 mL of deionized water. The solution was brought to a boil quickly with magnetic stirring. Upon boiling, 10 mL of 38.8 mM sodium citrate ($HOC(COONa)(CH_2COONa)_2 \cdot 2H_2O$) was quickly added. The solution changed from a pale yellow to dark blue and finally to a wine-red. At this point, the solution was allowed to heat for an additional 10 mins with stirring. The solution flask was removed from the heat and allowed to cool to room temperature with continued stirring. The synthesized AuNPs were characterized by UV-Vis spectrometry and TEM/EDS analysis.

2.2.4 Partitioning methods for separation of AuNP-aptamer complex

2.2.4.1 Dilution and preparation of AuNPs

Six 1.5 mL Eppendorf tubes were placed in a tray and labeled as control (3) and test (3) samples. 1 mL of 12 nM AuNPs was prepared from stock AuNP solution. 210 µL of 12 nM AuNPs was placed in the sample tubes labeled test and 210 µL of deionized water was placed in the tubes labeled control.

2.2.4.2 Preparation of aptamer dilutions

1 mL of 1 µM DNA aptamer was prepared and heated to 90°C for 5 mins and allowed to cool to room temperature for approximately 15-30 mins. When 2 sequences were added to AuNPs competitively, 1 mL of each sequence was prepared at a concentration of 1 µM. 1 mL of each sequences was mixed together in the same 15 mL tube, divided into 3 1.5 mL Eppendorf tubes and heated together for 5 mins to 90°C and cooled to room temperature for 15-30 mins.

2.2.4.3 Preparation of target molecule (OTA)

Purchased ochratoxin A (OTA) (approximately 1 mg) was dissolved in 1 mL of deionized water and placed on a shaker at room temperature overnight. The solution was filtered through 0.5 mL Corning Costar Spin-X centrifuge filter tubes. The filtrate was collected and quantified by UV-Vis absorption spectroscopy at 330nm. 10 µM of OTA was prepared in deionized water and stored at room temperature.

2.2.4.4 Introduction of aptamer to AuNPs

100 µL of 1 µM DNA was added to control samples and test sample tubes containing 210 µL of 12 nM AuNPs. The tubes were vortexed quickly and allowed to incubate at room temperature for 30 mins.

2.2.4.5 Removal of non-binding DNA sequences

2.2.4.5.1 Filtration

After 30 mins, the tubes were centrifuged for 30 mins at 14,000 g in 50 kDa size Amicon centrifuge filter tube. The supernatant solution was removed and placed in the new 1.5 mL tube. Non-binding fluorescein labeled DNA analyzed for the capacity of AuNPs was measured immediately on a fluorescence spectrophotometer (Horiba Jobin Yvon, USA) with a SpectrAcq controller.

2.2.4.5.2 Agarose gel electrophoresis

After 30 mins, the solution was mixed with 25% glycerol volume ratio and vortexed quickly. 80 µL of each tube of DNA was loaded into different individual wells and the gel was run at approximately 160 V for approximately 2-3 hours.

2.2.4.5.3 Centrifugation

After 30 mins, the tubes were centrifuged for 30 mins at 12,000 g. The supernatant solution was removed and placed in the new 1.5 mL tube. Non-binding fluorescein labeled DNA analyzed for the capacity of AuNPs was measured immediately on a fluorescence spectrophotometer (Horiba Jobin Yvon, USA) with a SpectrAcq controller. When two sequences were added, the non-binding fluorescein labeled DNA

sequences were placed on Savant AES2010 SpeedVac overnight or until dry and later analyzed by PAGE.

2.2.4.6 Introduction of target molecule (OTA)

100μL of 40 μM OTA and was added to the AuNPs after removal of non-binding DNA sequences. The tubes were once again vortexed quickly, allowed to incubate at room temperature for 20 mins and then centrifuged for 30 mins at 12,000 g. on a shaker at a low setting. This supernatant solution was removed and collected in the new 1.5 mL tubes. The tubes were placed on Savant AES2010 SpeedVac overnight or until dry and later analyzed by PAGE

2.2.4.7 PAGE analysis of AuNP-aptamer structure bias and multilayer effect

The collected DNA sequences were mixed with fomamide in a 1:1 volume ratio, vortexed quickly and heated to 90°C for 5 mins. 80 µL of each tube of DNA was loaded into different individual wells and the gel was run at 300 V for approximately 2-3 hours.

2.2.4.8 Imaging and analyzing the PAGE gel

After the gel run was complete, the gel was placed on a 20 cm by 20 cm fluorescent dye loaded TLC plate with plastic wrap. The gel was imaged using an Alpha Imager Multi Light Cabinet (Alpha Innotech). The intensity of each UV-Vis absorption band was found and analyzed with Image J software.

2.2.4.9 Fluorescence-based analysis of AuNP capacity for ssDNA aptamers

Fluorescence spectra were recorded on a fluorescence spectrophotometer (Horiba Jobin Yvon, USA) with a SpectrAcq controller with an excitation wavelength of 495 nm and an emission wavelength of 400- 600 nm (6fam fluorescein).

2.2.5 Salt-induced aggregation analysis of centrifugation assay design

Aggregation was induced at various stages of the AuNP centrifuge assay; before removal of supernatant, after removal of supernatant or after the addition of target. After centrifugation, the centrifuged tubes and their associated control tubes were vortexed quickly. 70 µL of 0.25 M sodium chloride (NaCl) was added to each tube. The tubes were vortexed quickly and allowed to incubate for 5 mins at room temperature. After incubation a picture was taken and the UV-Vis absorption spectra was measured using a Cary 300 Bio UV-Vis spectrometer (Varian, USA) within 30 mins of adding NaCl.

2.2.6 Transmission electron microscopy (TEM)

AuNPs were prepared as described in section 3.2.2. and analyzed at each step during synthesis. Transmission electron micrographs were taken with a FEI Technai G2 F20 TEM at the Carleton University Nano-imaging Facility, with a field emission source at a voltage of 200 kV using Gatan Microscopy Suite 2V. All images were taken on dry 300 mesh x 83 μm pitch carbon coated copper TEM grids at room temperature. Grids were prepared by placing 4 μL of AuNPs on a TEM grid. The TEM grids were allowed to dry for 4 -24 hours depending on the solvent. Images were taken at 1-2 μm, 100- 200 nm and 5- 10 nm for each grid.

2.2.6.1 TEM Energy-dispersive X-ray spectroscopy (TEM/EDS)

EDS of each AuNPs sample was taken at a 20 degree take off angle with an Oxford X-max 80mm EDS detector using Aztec software.

2.3 Results and Discussion

2.3.1 Optimization of AuNP-aptamer centrifugation assay conditions

As a starting point to determine whether AuNPs could serve as a potential platform for SELEX, we developed a AuNP-aptamer centrifugation assay to investigate the interaction between various single-stranded DNA aptamers and citrate capped AuNPs. Specifically, we were interested in the DNA loading capacity onto AuNPs, if there was a bias between DNA aptamer structures and lengths, and the extent of monolayer or multilayer formation on the AuNP surface. We also carefully considered the conditions used in the classical aptamer AuNP bioassay, in particular the ratio of DNA to AuNP concentrations (typically 40:1) (Table 2.1).

To measure the aptamers adsorbed to the AuNP surface, the non-binding aptamers must be removed for analysis by difference. To achieve this, centrifugation was applied to create a pellet of AuNPs. Initially, this was done using the same low volume conditions applied in the AuNP bioassay (*e.g.,* 6 μL of 10 μM DNA aptamer is added to 135 μL of 11 nM AuNPs), however, to accurately remove and measure the supernatant, the assay volume was increased while keeping the concentration ratios constant (Table 2.1). To further mimic the AuNP bioassay, all other conditions remained the same (*e.g.,* incubation time was kept at 30 mins).

Table 2.1 Conditions for the AuNP bioassay and the designed AuNP centrifugation assay

	Concentration added (M)	Volume added (μL)	Final assay concentration (M)	Final assay concentration ratio	Final assay volume (μL)	Final amount (mol)	Molar ratio
AuNP salt aggregation assay conditions							
ssDNA aptamer	1.0×10^{-5}	6	4.3×10^{-7}	40	141	6.0×10^{-11}	40
AuNP	1.1×10^{-8}	135	1.1×10^{-8}	1	141	1.48×10^{-12}	1
AuNP centrifuge assay conditions							
ssDNA aptamer	1.0×10^{-6}	100	3.2×10^{-7}	40	310	1.0×10^{-10}	40
AuNP	1.2×10^{-8}	210	8.1×10^{-9}	1	310	2.5×10^{-12}	1

2.3.2 Head-to-head studies reveal importance of partitioning methods for AuNP SELEX

The partitioning method for investigating AuNP-aptamer interactions was rationally chosen based on the fact that the separation technique used during SELEX should be compatible with the future testing conditions and well suited for the type of target. Therefore, the partitioning method should be chosen for a small molecule target that is free in solution. AuNP-based SELEX would require separation at two different

stages during each round of the selection process. First, the sequences that successfully adsorb onto the AuNP surface must be separated from the sequences that remain in solution. Next, the small molecule target is introduced, and the previously isolated AuNP-aptamer complex and target are allowed to incubate in solution. At this point, the partitioning method is used once again to separate the putative aptamer sequences that leave the AuNP surface to preferentially bind to the target molecule in solution from the non-binding sequences that remain adsorbed to the AuNP surface (Figure 2.6).

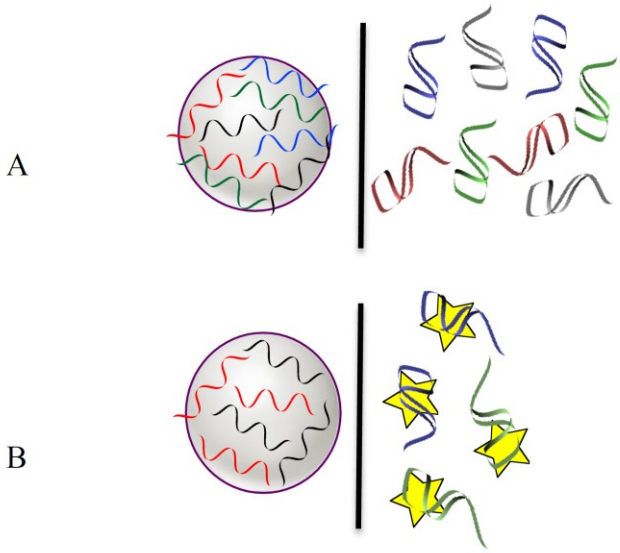

Figure 2.6 Partitioning steps required during AuNP based SELEX. A) displays the partitioning step required between ssDNA sequences (coloured ribbons) on the AuNP surface and sequences that remain in solution. B) illustrates how the ssDNA sequences (blue and green ribbons) with affinity for the target molecules (yellow star) must be separated from sequences (red and black ribbons) remaining on the AuNP surface

From the possible SELEX partitioning methods, filtration, gel electrophoresis and centrifugation were considered the best options for AuNP SELEX partitioning. This is

because these separation techniques are ‘in solution’ methods, meaning that they do not require an additional solid support matrix such as a column or bead.[24]

First, we attempted to use filtration as a partitioning method to separate the aptamer-AuNP complex from free aptamer in solution based upon a difference in size. By quantifying the amount of ssDNA that passed through the filter and comparing this amount to a control, we were able to calculate (by subtraction) the amount of ssDNA adsorbed to the AuNP surface. The pore size of the filter must be within a specific range, as it is required to be smaller than the AuNPs but large enough to let free ssDNA aptamers in solution pass through the membrane. To ensure the retention of approximately 13 nm AuNPs, a pore size of 50 kDa was chosen. Typically when washing our ssDNA sequences which are between 30-100 bases, 3 kDa membrane pore size is required. Therefore, there is theoretically a small range of pore sizes that will successfully separate the AuNPs from the ssDNA aptamers in solution. Regardless, a 50 kDa size Amicon centrifuge filter tube was investigated as a separation technique. This method for separation was problematic for a number of reasons. First, the available centrifuge tube with this pore size is designed to concentrate the sample. Therefore, not all the free ssDNA passed through the filter during the first separation and required multiple washes to ensure all the ssDNA in solution was filtered through the membrane. These required washes could affect the adsorption equilibrium further. Secondly, it was found that the membrane had an affinity for the AuNPs as the filter appeared wine-red in colour after filtration. This colour was removed after vortexing the filter tube, however, the AuNPs could block the pores during filtration and would interfere with separation. Finally, the centrifugal force required (14,000 g for 30 min) was too high when

considering that the ssDNA-AuNP complex is held together via proposed non-covalent interactions. With the combination of these challenges, other partitioning methods were considered.

We next examined gel electrophoresis as a partitioning method. Previously Pellegrino et al. successfully employed gel electrophoresis to study the difference in conjugate diameter with increasing ssDNA length. The size of the AuNP-ssDNA conjugate was analyzed for both covalently bound and adsorbed DNA. It is suggested that, even non-covalent interactions between ssDNA and AuNPs, result in a size difference that can be analyzed by the migration of the conjugate through the gel.[83] Zhang and co-workers also used gel electrophoresis to study the interactions between ssDNA and AuNPs.[79] In this work, they suggest that the adsorption of ssDNA results in an increase in the overall negative charge of the complex. The charge of the complex is considered to be the main contributing factor the migration of the ssDNA-AuNP complex, in comparison to an increase in size slowing down the migration.[79] Based on this, we investigated whether putative aptamers in solution could be separated from sequences adsorbed on the AuNP surface via agarose gel electrophoresis. However, there is one important difference for our work: the difference in size between free ssDNA in solution and the ssDNA-AuNP complex is much greater than a difference in the charge of the species.

Unfortunately, we were unable to optimize the procedure to work as a reliable partitioning method. Specifically, a clear distinction between two bands in the gel was not obtained. As a result, the percentage of ssDNA on the AuNP surface could not be determined. It is important to note that the previously reported methods used gel

electrophoresis to study the difference in ssDNA adsorption with different DNA lengths and assay conditions. These studies were not assessing the amount of ssDNA on the surface compared to the amount of ssDNA in solution, but rather how far the complex migrated in the gel relative to another sample. Despite our efforts towards optimizing the agarose gel percentage, running time, and voltage, two bands (one for ssDNA and one for the ssDNA-AuNP complex) could not be resolved and the one band was coincident with the unmodified AuNPs. This rendered gel electrophoresis unsuitable for our AuNP SELEX partitioning application.

Finally, the separation of AuNPs from non-binding DNA aptamers was attempted via centrifugation. In order to test the required centrifugation speed for sufficient separation of 13 nm AuNPs from solution, various centrifugation speeds were tested. Centrifugation of 20 nm AuNPs has been previously analyzed using a range of speeds (3,000-11,000 g) and times (10-60 mins). It was reported that approximately 80% of 20 nm AuNPs were separated at a centrifugal speed of 7,000 g for 20 mins. Based on these methods and considering the AuNP size difference, AuNPs were centrifuged for 30 mins at various speeds (5,000-12,000 g). Visually, a difference in the colour of the supernatant removed after centrifugation was noted (Figure 2.7). However, given that visual observation is not a reliable method for determining the presence of AuNPs in solution, the supernatant removed after centrifugation was analyzed by TEM with EDS. The TEM images suggest that nanoparticles remain in solution, even after centrifugation at the highest analyzed centrifugal speed (Figure 2.8). To continue with the following experiments, we chose a centrifuge speed of 13, 000 g in order to strike a balance between several factors. Specifically, to reduce the number of AuNPs left in solution as

observed by our results at 12,000 g, the speed must be higher. Conversely, to ensure that the aptamer-target interaction is maintained, speeds below 14,000 g are preferred.

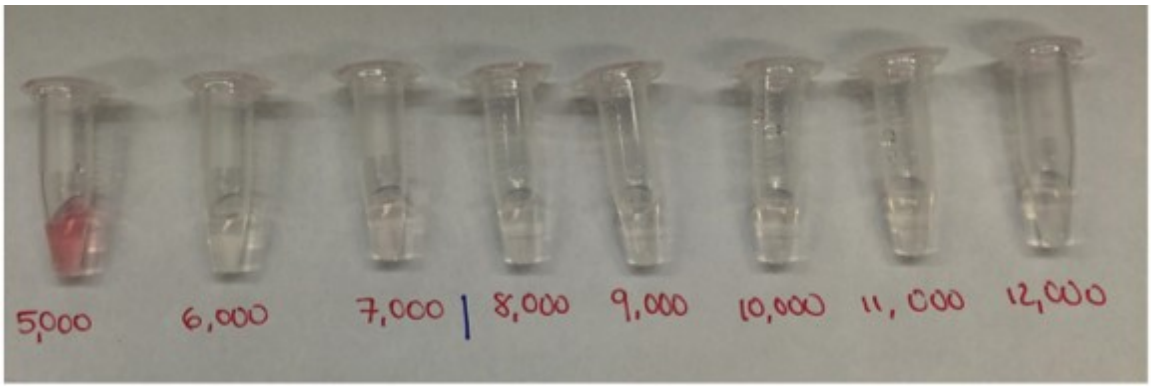

Figure 2.7 Image of the supernatant solution removed after centrifuging a 11 nM citrate capped AuNP sample for 30 mins at various centrifuge speeds (5,000- 12,000 g)

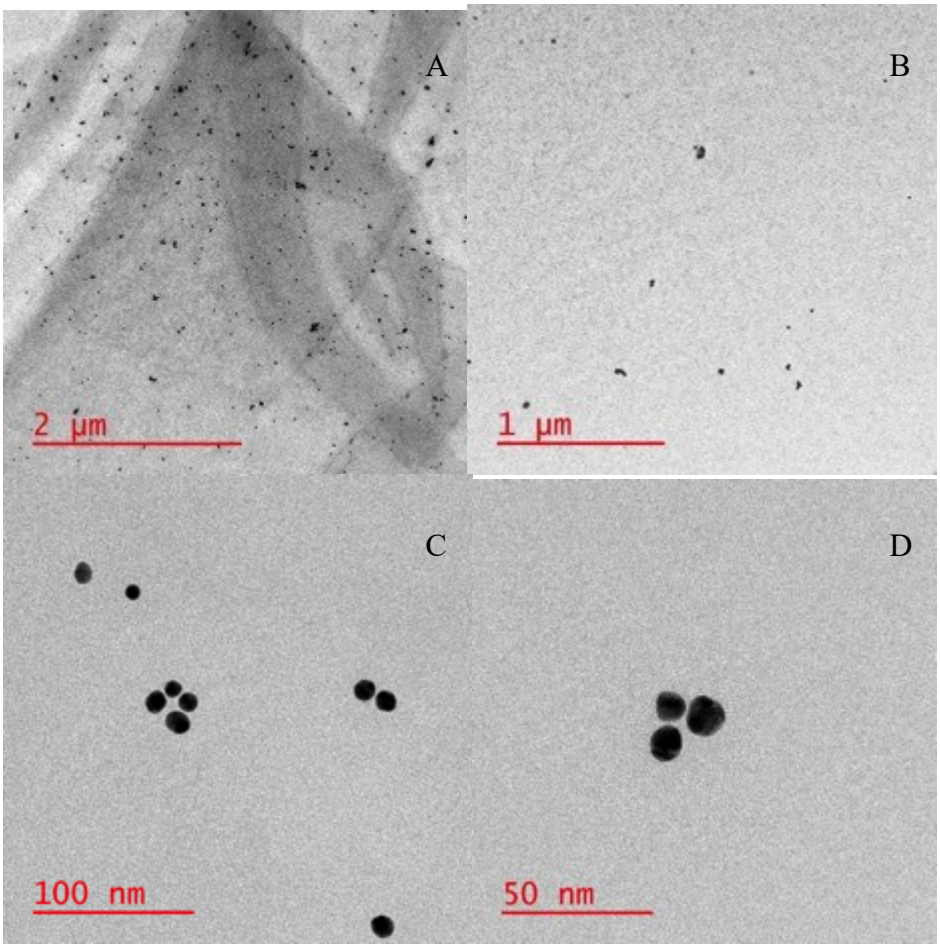

Figure 2.8 TEM images of AuNPs in the supernatant solution after centrifuging the AuNP sample for 30 mins at 13,000 g with various scale bars (A) 2 µm, (B) 1 µm, (C) 100 nm and (D) 50 nm.

2.3.3 Determination of AuNP capacity for ssDNA aptamers

To use AuNPs as a platform for small molecule SELEX, the capacity of AuNPs for a DNA aptamer library must be assessed. If a large volume of AuNPs is required to adsorb the majority of a standard ssDNA aptamer SELEX library, AuNP SELEX would be difficult to manipulate (*e.g.,* requiring large volumes/ numbers of PCR reactions, etc). As a first step, 1.12.2[84] (an aptamer for ochratoxin A)[85–87] was used as a model to measure the capacity of the AuNP surface to adsorb a DNA library for SELEX.

Typically, the DNA library during SELEX ranges between 10-1000 pmol. Therefore, a constant amount of AuNPs (2.5 pmol, 12 nM) was added to various amounts of fluorescein labeled 1.12.2 aptamer (10-1000 pmol). The supernatant solution containing the non-binding 1.12.2 was removed and collected after centrifugation. The concentration of 1.12.2 was compared to the control sample to determine the percentage of aptamer adsorbed onto the AuNP surface. The calculated adsorbed values were plotted against the original amount of 1.12.2 aptamer added (Figure 2.9).

Interestingly, the ideal amount of 1.12.2 for a constant amount of AuNPs was found to be 100 pmol (Figure 2.9). At this amount, the ratio of DNA aptamer to AuNPs was the ideal 40:1 (final assay concentration) used in the AuNP bioassay.

Figure 2.9 describes the percentage of 1.12.2 in comparison to a control sample. Therefore, to better illustrate the results, Figure 2.10 displays the absolute amount of 1.12.2 adsorbed with respect to amount of 1.12.2 added. Given that the amount of 1.12.2 detected is in the sub nanomolar range, the large standard deviation between the three trials is acceptable. This analysis suggests that the surface of AuNPs (2.5 pmol) is saturated with adsorbed 1.12.2 aptamer upon addition of approximately 100 pmol 1.12.2 aptamer.

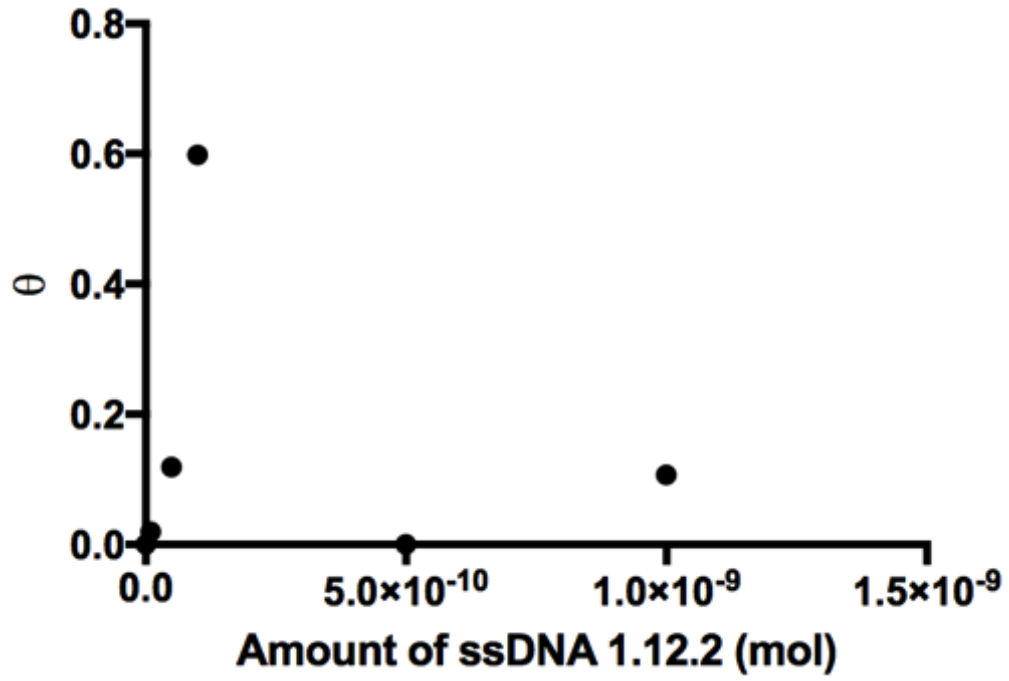

Figure 2.9 Percent of ssDNA adsorbed (θ) with respect to amount of ssDNA added (mol) determined by a Hill slope equation for the sequence 1.12.2

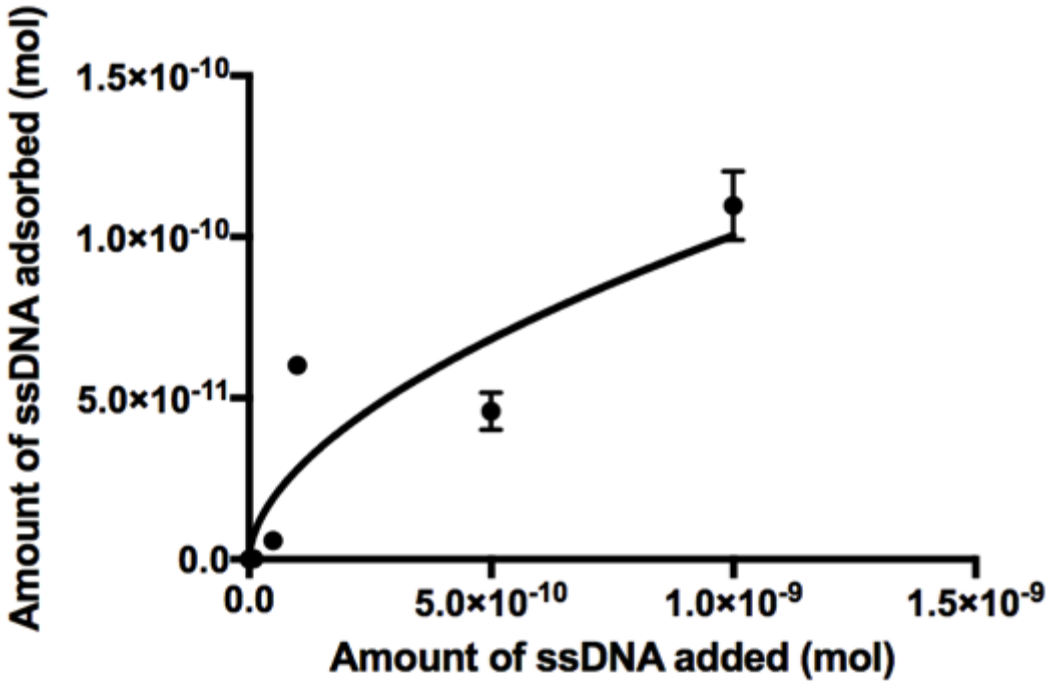

Figure 2.10 Percent of ssDNA adsorbed (mol) with respect to the amount of ssDNA added (mol) for sequence 1.12.2

To further confirm the adsorption of 1.12.2 to AuNPs at a 40:1 (final assay concentration ratio) of DNA aptamer to AuNPs we repeated the experiment with 100 pmol of 1.12.2, performing several replicates. The data supports that at this ratio, almost all of the DNA aptamer (1.12.2) was adsorbed onto the surface of AuNPs. The percent difference between the test and control samples was approximately 94.5 ± 1.7 % (Figure 2.11). It is suggested that this amount of AuNPs is 'at capacity' or saturated at approximately 100 pmol of 1.12.2 DNA aptamer.

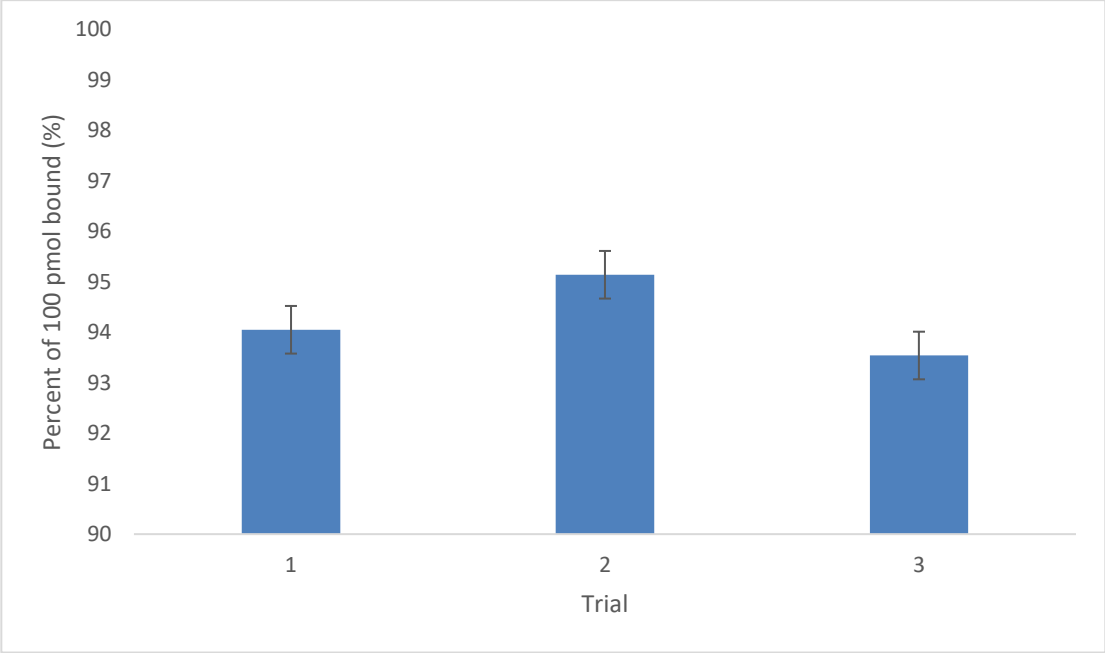

Figure 2.11 Percent of ssDNA adsorbed when 100 pmol of 1.12.2 was added to 2.5 pmol of AuNPs

We next compared our results to previous AuNP binding with a 44 base length sequence. To do this, the percent of DNA on the surface of the AuNPs was estimated against a control sample for a range of concentrations (10, 40, 70 and 100 pmol). Figure 2.12 clearly shows a larger difference in the amount of 1.12.2 adsorbed with an increase in the amount of DNA added. One drawback of this analysis is that the increase in

percent difference is partially due to the fact that there is bias between the detectable difference in fluorescence at various concentration of 5'-fluorscein-labelled aptamer. However, the Langmuir binding isotherm was modelled (Figure 2.12), and the K of adsorption was found to be 0.060 ± 0.014 nM^{-1}. This value is in agreement with previously determined adsorption K of 0.033 ± 0.004 nM^{-1} for a 44 base length sequence, with a slight variation being attributed to a difference in the ssDNA sequence and length.[79] In combination with our previously estimated isoterms over a wider range of 1.12.2 concentrations (10- 1000 pmol), it was suggested that a saturation of adsorption occurred at approximately 100 pmol or a 40:1 ratio.

Although this analysis can not provide an absolute capacity due to the high degree of error observed with this method of analysis, it was found reasonable that 100 pmol of DNA aptamer be used in a 40:1 ratio (DNA: AuNP) for further analysis. With this considered, for citrate capped AuNPs separated by centriguation it is estimated that 100 pmol (100 μL at 10 μM) can be absorbed onto 2.5 pmol of AuNPs (210 μL at 11 nM). If an initial SELEX library was comprised of approximately 1000 pmol of DNA, the required amount of AuNPs at 11 nM would be roughly 25 pmol or 2.3 mL. This volume is both reasonable and practical to be used as a small molecule SELEX platform. Although this method only provides an approximation, studying the capcity of citrate capped AuNPs for 1.12.2 in this way has assessed AuNP as a novel platform for small molecule SELEX.

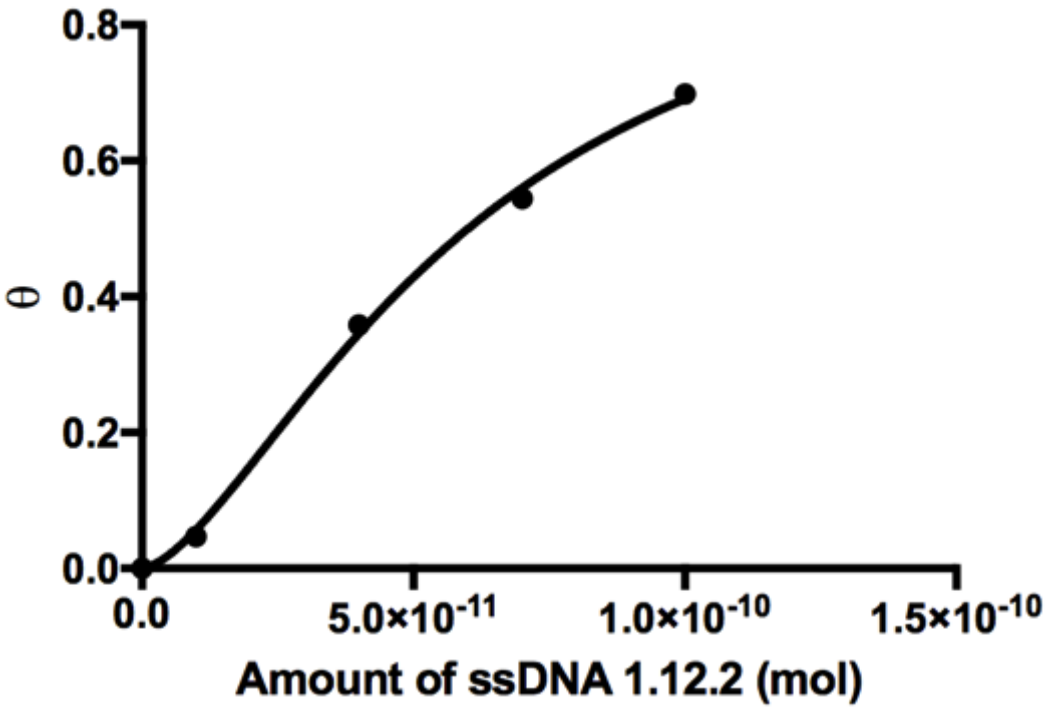

Figure 2.12 Percent of ssDNA adsorbed (θ) with respect to amount of ssDNA added (mol) determined by a Hill slope equation for the sequence 1.12.2

2.3.4 Investigating AuNP-aptamer interactions for SELEX conditions

2.3.4.1 Effects of aptamer structure and length on AuNP-aptamer interactions

We next examined the possible bias between structure and length for adsorption. If there is a difference in adsorption dependent on the sequence, desorption of sequences for a target molecule could be biased. To test this, aptamers of various lengths and structures were adsorbed to AuNPs and analyzed. A08m and H12 are two aptamers previously selected for the small molecule mycotoxin, OTA.[88,89] A08m is approximately half the length compared to H12, and the sequences are predicted to have different secondary structures based on DNAse analysis.[90,91] These sequences also yield different qualitative binding results with the AuNP bioassay.[50] The sequences were introduced

competitively to a known amount of AuNPs, removed, then separated and analyzed by PAGE. Figure 2.13 displays a representative gel of the control DNA sample of A08m and H12 in a 1:1 ratio and the DNA in the supernatant after separation. The intensity of the bands were then calculated and compared against a control sample. For A08m and H12, no measurable difference in adsorption was found (Figure 2.14). Within error, approximately 80% (81.9 ± 5.38 % for A08m and 82.2 ± 5.28 % for H12) of each sequence originally added was found to adsorb to AuNPs (Figure 2.14). There did not appear to be any preference for one aptamer length or structure over the other. Hypothetically, there may be a difference in adsorption with respect to length as the number of bases in the DNA sequence could influence adsorption kinetics.[79–81] However, our results suggest that there is no significant difference in the amount of adsorption relative to length or structure of the DNA sequence.

To confirm the generality of our results, another aptamer was tested. FB139 is an aptamer previously selected for another small molecule mycotoxin, Fumonisin B1 (FB1).[19,49] This sequence is approximately 3 times the length compared to A08m. Using the same method, there was no consistent or significant difference in the amount of adsorption between these two sequences (Figure 2.15). Again, approximately 80% (81.5 ± 5.93 % for A08m and 83.0 ± 5.04 % for FB139) of each sequence was found to be missing from the supernatant, and was assumed to be adsorbed to the AuNP surface (Figure 2.15).

Incubation time and centrifugation could all create bias in the developed assay. The longer sequences could have a stronger interaction with the surface of the AuNPs; however, the adsorption kinetic may be influences by the increased number of DNA

bases. The difference in length could promote the binding of longer sequences over shorter sequences as separation is achieved by centrifugation. These concerns are addressed in detail and tested experimentally in Section 2.3.4.2..

2.3.4.2 Non-specific removal of ssDNA aptamers from AuNP surface

To investigate the reliability of this assay as a partitioning method for SELEX, a proof–of-concept SELEX experiment was performed. In this experiment, two sequences were allowed to incubate with AuNPs at room temperature for 30 minutes. At this point, the solution was centrifuged to pellet the AuNPs, hypothetically containing the adsorbed ssDNA sequences. The supernatant solution was then removed and collected to estimate the amount of DNA sequences that did not adsorb onto the AuNP surface. This process would hypothetically leave only the aptamer sequences that originally adsorbed to the AuNP surface in solution. If a small molecule target (OTA) were introduced in solution, the aptamer sequences that preferentially bind the OTA would leave the AuNP surface. Centrifugation could again be used to pellet the AuNPs out of solution and allow separation of aptamers that remain on the AuNP surface from target-aptamer complexes.

First, two aptamer sequences (A08m and H12) that were both selected for the same target molecule (OTA) were compared.[88,89] Previous work indicated that H12 protects the AuNPs from salt aggregation regardless of target concentration; therefore, it is presumed that the aptamer fails to leave the nanoparticle surface.[50] Considering this, it is expected that A08m will leave the AuNP surface more readily than H12 resulting in a higher concentration of A08m in the supernatant. Figure 2.14 shows that in our experiments, this was not the case, and the amount of A08m and H12 in the supernatant was approximately equal. The amount of A08m removed from the AuNP surface when

OTA was introduced was estimated to be 4.05 ± 1.18 % and, the amount of H12 was approximately 4.51 ± 1.36 % (Figure 2.14).

Next, we tested aptamers to two different targets: A08m and FB139.[19,89] Hypothetically, since FB139 has no affinity for OTA, A08m should be removed more readily when OTA is introduced. The results did not support our hypothesis and the amount of A08m was relatively equal to FB139 when OTA was added (Figure 2.15). Using PAGE analysis, the amount of A08m and FB139 was found to be approximately 4.39 ± 2.40 % and 4.46 ± 2.35 %, respectively. These results where in agreement with the previous findings for A08m and H12. However, the non-specific removal of FB139 with OTA was concerning and prompted analysis of the proposed centrifugation separation method.

We next tested performed a negative control experiment. Warfarin is a small molecule that is similar in structure to OTA, but does not bind to the aptamer and thus is commonly employed as a negative control.[84] Again, aptamer A08m and H12 as well as A08m and FB139 were tested in the same, previously described, assay. Alarmingly, the amount of each sequence removed with OTA was comparable with the amount of each sequence removed with negative control (warfarin) and with a blank (water). When A08m and H12 were subjected to a water blank sample approximately 9.49 ± 0.36 % and 7.41 ± 1.97 % were found in the supernatant, respectively. Similarly, when A08m and FB139 were subjected to a water blank sample approximately 8.89 ± 0.33 % of A08m and 8.92 ± 0.67 % of FB139 were removed into solution. When A08m and H12 were introduced to warfarin in solution, approximately 8.17 ± 0.36 % of A08m and 6.27 ± 3.01 % of H12 were found in the supernatant. Likewise, approximately 9.99 ± 2.06 % of

A08m and 8.86 ± 1.83 % of FB139 were estimated to be removed form the AuNP surface with warfarin. This suggests that the sequences appeared to be removed non-specifically. While analysis by PAGE results in a relatively high margin of error; the findings suggest that centrifugation as a separation method may be playing a role in the unexpected results.

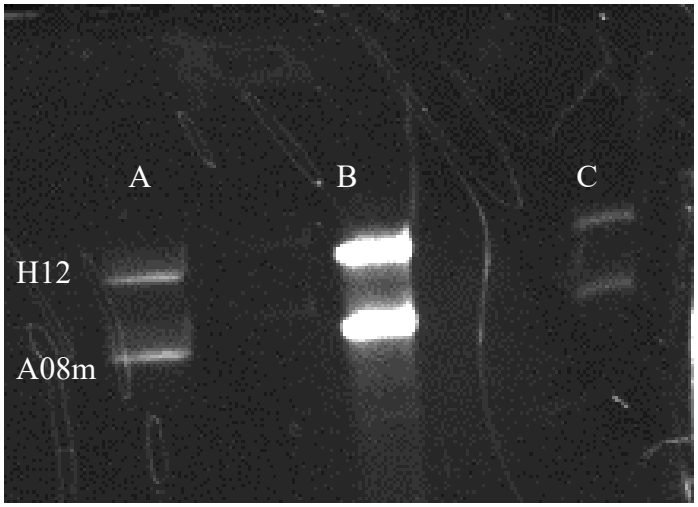

Figure 2.13 Representative image of PAGE gel analysis. 10% control of A08m and H12 (A), amount of A08m and H12 not adsorbed (B) and amount of A08m and H12 removed with the target molecule, OTA (C).

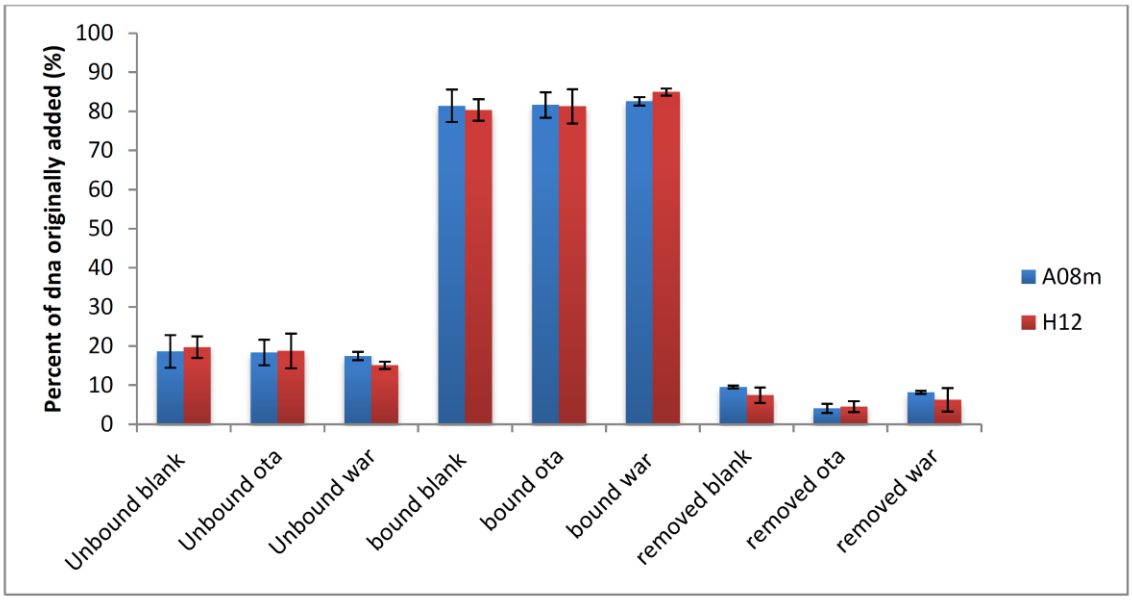

Figure 2.14 Analysis of A08m and H12 adsorbed onto AuNPs and removed with target (OTA), a negative control (warfarin) and a blank (water). The amount of ssDNA for each sequence is represented as a percentage of the total amount of each sequence originally added

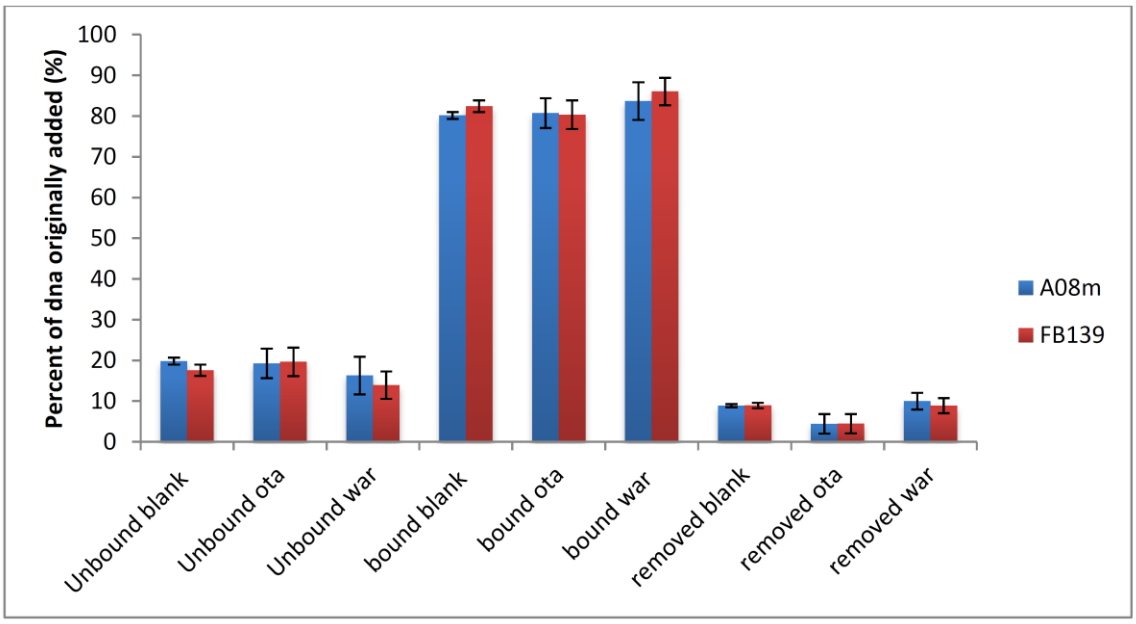

Figure 2.15 Analysis of A08m and FB139 adsorbed on AuNPs and removed with target (OTA), a negative control (warfarin) and a blank (water). The amount of ssDNA for each sequence is represented as a percentage of the total amount of each sequence originally added

2.3.5 Challenges with centrifugation as a separation technique for SELEX

We next examined the effects of centrifugation on the non-covalent interaction between AuNPs and ssDNA. First, the interactions between AuNPs and A08m after experiencing various speeds of centrifugation were investigated. In this experiment, the same concentration of AuNPs (210 μL, 11 nM) and A08m (100 μL, 10 μM) were added to each tube. After incubation, the tube was centrifuged at the appropriate speed (between 5,000 and 12,000 g). The addition of 0.25 M NaCl resulted in salt induced aggregation of the AuNPs regardless of speed. It was suggested that there was an increase in aggregation proportional to increasing speed. Although a slight variation in the degree of aggregation, even the sample that experienced the lowest speed (5,000 g) aggregated with the addition of salt. The previous section determined the highest speed (12,000 g) was required for separation and even at a speed of 13,000 g a small percentage of AuNPs remained in solution. Salt induced aggregation following centrifugation suggested that the force of the centrifuge used to separate AuNPs from solution affected the non-covalent interactions between ssDNA aptamers and AuNPs (Figure 2.16).

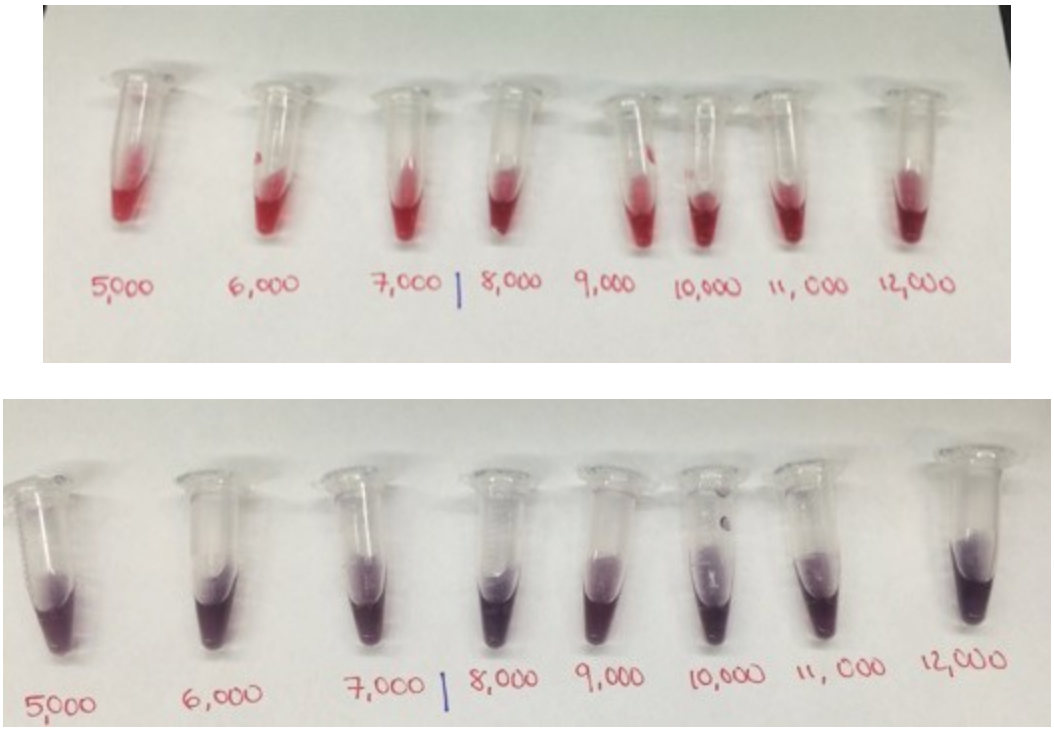

Figure 2.16 Image of AuNP-A08m sample after centrifugation for 30 mins at various centrifuge speeds (5,000- 12,000 g). The pelleted AuNPs were re-suspended in solution (top) and a solution of 0.25 M NaCl was introduced to test salt-induced AuNP aggregation (bottom).

The difference in aptamer adsorption with and without centrifugation (12,000 g) was analyzed using aptamers at various lengths: 1.12.2 (36 nts), Dop (58 nts) and FB139 (96 nts).[19,84,92] Each aptamer was incubated with AuNPs at room temperature for 30 minutes. Following this incubation, half of the samples for each sequence (three trials) were centrifuged at 12,000 g for 30 minutes. The other half of the prepared samples for each sequence (three trials) was left un-centrifuged for 30 minutes. Control samples, of AuNPs without DNA were prepared for comparison. It is reported that the adsorption of ssDNA can protect nanoparticles from salt induced aggregation. Based on this assumption, salt induced aggregation can infer if the aptamers in solution are adsorbed to the surface of the AuNP or not.

A picture of the samples was taken before and after the addition of NaCl (Figure 2.17) and the UV-Vis absorption spectra for each sample were obtained via a Cary 300 Bio UV-Vis Spectrometer (Figure 2.18). Here, only the shortest aptamer sequence (1.12.2) differed in salt induced aggregation after centrifugation for 30 minutes at 12,000 g. Although Dop and FB139 samples did not experience these same effects, this is a notable bias between aptamer lengths when using centrifugation as a separation method. It was also observed that the control without any ssDNA was extremely aggregated after this centrifugation speed (Figure 2.17). This aggregation was so extensive, that this sample could not be analyzed by UV-Vis spectrometry.

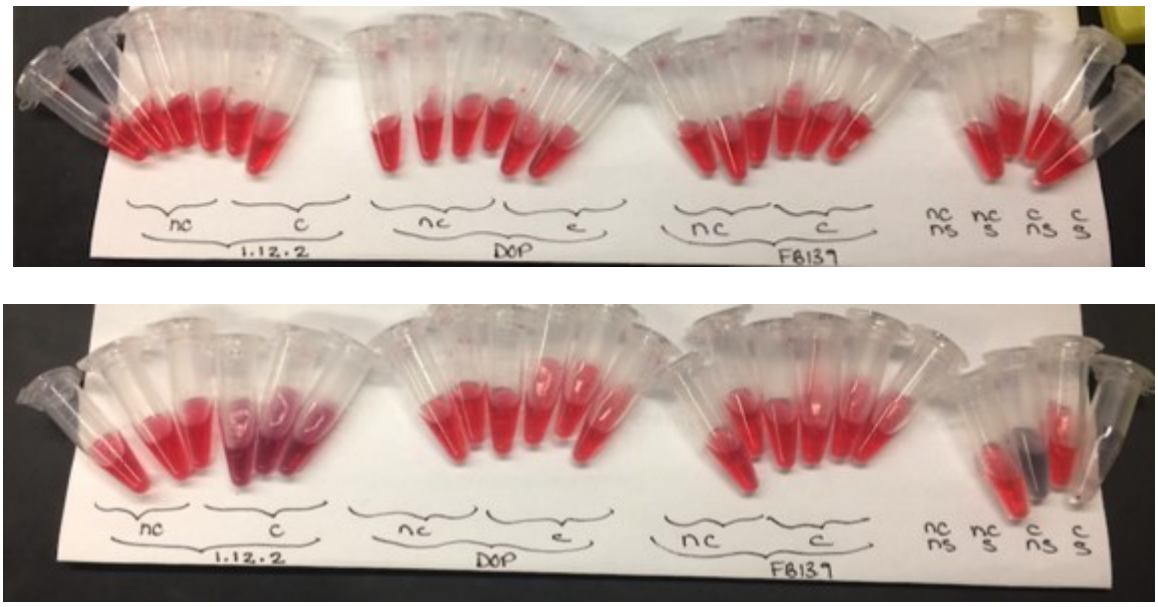

Figure 2.17 Image of AuNP-ssDNA sample with and without centrifugation for 30 mins at 14,000 g. Various lengths of aptamer sequences were tested: 1.12.2 (36 bases), Dop (57 bases) and FB139 (96 bases. The pelleted AuNPs of the centrifuged samples were re-suspended in solution (top) and a solution of 0.25 M NaCl was introduced to test a difference in salt-induced AuNP aggregation (bottom).

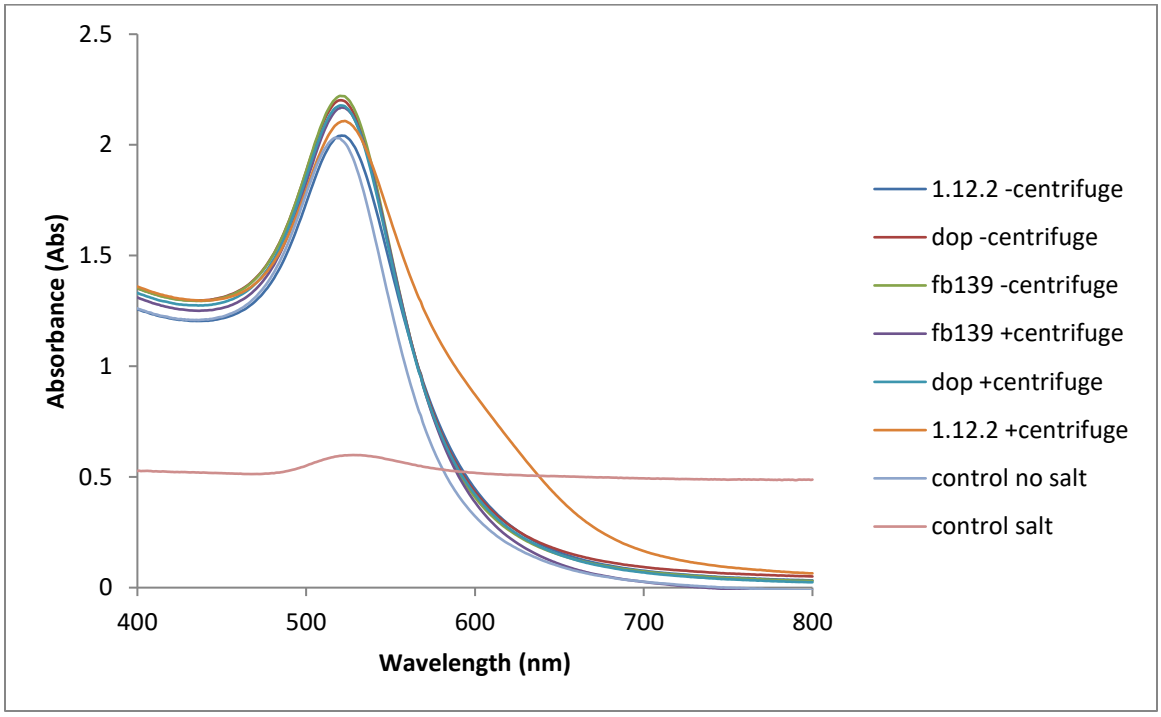

Figure 2.18 UV-Vis spectroscopy analysis of the salt-induced AuNP aggregation study previously described (Figure 2.16).

Finally, salt induced aggregation was applied after the addition of target to investigate if there was adsorbed aptamer on the surface of the AuNPs at this stage. Previous results suggested that approximately 80% of the ssDNA aptamer added is adsorbed onto the surface of the AuNPs and that between approximately 4- 10% of the ssDNA originally added is removed non-specifically with target (section 2.3.4.2); therefore some of the adsorbed aptamer must remain on the surface of the AuNPs. Although the samples aggregated more than expected, no one sample appeared to aggregate more than the other (Figure 2.19).

This supports that through the centrifugation assay, ssDNA aptamers are removed from the surface of AuNPs non-specifically for warfarin and water. In addition, the

results of the salt aggregation assay do not agree with previous PAGE analysis. PAGE analysis predicted that after the addition of target, approximately 75% of the original ssDNA aptamer originally added remains on the surface of the AuNPs. However, with the high degree of salt induced aggregation of the AuNPs at this stage, it is unlikely that 75% of aptamer remains on the surface. The force of centrifugation required to pellet the AuNPs out of solution may affect the non-covalent interactions between ssDNA aptamers and AuNPs. Thus, while there is some degree of error associated with every separation method, centrifugation is likely not viable for AuNP-based SELEX.

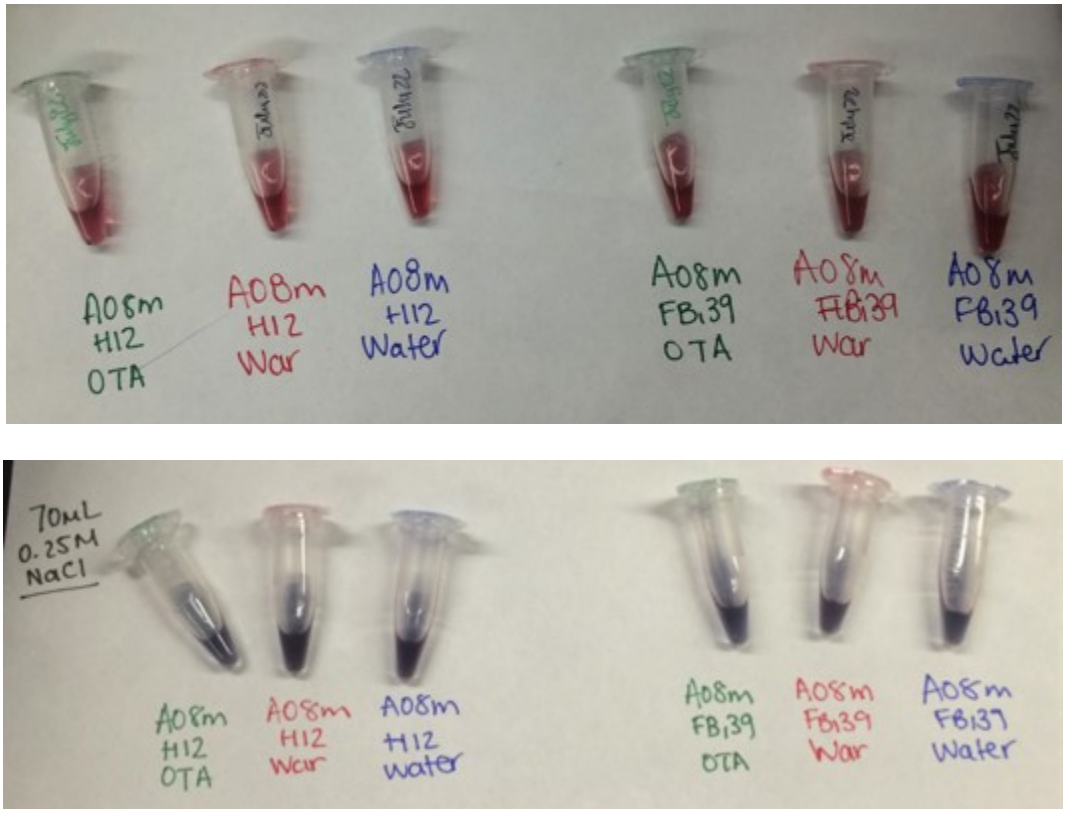

Figure 2.19 Image of AuNP-A08m sample after target incubation and centrifugation for 30 mins at 14,000g. The target (OTA), a negative control (warfarin) and a blank sample (water) were tested. The pelleted AuNPs were re-suspended in solution (top) and a solution of 0.25 M NaCl was introduced to test salt-induced AuNP aggregation (bottom).

2.3.6 The impact of aptamer modifications on the efficacy of the AuNP bioassay

To investigate if aptamer modifications influence the interaction between ssDNA and AuNPs, various 5' chemical modifications were tested with AuNP bioassay. First, unmodified A08m was compared to A08m modified with fluorescein (A08mF) or with biotin (A08mB). A08m modified with biotin appeared to protect the AuNPs more readily than the other analyzed A08m sequences (Figure 2.20). Considering the chemical structure of biotin, this is likely attributed to the strong interaction between sulfur and gold.

Next, the AuNP bioassay results before and after separation of AuNP by centrifugation were compared. Figure 2.20 displays the difference in salt-induced AuNP aggregation for A08mF and A08mB before and after centrifugation. The centrifuged samples were re-dispersed in solution and a 0.25 M NaCl solution was added to each tube. Not only did this study support previous findings that suggested there a difference in salt induced aggregation between A08mF and A08mB, but this experiments suggests that centrifugation influences the interaction between A08m(F/B) and the AuNPs. Both modified A08m sequences appear to be affected by separation with centrifugation. Although preliminary and specific for the A08m sequence, these results indicate that the aptamer modification required for future applications should be involved during a AuNP based SELEX process.

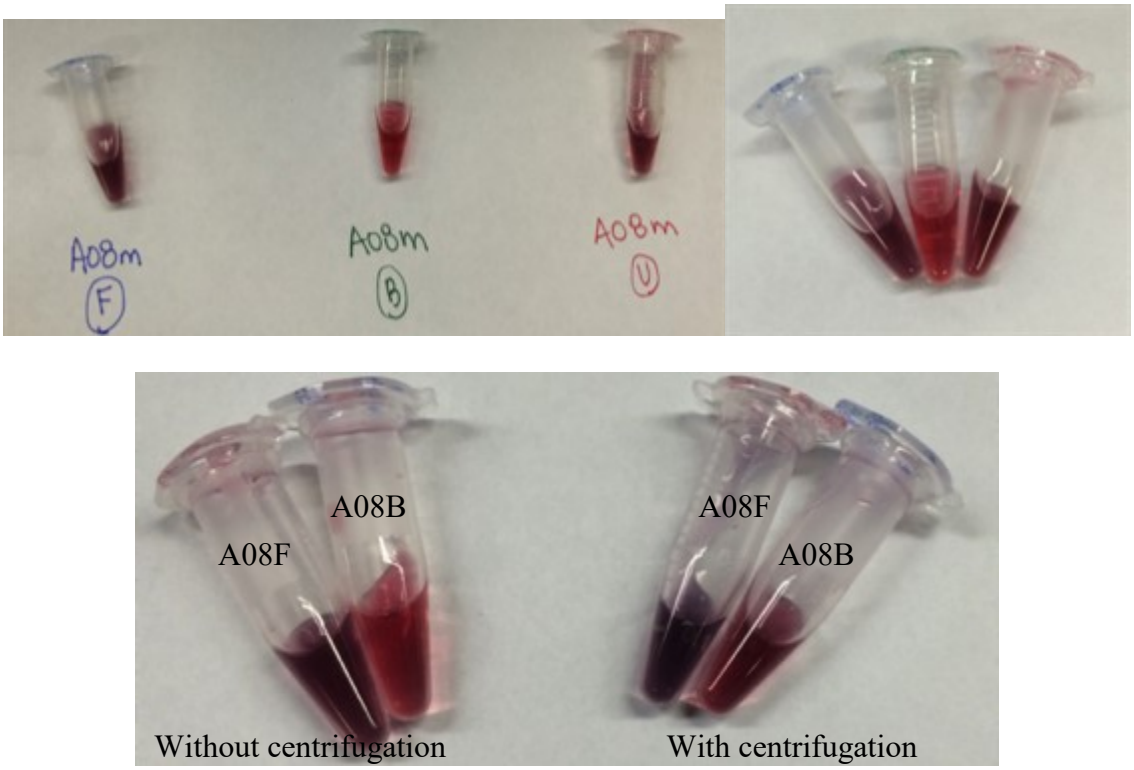

Figure 2.20 Image of AuNP-A08m samples. Various aptamer modification were tested, biotin labeled (B), fluorescein labeled (F) and the unmodified sequence (U). The various modified A08m sequences were tested through the salt- induced aggregation assay without centrifugation (top). A08F and A08B were compared with (right) and without (left) centrifugation of the AuNPs at 14,0000 g for 30 mins (bottom).

2.4 Conclusions

This chapter aimed to find a reliable separation method to act as a partitioning technique for a potential AuNP-based SELEX. Both filtration and gel electrophoresis presented a number of limitations. For example, due to the membrane matrix, available filtering systems, and the size of the AuNPs, filtration was not suitable. Similarly, the difference in size was not sufficient to achieve separation of ssDNA and ssDNA-AuNP conjugates via gel electrophoresis.

Centrifugation was the most promising of the investigated techniques. This method was able to estimate a capacity of citrate capped AuNPs for a 36 base DNA aptamer. Although ssDNA adsorption was apparent and the capacity of a DNA aptamer could be determined, the ability to remove ssDNA aptamers selectively for a specific small molecule target was a challenge. The amount of aptamer removed from the AuNP surface for a specific target was not significantly more than the amount removed for a water blank or negative control, suggesting that centrifugation as a separation technique results in the non-specific removal of aptamers from the gold nanoparticle surface.

The colourimetric properties of the salt induced aggregation assay helped to assess the effects of the centrifuge on the interactions between ssDNA and AuNPs. The centrifugal force required to pellet the AuNPs out of solution, was found to negatively influence this interaction. More specifically, salt induced aggregation results suggested that the effect of the centrifuge during separation was related to the length of the sequence. Through centrifugation and salt-induced aggregation, this work supports the idea that longer DNA sequences are not removed from the AuNP surface as easily as shorter DNA sequences. Most importantly, the lack of specificity with centrifugation makes it unsuitable as a partitioning method for SELEX. This warranted the development of a novel core-shell nanoparticle platform for a quick, more gentle separation method (Chapter 3).

2.5 Acknowledgements

I would like to thank Maureen McKeague for her assistance in designing and optimizing these preliminary centrifugation assay conditions for AuNP-based SELEX.

Chapter 3: Preparation and optimization of core-shell gold coated magnetic nanoparticles (Fe_3O_4-AuNPs) for biosensing assays

3.1 Introduction

3.1.1 Magnetic particles as a partitioning method

For decades, magnetic-based separation has been one of the most widely applied and versatile methods for partitioning samples in the field of biotechnology. However, magnetic-based separation applied to the field of bionanotechnology is relatively unexplored, having only gained recent popularity with the growth in nanotechnology.[93] Many common separation methods rely upon the difference in size, mass, or binding affinity of a sample. However, magnetic separation can be more useful and reliable due to the non-magnetic nature of most biomolecules.[93] Furthermore, the quick and gentle nature of magnetic separation provides a number of advantages over other separation techniques such as centrifugation, filtration, or chromatography.

Magnetic particles in particular are attracting attention for use in biotechnology because of their versatility: they can be functionalized with various ligands[93–95] (amines, carboxyls, etc) or coated with different materials[96,97] (silica, cobalt, gold, etc). For example, a magnetic bead assay was developed to facilitate measuring the binding affinity of aptamers to small molecules.[89,98] In this assay, the small molecule target is covalently immobilized to a magnetic bead. When the aptamer is introduced in solution, the aptamer sequences that bind to the target molecule on the magnetic bead can be separated from the non-binding aptamers when the magnetic beads are captured from

solution (Figure 3.1). Using magnetic beads with a highly crossed linked coating additionally reduces non-specific binding with the partitioning surface, thus providing a more accurate measurement of aptamer affinity.[1]

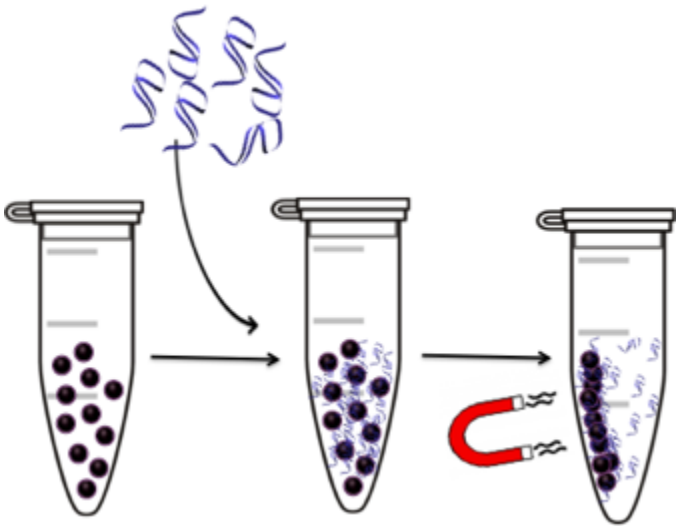

Figure 3.1 Illustration of core-shell gold-coated magnetic nanoparticles (Fe_3O_4-AuNPs) as a partitioning method for small molecule SELEX. ssDNA (blue ribbon) adsorbed onto the surface of the AuNPs (purple spheres) can be separated from non-binding sequences that remain in the supernatant solution.

To achieve separation on biomolecules, magnetic nanoparticles must be drawn towards a magnetic source, ultimately allowing the particles to be removed from solution. To achieve this, the applied magnetic force (F_m) must be greater than the particle diffusion and other combined forces (including gravitational, inertial, viscous and buoyancy). This can be described in the equation for the magnetic force (F_m) exerted on a particle:

$$F_m = \frac{V_p \Delta x}{\mu_0} (B.\nabla)\, B \qquad \textbf{Equation 10}$$

where V_p is the volume of the particle (m^3), Δx is the difference between the magnetic susceptibility of the particle and the medium, μ_0 is the permeability of vacuum and B is the applied magnetic field (T).

From the equation, it is clear that several properties can be tuned to achieve successful magnetic separation. For example, the size and magnetisability of the nanoparticles determines the magnetic strength required to successfully capture the magnetic nanoparticles from solution. In addition, the viscous force exerted on the nanoparticles is influenced by concentration and the solubility of the particles or associated capping agent on the surface of the particle in solution.[93]

3.1.2 Core-shell nanoparticles

A nanoparticle of one material (inner core) can be coated with another material (outer shell) to form a nanoparticle with a core-shell structure consisting of two different materials. This system is advantageous as it provides a single nanoparticle with multiple functions and overall increased functionality of the system. For example, an otherwise non-magnetic material such as gold, cobalt or silica could be combined with iron oxide in a core-shell model, to obtain magnetic properties.[97] Due to the multi-functionality of these nanostructures, core-shell nanoparticles are growing in popularity for a wide range of applications including biomedical[99,100] and pharmaceutical[101] applications, catalysis[52,102], electronics[103,104] and enhancing photoluminescence[105–107]. From a more specific standpoint, biotechnology has benefited from the use of core-shell nanoparticles in drug delivery and release[100,108,109], bioimaging[100,110,111], and biosensing[112,113]. As an

example, coating otherwise toxic nanoparticles with a biocompatible material facilitates biocompatibility and *in vivo* applications.[114]

An important feature of the core shell nanoparticle structure is that the chemical or physical properties of a nanoparticle surface can be altered without losing the properties provided by the core material.[115] For instance, porous silica has been used to control drug delivery, while magnetic iron oxide cores have been used for imaging.[116] However, the interface of the core and shell also influences the chemical and physical properties.[117,118] Thus, the final properties of the core-shell nanoparticle must be carefully characterized and considered based on the application on interest.

Core-shell nanoparticles may differ in size, shape, thickness, surface morphology, and materials. They also may differ by their coverage. Some examples include spherical, hexagonal, multiple small core, movable core and nanomatryushka. However, the complete covering of a spherical nanoparticle with another material, known as concentric spherical, is currently the most common form of core-shell nanoparticles. In terms of materials, core-shell nanoparticles can be divided into the following categories: inorganic/inorganic, organic/organic, inorganic/organic or organic/inorganic. Among the various types of core shell nanoparticles, inorganic/inorganic core-shell nanoparticles are the most commonly studied.[97]

The resulting size and coating of the core shell nanoparticle is very important to control for particular application. For example, size is inversely proportional to specific surface area and the energy gap between the valence and conductance bands. Therefore, a smaller nanoparticle can provide greater optical and quantum mechanical properties through an increase in the nanoparticle's specific surface area and energy band gap.[97,119]

Furthermore, *in vivo* applications such as bioimaging and drug delivery require a core-shell nanoparticle that is less than 50-100 nm in size. This is because small nanoparticles (<50 nm) are able to accumulate in tumors, which is a primary *in vivo* bioimaging application of core shell magnetic nanoparticles.[97,120] While synthesis of inorganic core shell nanoparticles can be achieved using a variety of chemical methods such as reduction[121,122], hydrolysis[121,122], microemulsion[123], thermal (solvo or hydro)[124–126], and precipitation[127,128], unfortunately, synthesizing small core-shell nanoparticles with a uniform coating and size distribution is challenging.[97] A number of parameters have been reported to control the size and coating of core-shell nanoparticles. Among these, temperature in the presence of core surface modification is commonly used to control the reaction kinetics during core-shell nanoparticle synthesis.[97] For example, Xuan et al. showed that a low temperature is generally used to achieve a uniform shell coating when the core nanoparticle surface is modified.[125]

3.1.2.1 Core-shell gold-coated magnetic nanoparticles (Fe_3O_4-AuNPs)

There are several chemical and physical properties that currently limit the potential of magnetic nanoparticles in certain applications. First, magnetic nanoparticles have relatively low electrical conductivity and poor optical properties.[129,130] Second, magnetic nanoparticle have a large surface area to volume ratio and a low surface charge (at neutral pH). As a result, they are unstable and often aggregate in solution.[130,131] Finally, these particles are not easily functionalized due to their restricted compatibility with a number of surface chemistry modifications. Which limits the stability of magnetic nanoparticles in solution and their use in biosensor applications.[130,132]

Using core-shell nanoparticles can resolve these aforementioned limitations, without losing the magnetic properties of the nanoparticle. For example, if a magnetic nanoparticle (core) is coated (shell) with a noble metal such as Au, the magnetic properties should be maintained. However, the core-shell nanoparticle surface also exhibits the chemical and physical surface properties associated with gold. This enhances the nanoparticle biocompatibility[133,134], bioaffinity[135], optical properties[136], chemical stability[137], and conductivity[130,138]. This has resulted in the use of core-shell gold coated magnetic nanoparticles in a variety of applications; including bioseparation[134], electrochemical sensors[139], bioimaging[140] and targeted delivery[130,141].

There are a number of reported methods for the synthesis of core shell Fe_3O_4-AuNPs including hydroxylamine seeding[135], reverse micelle[142], ϒ-ray radiation[143], laser ablation[144], sonochemical[145] and wet chemical reactions[146], layer-by-layer electrostatic deposition[147], and photochemical reduction[148,149]. However, many of these methods produce large core-shell particles (approximately 60 nm) or involve pre-formed AuNPs as a precursor in the reaction.[149] More recently, the sequential formation of Fe_3O_4 core and Au shell has been documented to successfully produce monodispersed, well-defined core-shell Fe_3O_4-AuNPs with an average size of 5-15 nm (and Au coating of 0.5- 2.0 nm).[124]

3.1.2.1.1 Synthesis of Fe_3O_4 by solvothermal methods

First, magnetic nanoparticles must be synthesized as the core material. Commonly, magnetic nanoparticles are synthesized using solvothermal methods. Recently, Wang et al. reduced $Fe(acac)_3$ with 1,2- hexadecanediol in the presence of two

capping agents, oleic acid and oleylamine to produce Fe_3O_4 seeds.[124] While several other methods have been reported, the thermal deposition of $Fe(acac)_3$ in a high temperature boiling organic solvent results in the production of stable, mono-disperse Fe_3O_4 nanoparticles. Furthermore, including oleic acid and oleylamine as capping agents was shown to control the formation, stability, and future coating of Fe_3O_4 nanoparticles.[149] Finally, the synthesis temperature synthesis and the ratio of oleic acid to oleylamine allows the size of Fe_3O_4 nanoparticles to be fine-tuned, permitting the formation of Fe_3O_4 nanoparticles at various sizes. Oleylamine acts as both a capping and reducing agent simultaneously. The combination of oleylamine with other reducing agents has been shown to improve the overall synthesis and uniform formation of Fe_3O_4 nanoparticles at various sizes.[124,149]

3.1.2.1.2 Direct Au coating of Fe_3O_4 nanoparticles

Synthesized magnetic nanoparticles can be coated with Au to form core-shell Fe_3O_4-AuNPs. This simple synthetic process in organic solvent, is found to successfully achieve a thin, uniform coating of gold on pre-synthesized magnetic nanoparticle (< 7nm). When $Au(CH_3COO)_3$ is reduced by 1,2- hexadecanediol, gold is deposited on the surface of the pre-formed Fe_3O_4 nanoparticles. If the surface of Fe_3O_4 nanoparticles is modified with oleylamine and oleic acid, these capping agents must be removed from the surface for gold to be deposited as a shell. The partial desorption of the capping agents from the core nanoparticle relies upon a thermally active process and requires a temperature between 180- 190°C. As this is a thermal process, the reaction temperature significantly affects the success of the core-shell nanoparticle formation. The following

describes the coating process; (A) $Au(CH_3COO)_3$ is reduced by 1,2- hexadecanediol in the presence of oleic acid and oleylamine at a temperature of 180-190°C, (B) thermally active partial desorption of the capping layer occurs, (C) the reduction of $Au(CH_3COO)_3$ results in deposition of Au on the surface of the exposed surface of the magnetic nanoparticles, and (D) the re-encapsulation of the Au shell with oleylamine and oleic acid (Figure 3.2).[124,149]

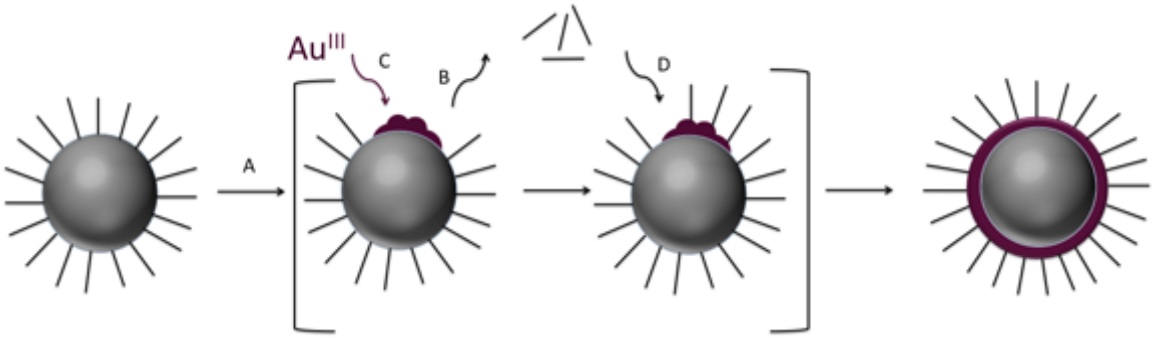

Figure 3.2 Illustration the coating process; (A) $Au(CH_3COO)_3$ is reduced by 1,2- hexadecanediol in the presence of oleic acid and oleylamine at a temperature of 180-190°C, (B) thermally active partial desorption of the capping layer occurs, (C) the reduction of $Au(CH_3COO)_3$ results in deposition of Au on the surface of the exposed surface of the magnetic nanoparticles, and (D) the re-encapsulation of the Au shell with oleylamine and oleic acid

3.1.3 Phase transfer of inorganic nanoparticles

Often, synthesized nanoparticles must be transferred from a non-polar to polar solvent or vice versa to be suitable for the application-of-interest. In particular, some successful reducing and capping agents used for the synthesis of core-shell nanoparticles are organic and non-polar; often this environment is preferred for synthetic ease and success.[124,150] However, biotechnology applications typically require a polar, aqueous solvent, such as water.[2,64,65] Unfortunately, removing a nanoparticle's capping agent

quickly or without replacement can result in aggregation or agglomeration. Similarly, the dispersion of nanoparticles in a solvent unsuited for the current surface modification results in the same loss. Thus, a method to transfer the synthesized nanoparticles from an organic phase to aqueous solution is desired.[151]

Many phase transfer techniques have been reported that alter the solubility of nanoparticles without losing the stability provided by surface modifications. Functionalization[152], ligand exchange[153], and electrostatic interactions[154] are exploited to develop a number of nanoparticle phase transfer methods. It has been reported that transferring synthesized nanoparticles post synthesis, with additional stabilizing agents, is beneficial. Although this requires two separate steps for synthesis and transfer, there is greater control over particle size, shape and dispersity.[151] Maintaining stability while transferring nanoparticles from one phase to another is a challenge. Therefore, understanding and improving these methods is required to expand the versatility of nanoparticle solubility, while preserving the stability of the synthesized nanoparticles.[151]

3.1.3.1 Phase transfer of Fe_3O_4-AuNPs using DMAP

Previously reported ligand exchange methods for the phase transfer of AuNPs from organic solvent to aqueous media and vise versa were limited by reaction time.[155] To address this, Gittins and Caruso reported a rapid ligand exchange phase transfer of AuNPs which utilizes 4-dimethyl(amino)pyridine (DMAP) as a capping and stabilizing agent. In this work, AuNPs previously synthesized and capped with tetraalkyl ammonium salts were effectively transferred into water with the use of DMAP (Figure 3.3). Gittins and co-workers proposed that DMAP crosses the solvent barrier and forms a labile

acceptor-donor complex with the metal surface atoms.[156] It is found that DMAP interacts with the gold nanoparticle surface through the endocyclic nitrogen. This arrangement directs the exocyclic nitrogen outwards, away from the nanoparticle, resulting in a positive surface charge (Figure 3.4). The ligand exchange and subsequent surface charge triggers the transfer of the nanoparticles into the aqueous layer (Figure 3.5).[157]

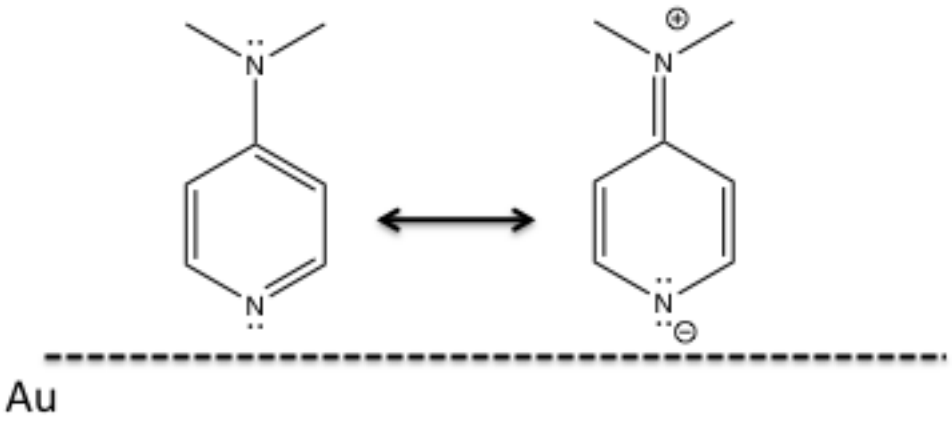

Figure 3.3 Chemical structure and resonance form of 4-di(methylamino)pyridine (DMAP). This figure illustrates the orientation of DMAP on the AuNP surface.

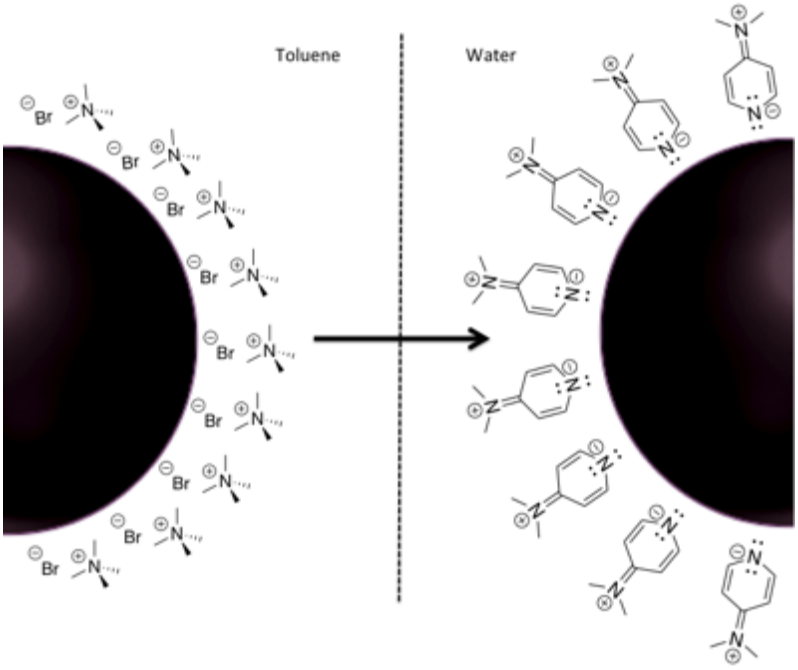

Figure 3.4 Illustration of the reported ligand exchange phase transfer of AuNPs from toluene (capped with tetramethylammonium bromide (TAOB)) using DMAP

Recently, DMAP has been reported to be a versatile ligand for gold nanoparticle stabilization and nanoparticle transfer. When considering replacing oleylamine and oleic acid with DMAP, the bond strength between the ligands and the gold nanoparticle surface must be compared. Adsorption of the endocyclic nitrogen of DMAP, is proposed to displace of the primary amine of oleylamine on the AuNP surface through a ligand exchange. Compared to the primary amine of oleylamine, DMAP creates a stronger bond with the gold atoms on the nanoparticle surface. This is attributed to the charge localization of the DMAP conjugate acid, which raises the energy of the lone pair on the nitrogen atom.[157] The position of the ligand's HOMO and LUMO orbitals in relation to the Fermi level of Au determines the strength of the Au-ligand interaction. This is further explained by the Hard-Soft Acid-Base theory.[158] When metals (including Au) are in a 0

oxidation state, they are considered a soft acid.[159,160] HSAB classifies DMAP as a borderline to soft base, while the primary amine of oleylamine is a relatively hard base. Therefore, a soft base, like DMAP, interacts more strongly with the gold nanoparticle surface in comparison and will likely replace oleylamine via phase transfer.

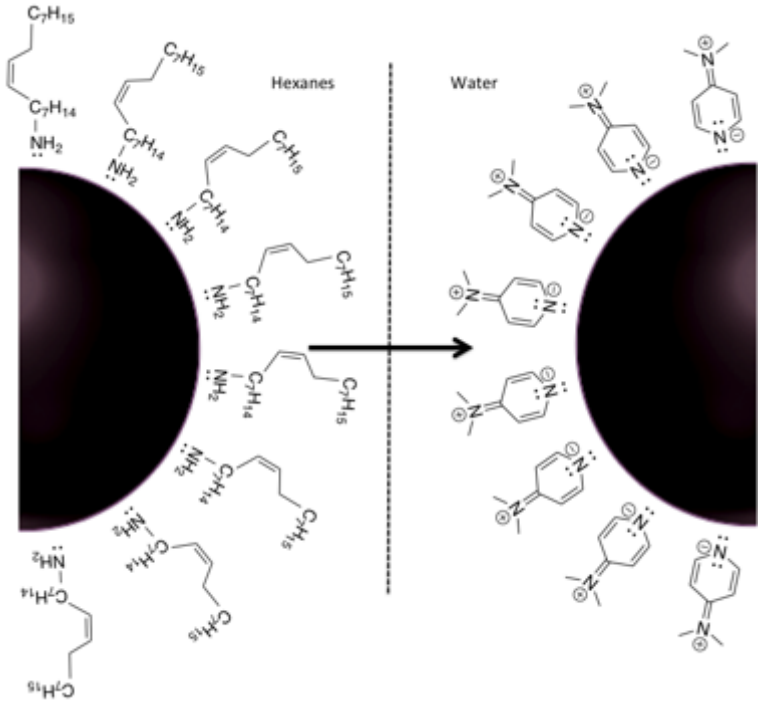

Figure 3.5 Illustration of the purposed ligand exchange phase transfer of AuNPs from hexanes (capped with oleylamine and oleic acid) into aqueous solution using DMAP

3.1.4 Characterization of core-shell nanoparticles

The advancement of nanoparticle synthesis has resulted a need for reliable characterization techniques. There are many methods to characterize nanoparticles. Common examples include high resolution transmission electron microscopy (HRTEM) with Energy-dispersive X-ray spectroscopy (EDS), X-ray diffraction (XRD), and UV-Vis absorption spectroscopy (UV-Vis).[150] Briefly, HRTEM is capable of imaging

nanoparticles by transmitting a high energy beam of electrons through a sample[161], XRD determines the crystallinity of the material based on Bragg's law[162] and UV-Vis determines the SPR absorption of the nanoparticle[163]. Typically, HRTEM is used as it can observe the size, dispersion, and single particle composition, which are particularly important for core-shell species. Furthermore, when the sample is exposed to a high energy electron source through HRTEM, EDS can provide spatially resolved elemental data of the sample by analyzing emitted X-rays.[161] Although HRTEM is the most commonly used technique for core-shell nanoparticle analysis, other characterization techniques such as UV-Vis and XRD are often used to support the HRTEM results.[150]

3.1.5 Chapter objectives

This core-shell Fe_3O_4-AuNP model is attractive as a quick and gentle separation method for our SELEX application. Therefore, the goal of this chapter was to obtain Fe_3O_4-AuNPs and investigate this platform as a possible SELEX partitioning method. The magnetic core allows the position of the nanoparticle in solution to be controlled with an external magnetic field. Simultaneously, the gold shell provides the necessary surface properties and biocompatibility to mimic AuNP-based aptasensors. The size of the formed core-shell Fe_3O_4-AuNPs is important to consider for our SELEX application, as we aim to mimic future testing conditions in which 13-15 nm sized AuNPs are used. In addition, the synthesized Fe_3O_4-AuNP must be monodisperse and stable in solution. We first characterized purchased Fe_3O_4-AuNPs with additional HRTEM and EDS analysis. Our analysis suggested that the purchased nanoparticles were not Fe_3O_4-AuNPs but some variation of two separately formed individual nanoparticles (Fe_3O_4 nanoparticles and

AuNP). Upon determining this irregularity, we investigated previously reported methods to synthesize Fe_3O_4-AuNPs with the necessary properties. The core Fe_3O_4 nanoparticle was prepared in a high temperature boiling organic solvent. Compared to other Fe_3O_4-synthesis methods, this method is found to yield stable, monodisperse Fe_3O_4 nanoparticles.[150] Furthermore, these Fe_3O_4 core nanoparticles are stabilized with a capping agent, which can easily be coated with Au through a thermal process to produce small, uniform core-shell nanoparticles. The synthesized Fe_3O_4-AuNPs were characterized with HRTEM with EDS and UV-Vis absorption spectroscopy. Although this method is reported to successfully synthesize small, uniform Fe_3O_4-AuNPs, our application requires that the nanoparticles be transferred to an aqueous media. Previously reported phase transfers resulted in aggregation and loss of product.[164] This led us to investigate DMAP ligand exchange as a more gentle phase transfer technique.[151,156,157] The transferred DMAP capped Fe_3O_4-AuNPs were validated through HRTEM with EDS, UV-Vis spectroscopy, and solubility tests.

3.2 Experimental

3.2.1 Materials

Iron (III) acetylacetonate ($Fe(acac)_3$), 99%, oleylamine (70%), oleic acid (99%), phenyl ether (99%), anhydrous sodium citrate (99%) , 4-dimethyl(amino)pyridine (99%) and other solvents (hexanes, toluene and absolute ethanol) were purchased from Sigma-Aldrich (Oakville, ON, Canada). 1, 2- hexadecanediol was purchased from VWR (Mississauga, ON, Canada). Gold (III) acetate ($Au(ac)_3$) was purchased from Alpha Aesar (Haverhill, Massachusetts, USA). 300 mesh x 83 μm pitch copper TEM grids were

purchased from Ted Pella (Redding, CA, USA). All glassware used for the Fe_3O_4-AuNP synthesis was washed with aqua regia (3:1 mixture concentrated HCl/HNO_3) and rinsed thoroughly with deionized water. The glassware was then rinsed with acetone before being dried in an overnight or until used for synthesis. Unless otherwise specified, all synthetic procedures were performed using standard Schlenk techniques under an argon (5.0, 99.999 %) atmosphere.

3.2.2 Synthesis of gold-coated magnetic nanoparticles (Fe_3O_4-AuNPs)

3.2.2.1 Preparation of iron oxide (Fe_3O_4) nanoparticles

0.71 g of $Fe(acac)_3$ was dissolved in 20 mL of phenyl ether with 2 mL of oleic acid and 2 mL of oleylamine with vigorous stirring. Once dissolved, 2.58 g of 1, 2-hexadecanediol was added in one portion and a water cooled condensing column was fitted to the flask. The solution was slowly heated to 210°C, and kept at reflux for 2 hours at this temperature. After 2 hours, the bright red suspension appeared dark brown in colour, and was allowed to cool to room temperature under argon overnight.

3.2.2.2 Coating Fe_3O_4 with gold to synthesize Fe_3O_4-AuNPs

10 mL of previously prepared Fe_3O_4 in phenyl ether was added to 30 mL of phenyl ether with vigorous stirring. To this solution, 0.83 g of $Au(ac)_3$,3.1 g of 1,2-hexadecanediol 0.5 mL of oleic acid and 3 mL of oleylamine were added. This suspension was then heated slowly (10°C/ min) until 180- 190°C and maintained at this temperature under reflux for 3 hours. The solution was allowed to cool to room temperature under argon overnight. 5 mL of the solution was transferred to a 125 mL

Erlenmeyer flask and 15 mL of ethanol was added to it. . The solution was agitated gently resulting in a visible aggregation of the nanoparticles, and the flask was then placed on top of 6 rare earth magnets for 5-10 mins to magnetically separate the particles from the supernatant solution. The supernatant solution was decanted as waste and the precipitated nanoparticles were washed three times with 15 mL of absolute ethanol. The nanoparticles were then redispersed in a solution of 10 mL of hexanes, 0.25 mL of oleic acid and 0.25 mL of oleylamine. This procedure was repeated multiple times to obtain 3 samples of Fe_3O_4-AuNPs in hexanes. Solutions appeared dark red-purple in colour, and were stored in glass covered by foil at room temperature.

3.2.2.3 Organic-aqueous phase transfer of Fe_3O_4-AuNPs nanoparticles

The following methods were not performed under Ar.

3.2.2.3.1 Sodium citrate ligand exchange

5 mL of prepared Fe_3O_4-AuNPs in hexanes was precipitated by magnetic separation using 15 mL of ethanol. The nanoparticles were washed 3 times with 15 mL of 100% ethanol and redispersed in 3 mL of TMAOH. 0.04 g of sodium citrate is added and the pH of solution was slowly adjusted to approximately 6.5 with dilute HCl using a pH meter. The solution was sonicated at room temperature for 15 mins. The nanoparticles were then collected on a magnet and redispersed in Milli-Q deionized water and sonicated for 5 mins at room temperature. Alternatively, the nanoparticles where redispersed in 3 mL of TMAOH containing 0.04 g of sodium citrate, and 3 mL of

TMAOH containing 0.4 g of sodium citrate. The TMAOH was also added drop wise and to nanoparticles in ethanol incrementally.

3.2.2.3.2 4-(Dimethylamino)pyridine (DMAP) phase transfer

0.5 M DMAP solution was prepared by adding 0.68 g of DMAP into 1 mL of Milli-Q water. 1 mL of Fe_3O_4-AuNPs was added to a 1 mL aliquot of 0.5 M aqueous DMAP solution in a glass vial. Two phases were observed, a dark purple hexane layer (top) and a clear aqueous layer (bottom). The phases were thoroughly mixed with vigourous stirring for 1 hour. At this time, the top hexane layer appeared light purple to clear and the bottom aqueous layer appeared dark purple suggesting that the nanoparticles were successfully transferred into aqueous solution. The bottom layer was transferred to a new glass vial and purified by washing the nanoparticles with a 0.5 M DMAP solution via magnetic separation.

3.2.3 Fe_3O_4-AuNPs characterization

3.2.3.1 UV-Vis spectroscopy

Fe_3O_4-AuNPs were prepared as described in section 3.2.2. The UV-Vis absorption characterization of the Fe_3O_4-AuNPs was performed using a Cary 300 Bio UV-Visible spectrophotometer (Varian, Santa Clara CA).

3.2.3.2 Transmission electron microscopy (TEM)

Fe_3O_4-AuNPs were prepared as described in section 3.2.2. and analyzed at each step during synthesis. Transmission electron micrographs were taken with a FEI Technai G2 F20 TEM at the Carleton University Nano-imaging Facility, with a field emission source at a voltage of 200 kV using Gatan Microscopy Suite 2V. All images were taken on dry 300 mesh x 83 μm pitch carbon coated copper TEM grids at room temperature. Grids were prepared by placing 4 μL of Fe_3O_4-AuNP (in various solvents) on a TEM grid. The TEM grids were allowed to dry for 4 -24 hours depending on the solvent. Images were taken at 1-2 μm, 100- 200 nm and 5- 10 nm for each grid.

3.2.3.2.1 TEM Energy-dispersive X-ray spectroscopy (TEM/EDS)

EDS of each Fe_3O_4-AuNPs sample was taken at a 20 degree take off angle with an Oxford X-max 80mm EDS detector using Aztec software.

3.2.3.3 Fe_3O_4-AuNPs size distribution analysis and lattice spacing

Transmission electron micrograph images were analyzed for nanoparticle size distribution using Image J software. The scale of the image was reset to the known scale of the TEM image. Bandpass filter and threshold were used to improve the resolution of the image for analysis. The area of each nanoparticle was determined with the nanoparticle analysis function. Using excel, the area of each nanoparticle was converted to diameter. A histogram was assembled for the frequency of each nanoparticle diameter.

The average nanoparticle diameter with standard deviation for a number of nanoparticles was calculated.

3.3 Results and Discussion

3.3.1 Characterization of purchased Fe_3O_4-AuNP

Magnetic gold nanoparticles (Fe_3O_4-AuNPs) were purchased (Nitparticles of Nitimmunotech, Spain). The company provided a scanning electron microscopy (SEM) image and UV-Vis absorption spectrum of the product (Figure 3.6). Since the purchase of this product, the company has added high resolution transmission electron microscopy (HRTEM) characterization to the documentation datasheet (Figure 3.6).[165]

Upon obtaining this sample of Fe_3O_4-AuNPs, it was further characterized by TEM/EDS. Figure 3.7 suggests the presence of two separate, co-existing nanoparticles within the same solution. Documented characterization provided by the company, such as SEM and UV-Vis, would not necessarily display uncoated iron oxide nanoparticles that are visible with TEM/EDS. This is due to the low density of iron oxide relative to gold. The provided HRTEM was not accompanied with EDS analysis which is a shortcoming in the data.

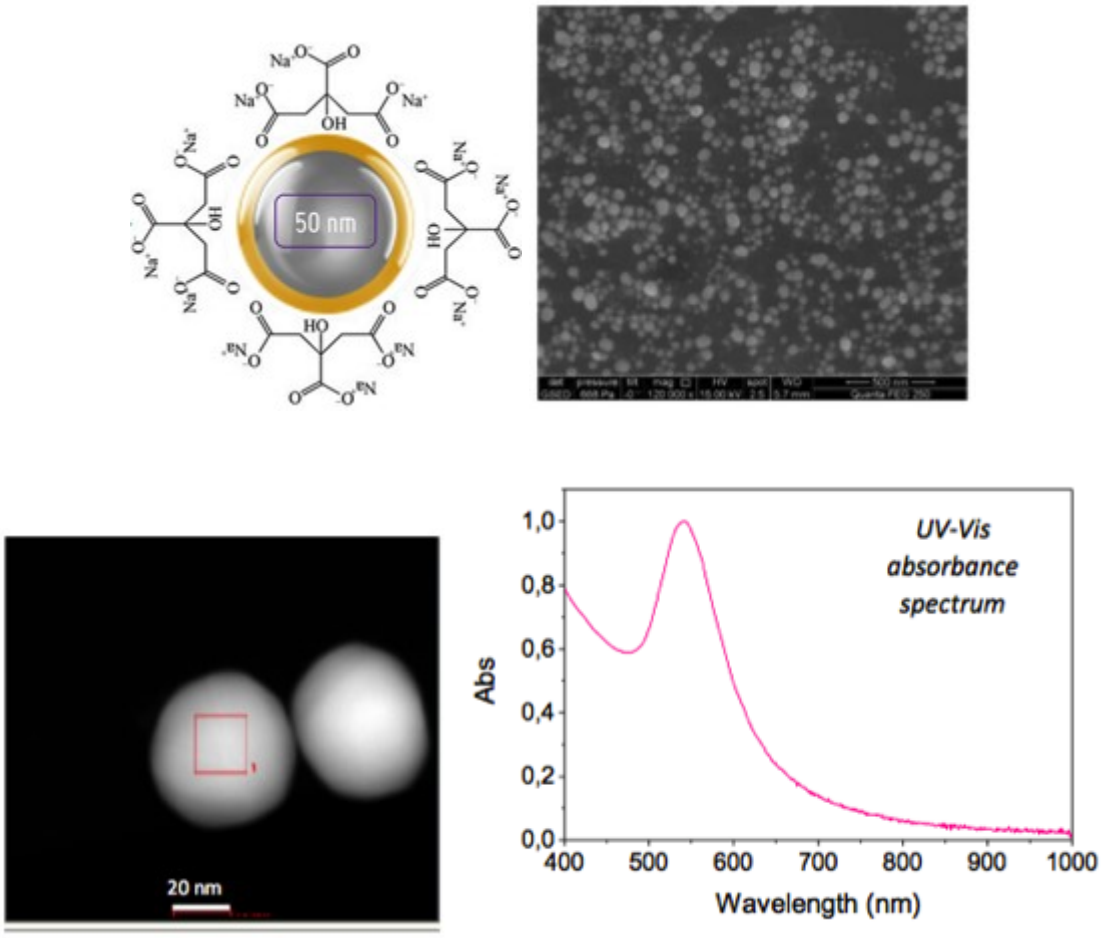

Figure 3.6 Obtained documentation of purchased Fe_3O_4-AuNPs including an illustration of the citrate capped core-shell Fe_3O_4-AuNPs (top left), SEM image (top right), HRTEM (bottom left) and UV-Vis absorption spectrum (bottom right).

Our analysis was not consistent with the documentation provided by the company. These nanoparticles were analyzed by HRTEM/EDS and found to be iron oxide nanoparticles without gold-coating and gold nanoparticles without an iron oxide core (Figure 3.7-3.8). As the reported synthesis included purification by magnetic separation, AuNPs without a magnetic core should be removed from the final product. With this considered, there is a chance that the larger particles are bound to magnetic particles, but are not core-shell structures. The reported molar concentration of the purchased product

is 0.05 nM with a particle concentration of $3.2x10^{-10}$ particles/mL.[165] At this concentration, the colloidal suspension of Fe_3O_4-AuNPs was a clear solution by eye. This relatively low concentration would be an inefficient separation or partitioning method, since most biomolecular interactions have dissosication constants (K_d values) in the high nanomolar range. In particular, SELEX begins with 1000 pmol of DNA, and thus 25 pmol of these purchased nanoparticles would be required as a platform. Therefore, one round of selection would require a 50 L volume of the nanoparticles at this concentration.

A final challenge encountered upon the analysis of the nanoparticles can be seen in the TEM/EDS results. Specifically, the samples displayed multiple impurities including cobalt, tin and vanadium. Such impurities may impede the separation effectiveness of the nanoparticles, or may lead to the isolation of aptamers to the contaminant molecules rather than the desired AuNP surface (Figure 3.9).

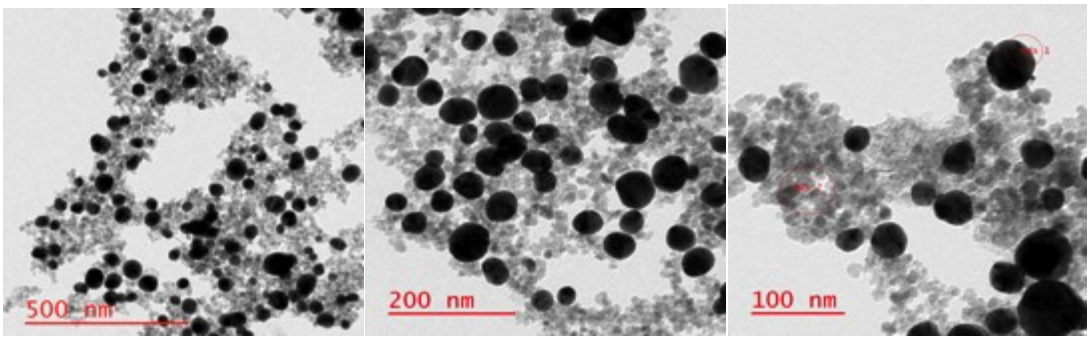

Figure 3.7 TEM analysis of purchased Fe_3O_4-AuNPs with various scale bars, 500 nm (A), 200 nm (B) and 100 nm (C).

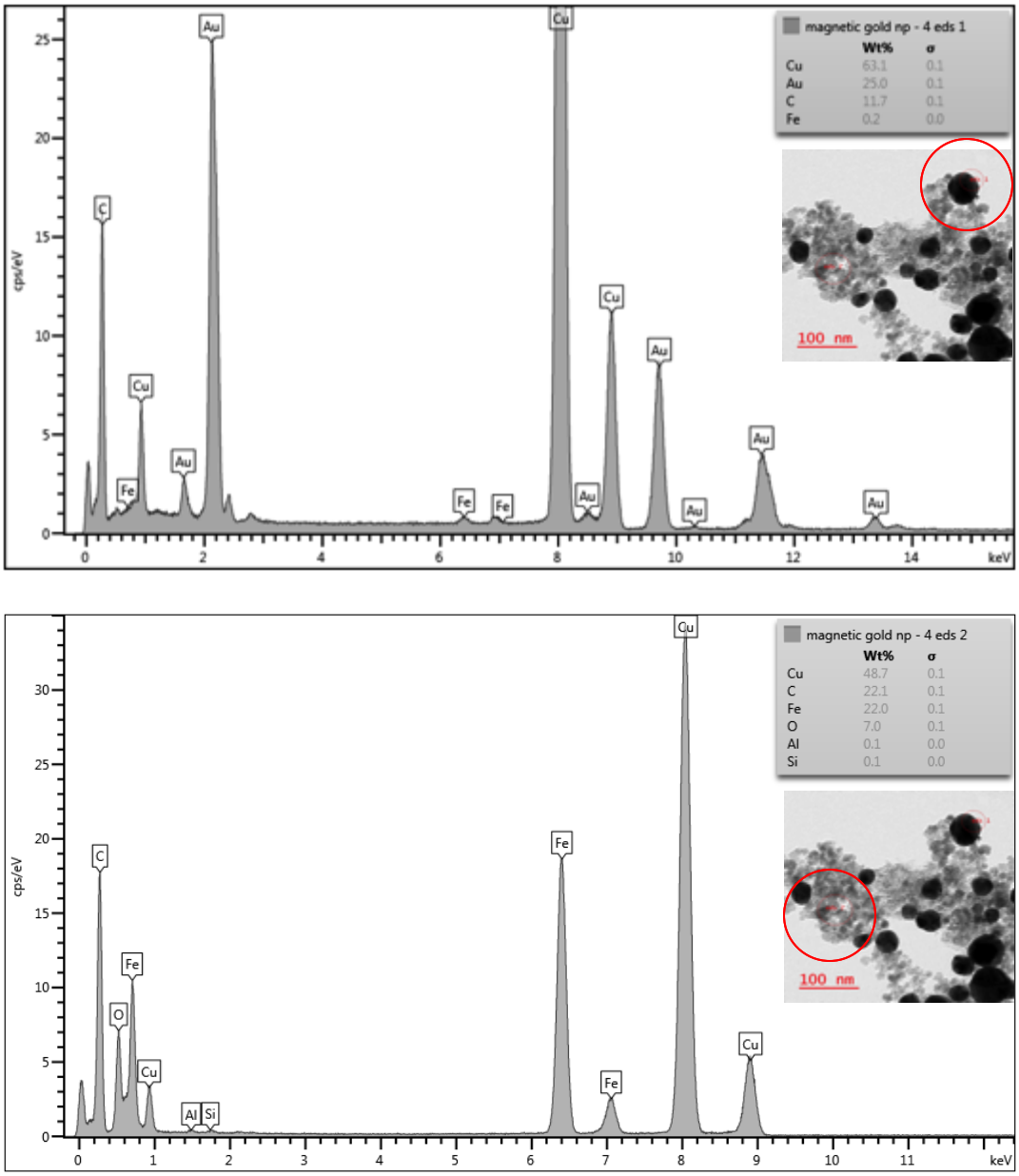

Figure 3.8 TEM image with corresponding EDS analysis; EDS 1 of darker nanoparticles (top) and EDS 2 of lighter nanoparticles (bottom), of purchased Fe_3O_4-AuNPs with a 100 nm scale bar

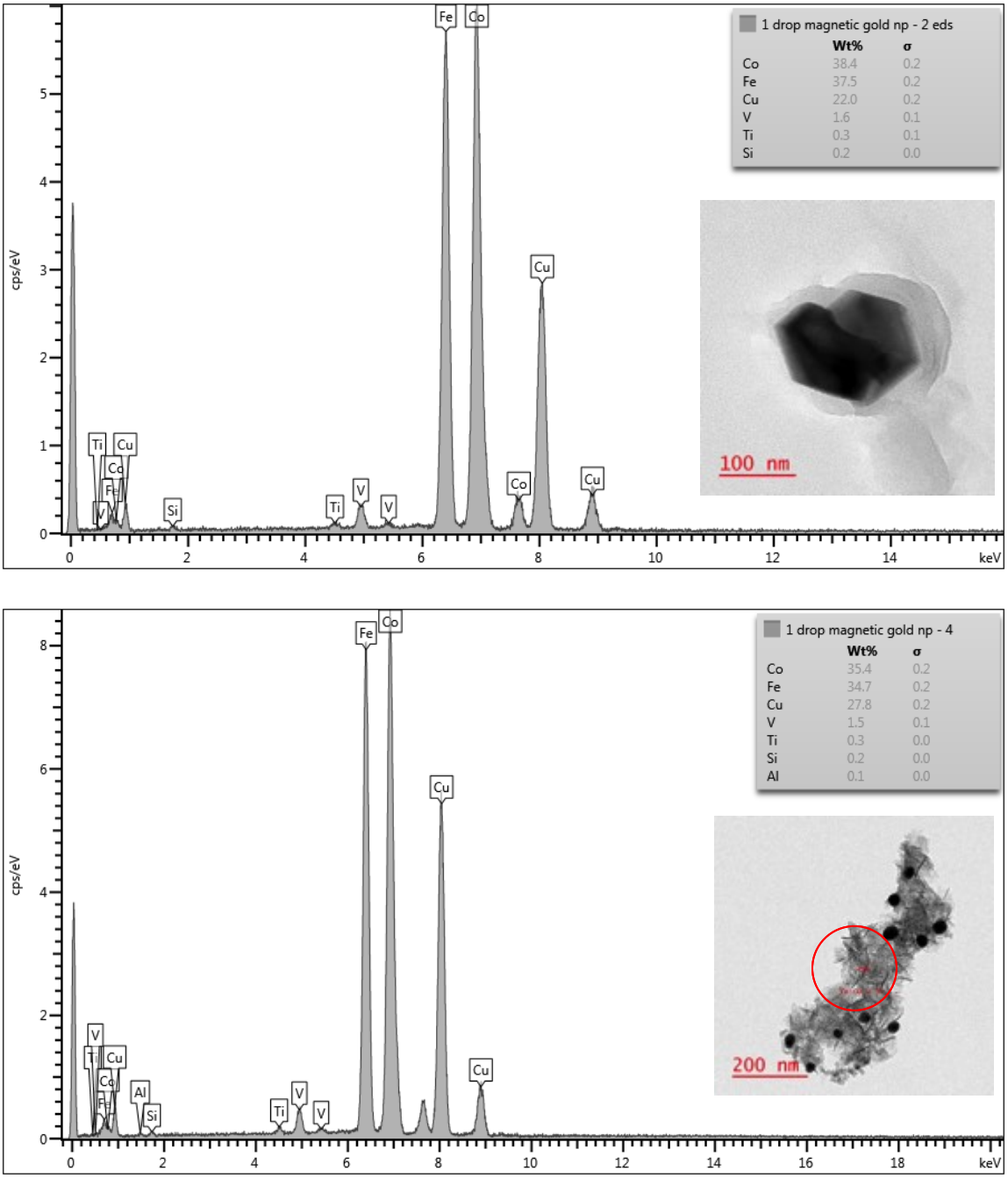

Figure 3.9 Example TEM images with corresponding EDS analysis of contamination within the purchased Fe_3O_4-AuNP sample with 100 nm and 200 nm scale bars

Based on the poor overall quality of the purchased nanoparticles: exposed Fe_3O_4 surfaces, low sample concentration, and the possible inclusion of other impurities such as

Ti, V and Co; these nanoparticles were determined to be insufficient for our purposes as a separation method for small molecule SELEX.

3.3.2 Optimization and characterization of Fe_3O_4-AuNP synthesis

3.3.2.1 Characterization techniques for synthesized Fe_3O_4-AuNPs

As previously described, synthesized core-shell nanoparticles can not be judged without comprehensive characterization. High-resolution transmission electron microscopy (HRTEM) is a valuable source of characterization, however contrast between the core and shell of synthesized Fe_3O_4-AuNP is often difficult to achieve through this technique. As previously mentioned, TEM is a technique capable of imaging nanoparticles by transmitting a high energy beam of electrons through a sample. The image is produced by differences in how the electrons are transmitted through a sample, which varies with crystallinity, atomic mass or thickness. Nanoparticles are an example of a specimen suitable for TEM analysis, as the product is very thin (<100 nm). Scanning electron microscopy (SEM) is used to analyze samples, including nanoparticles, by scanning a sample with a focused beam of electrons. Compared to TEM, SEM works by analyzing how the electrons interact with the atoms at the surface of a sample to relay an image. Although SEM is able to image the depth of a bulk sample to produce a 3-dimensional image, SEM is approximately an order of magnitude less sensitive than TEM and only analyzes the surface of a sample. Therefore, core-shell nanoparticles are not well suited for SEM and require analysis with HRTEM. Crystallography and composition analysis can be useful information; however, this analysis only provides the composition of the entire sample and not a single core-shell nanoparticle. For example,

X-ray diffraction (XRD) determines the crystalline material within a sample by exposing a sample to a high energy source of electrons and analyzing the diffracted angle via Bragg's law. Therefore, this technique can be used to compare the crystalline composition of Fe_3O_4, Au and Fe_3O_4-AuNPs and conclude the presence of core-shell particles. However, this analysis is also inconclusive in determining if the Au is coating the Fe_3O_4, and if the entire sample of Fe_3O_4 is evenly coated with Au. In some cases, the Fe_3O_4 diffraction peaks are absent when characterizing Fe_3O_4-AuNPs with XRD analysis.[150] This is attributed to the effects of gold as a heavy atom in comparison to Fe_3O_4, and explains further the difficulties with XRD as a characterization method for this core-shell product. Therefore, XRD results are somewhat inconclusive as this method confirms the presence of both Fe_3O_4 and Au in a sample, but not the composition of each nanoparticle individually. Similarly, electron dispersive X-ray spectroscopy (EDX), also known as EDS is unable to conclude that Fe_3O_4 is coated with Au within a single particle due to the depth sensitivity of the tool. This method is similar to XRD, however can theoretically provide elemental analysis of a single particle with HRTEM. The X-ray diffraction pattern on the surface of the nanoparticle is imaged by HRTEM and can be estimated with external software to assess the presence of gold. The lattice spacing for Au is 0.235 nm. In addition, a UV-Vis absorption spectrum of the core- shell nanoparticles can be insightful. Compared to AuNPs of the same size, a core Fe_3O_4 results in a slight red shift in the absorption, which can support other characterization methods. A thinner coating of Au on the Fe_3O_4 nanoparticles results in a spectrum that experiences a larger red-shift from that of AuNPs (~525 nm). This shift results in absorption of approximately 530- 540 nm for core- shell Fe_3O_4-AuNPs depending on the

thickness of the Au shell, which can be explained by Mie theory.[54,166] As previously mentioned, the UV-Vis absorption depends upon the SPR of the nanoparticle. Simply, Mie theory outlines the absorption and scattering of electromagnetic waves of light by uniform particles. A core-shell structure alters this scattering, with the bimetallic difference in material throughout the nanoparticle. The SPR of the overall system is affected, which results in a UV-Vis absorption shift.

3.3.2.2 Controlling temperature during synthesis improves gold coating

The initial synthesis of Fe_3O_4-AuNPs was based upon a previously reported procedure by Robinson and co-workers.[164] However, the goal of their work was to study the interaction between synthesized Fe_3O_4-AuNPs and thiolated DNA. We wanted to test whether the same procedure would be useful in the context of non-thiolated DNA aptamers. This study found that synthesizing Fe_3O_4-AuNPs nanoparticles with organic capping agents such as oleic acid, oleylamine and 1,2-hexadecanediol, compared to using aqueous based capping agents in other methods, is advantageous. In particular, while the synthesis, composition and characterization of Fe_3O_4-AuNPs was previously challenging, this approach has successfully provided stable, highly-monodisperse core-shell nanoparticles. Therefore, we performed, adapted and optimized this synthesis strategy to develop Fe_3O_4-AuNPs.

In our first synthesis of Fe_3O_4 nanoparticles, the solution was refluxed for 2 h at 180-190 °C as reported by Robinson et al.[164] This resulted in aggregated Fe_3O_4 nanoparticles with a non-uniform size distribution (Figure 3.10). However, because diphenyl ether was used as the synthesis solvent (boiling point of 258°C), we performed a second reaction with an increased reaction temperature (from 190°C to 258°C) to test

the effect of temperature on our synthesis. This change in temperature did not result in a significantly more mono-disperse Fe_3O_4 sample (Figure 3.11).

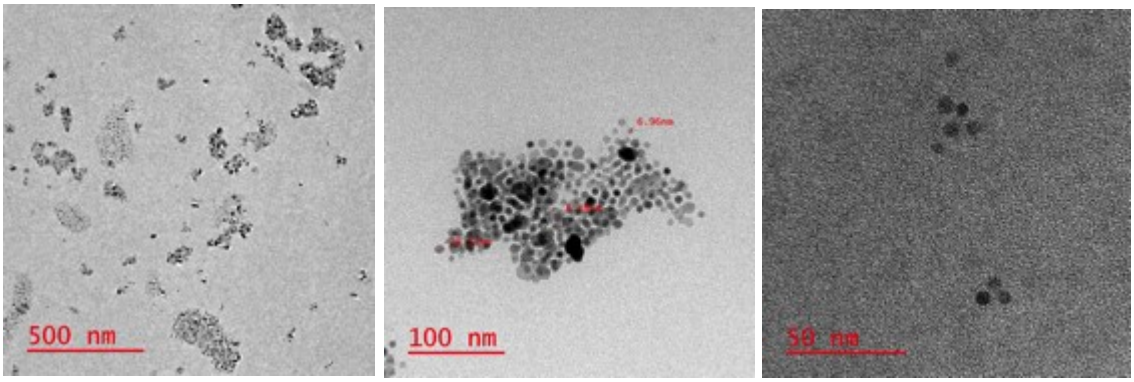

Figure 3.10 TEM images with 500 nm, 100 nm and 50 nm scale bars of synthesized Fe_3O_4 (batch 1) nanoparticle product from initial synthesis

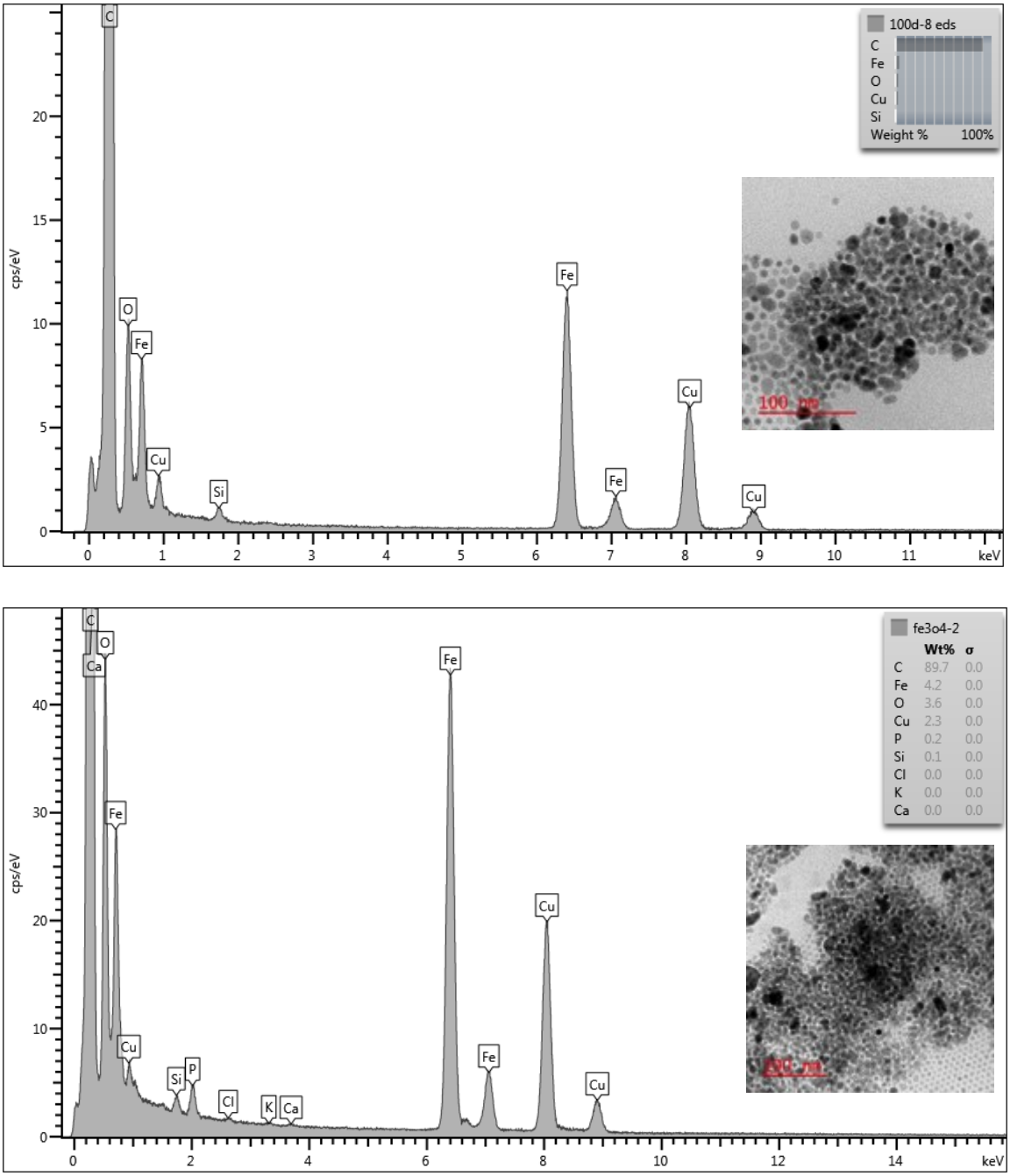

Figure 3.11 TEM image with corresponding EDS analysis with a 100 nm scale bar of synthesized Fe_3O_4 (batch 1) nanoparticle product from initial synthesis

As previously mentioned, it is reported that temperature is important for the gold coating process. To coat Fe_3O_4 with gold, we quickly heated the solution to 180-190°C under N_2 with vigorous stirring for 1.5 hours. Unfortunately, during this coating process, the temperature rapidly increased to 215-230°C. The resulting sample was characterized using TEM/EDS analysis. Figure 3.12 displays that mono-disperse coating of Fe_3O_4 with gold was unsuccessful, instead showing two distinct sizes of nanoparticles present in solution. These results are similar to that of the purchased Fe_3O_4-AuNPs. It is likely that some Fe_3O_4-AuNPs are present in solution, due to magnetic purification during synthesis. However, the size distribution of these particles is extremely non-uniform and it is possible that uncoated Fe_3O_4 or AuNPs without a magnetic core remain in solution.

Next, the two populations of nanoparticles were analyzed by TEM/EDS in an attempt to characterize and understand their composition. EDS analysis (Figure 3.13) of both the smaller and larger particles indicated peaks present that are characteristic to both iron and gold. However, EDS analysis of Fe_3O_4-AuNPs compared to Fe_3O_4 next to AuNPs is questioned. The second population had a documented iron weight percentage (wt%) 0.1-0.2 higher than, which is more than the amount of iron found within the TEM grid and is therefore distinctive of Fe_3O_4. Taken together, we propose that the synthesis yielded a population of smaller nanoparticles that are core-shell Fe_3O_4-AuNPs, as well as a population of larger particles that are AuNPs without a magnetic core. Therefore, at this point during the synthesis, it is possible that AuNPs without a magnetic core may remain in solution during magnetic separation. In order to improve the synthesis of Fe_3O_4-AuNPs, the size distribution and composition of nanoparticles must be improved. Although the composition and successful gold coating of Fe_3O_4 can be improved during

synthesis, uncoated Fe_3O_4 (AuNPs without a magnetic core) could potentially be separated from solution during a post synthesis phase transfer. This being said, size distribution of the synthesized Fe_3O_4-AuNPs must be improved during synthesis. It is reported that the temperature during synthesis is of most importance for stable, mono-disperse nanoparticles.[124,150] During the initial synthesis of Fe_3O_4-AuNPs it was observed that the temperature reached approximately 215-230°C very quickly, before the temperature was eventually reduced to 180-190°C within the 1.5 hour reaction. This rapid temperature spike during the reaction was assumed to be the main fault during this specific synthesis of Fe_3O_4-AuNPs.

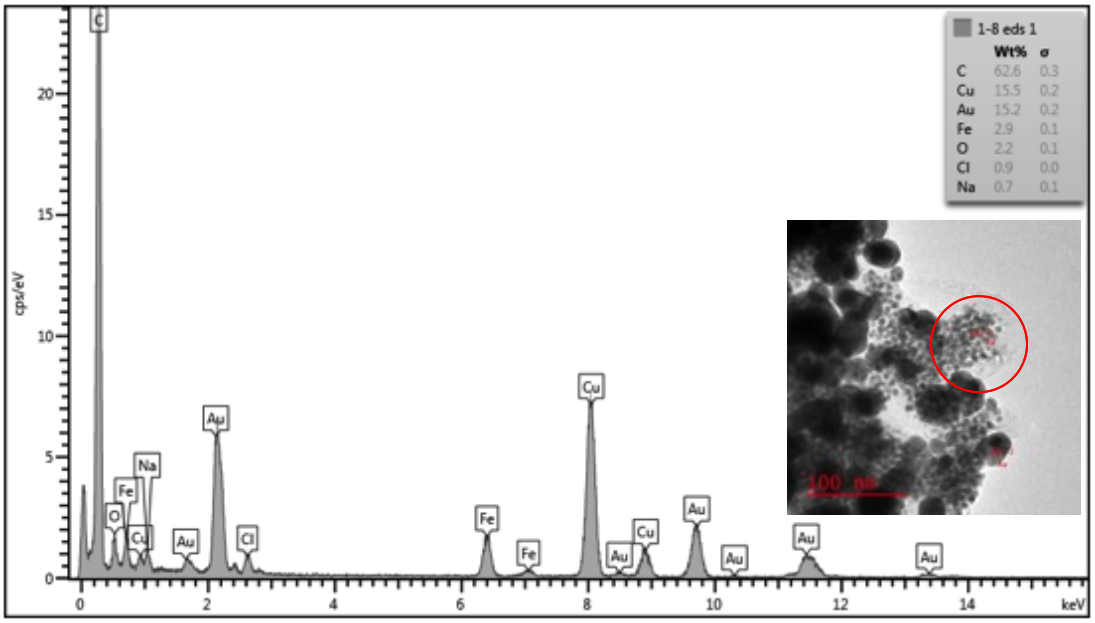

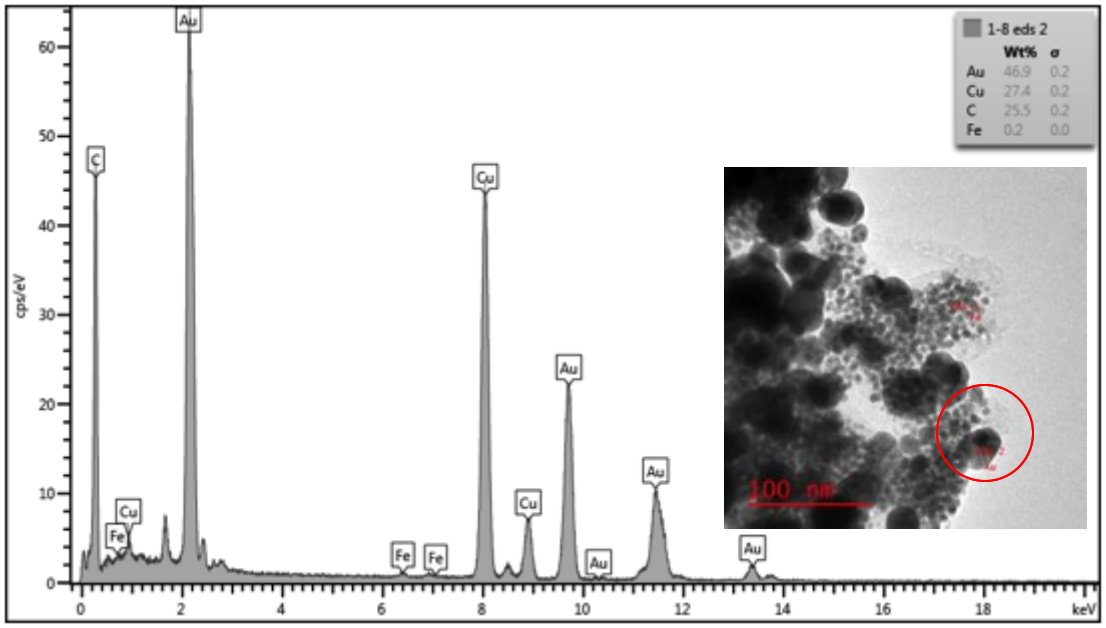

Figure 3.12 TEM image with corresponding EDS analysis; EDS 1 of smaller nanoparticles (top) and EDS 2 of larger nanoparticles (bottom), of synthesized Fe_3O_4-AuNPs (batch 1) with a 100 nm scale bar

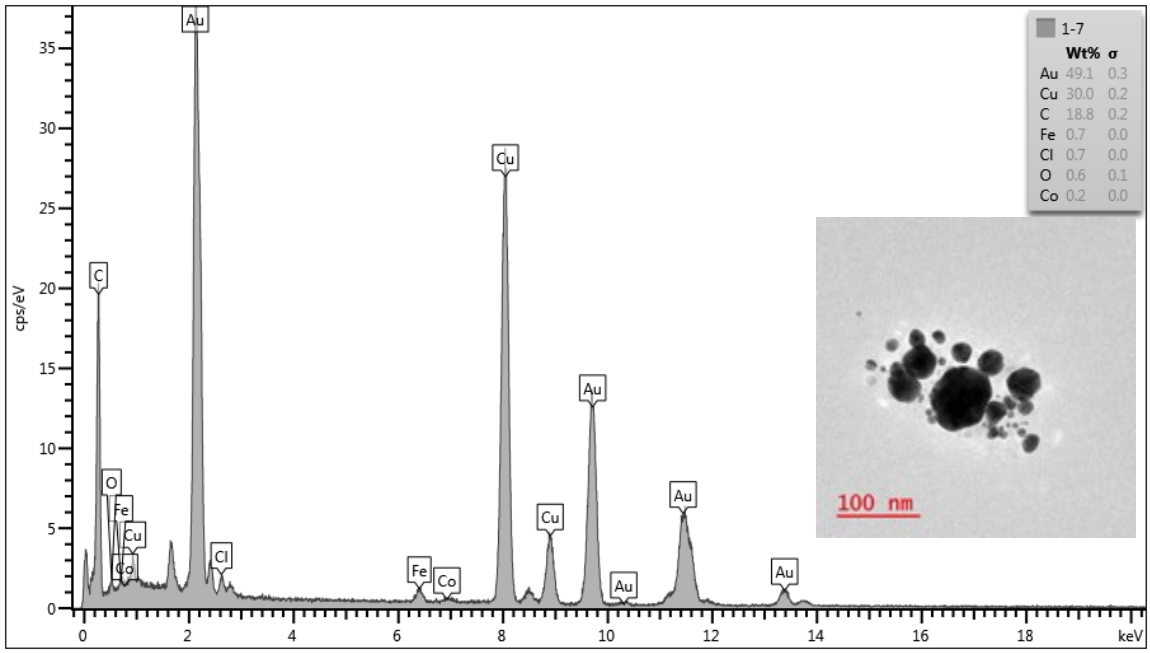

Figure 3.13 TEM image with corresponding EDS analysis of synthesized Fe_3O_4-AuNPs (batch 1) with a 100 nm scale bar

We next examined whether strictly maintaining the solution at 180-190°C for 1.5 hours would improve the formation of Fe_3O_4-AuNPs (Figures 3.14-3.15). TEM/EDS found that the Fe_3O_4-AuNPs resulting from this synthesis appear to be more uniform and consistent in comparison original synthesis (Figures 3.12-3.13). However, there is a large variance in the size of the synthesized Fe_3O_4-AuNPs (Figure 3.16-3.17). Furthermore, the composition of the nanoparticles is still inconsistent. TEM/EDS analysis shows that there is a mix of Fe_3O_4-AuNPs, Fe_3O_4 and AuNPs without a magnetic core. Through TEM/EDS, most of the synthesized nanoparticle were found to be either uncoated Fe_3O_4 or AuNPs without a magnetic core. Since the formation of Fe_3O_4-AuNPs was not prevalent, the synthesis was found to be unsuccessful. Nonetheless, we conclude that reaction temperature on size distribution and uniform coating of gold is an important source of improvement.

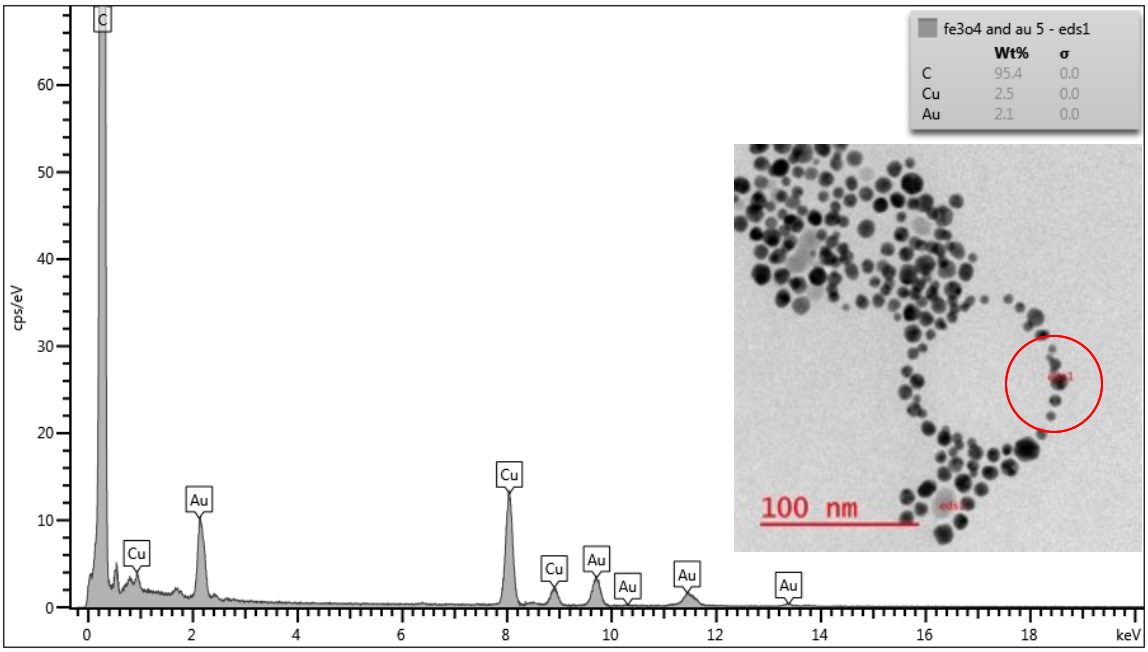

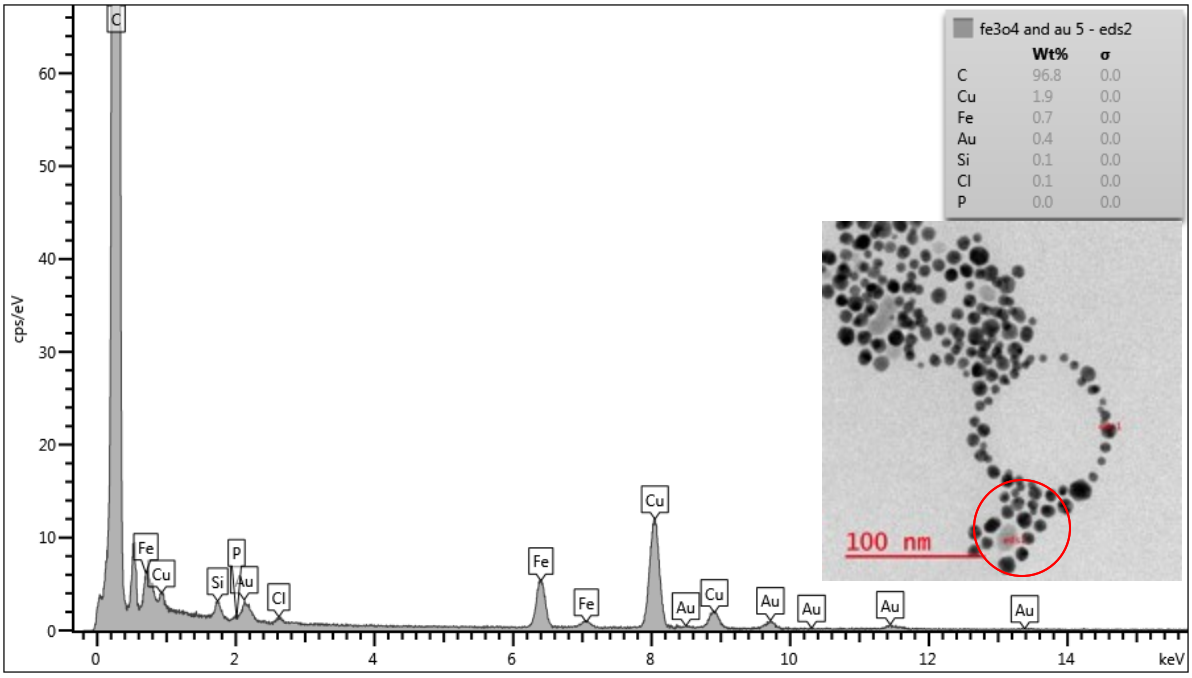

Figure 3.14 TEM image with corresponding EDS analysis of synthesized Fe_3O_4-AuNPs (batch 2) with a 100 nm scale bar. EDS 1 of darker nanoparticles (top) and EDS 2 of lighter nanoparticles (bottom).

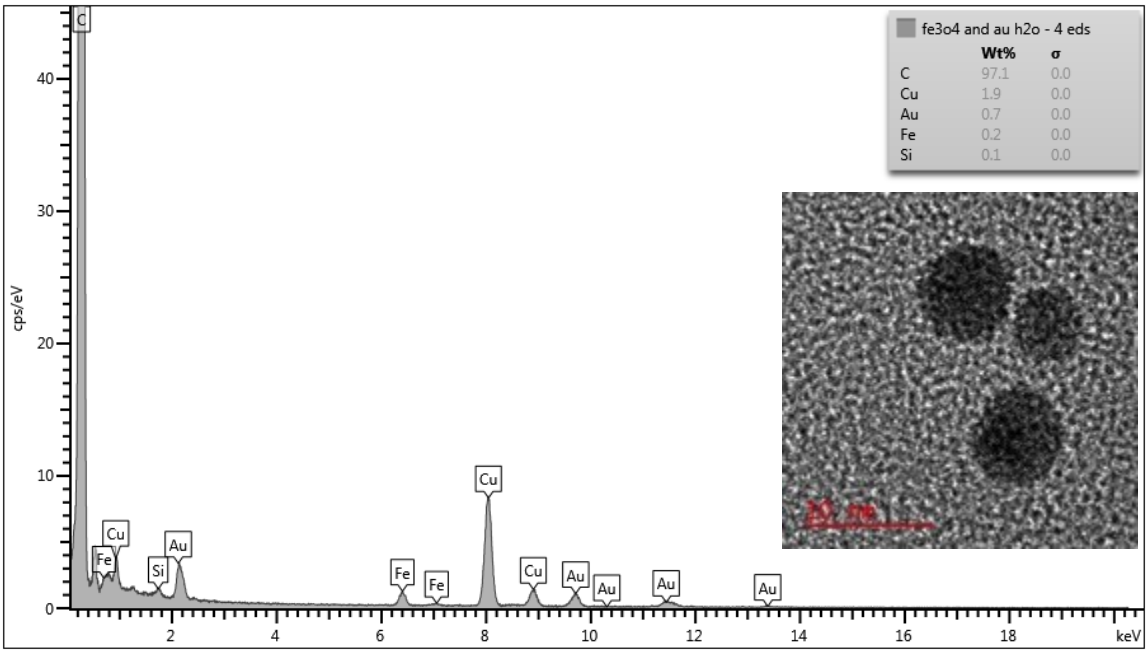

Figure 3.15 TEM image with corresponding EDS analysis of synthesized Fe_3O_4-AuNPs (batch 2) with a 10 nm scale bar

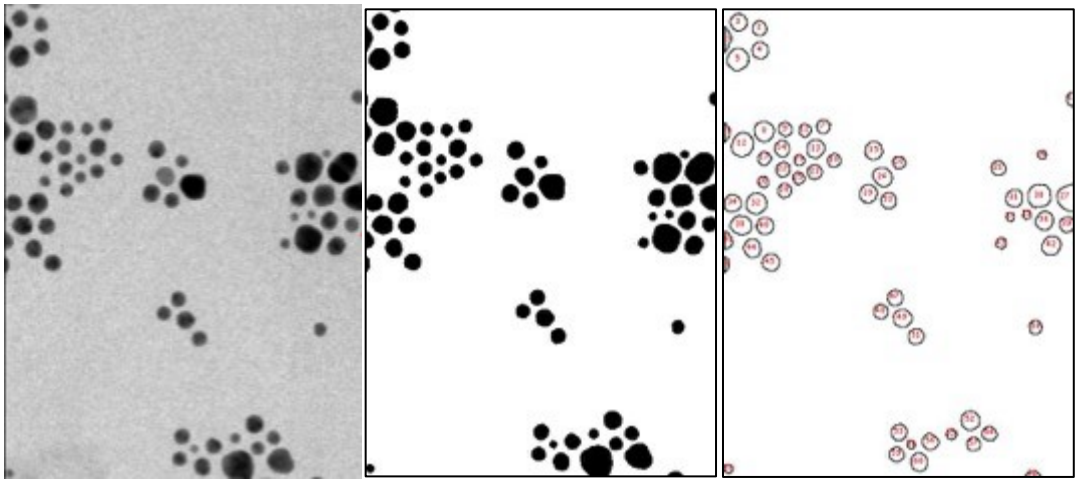

Figure 3.16 TEM image of synthesized Fe_3O_4-AuNPs (batch 2) (A) used for size distribution analysis outline (B) and area of nanoparticles (C)

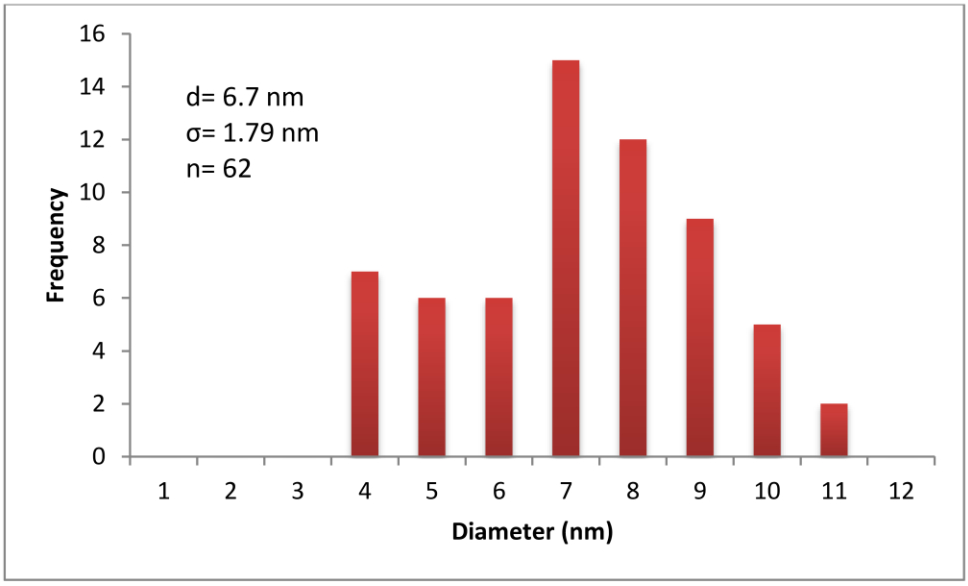

Figure 3.17 Histogram of synthesized Fe_3O_4-AuNPs (batch 2) with associated average diameter of the nanoparticles, standard deviation and number of particles analyzed. TEM image was analyzed with ImageJ software for the area of the nanoparticles.

3.3.2.3 A controlled increase further improves coating and distribution

A more controlled and incremental temperature increase throughout the synthesis was tested. Specifically, the Fe_3O_4 synthesis was preformed under reflux for 2 hours at 210 °C as reported by Wang and co-workers.[124] TEM/EDS analysis of Fe_3O_4 nanoparticles synthesized under these specific temperature conditions (Figures 3.18-3.19) showed more uniform and mono-disperse nanoparticles compared to the previous batch (Figure 3.11, 3.19). The TEM/EDS analysis also indicated an average diameter of the synthesized Fe_3O_4 to be 5.96 nm (σ= 0.23 nm, n=7) (Figure 3.18). Although the size of the synthesized Fe_3O_4 nanoparticles is approximately 1 nm smaller than that reported (the expected diameter of the Fe_3O_4 nanoparticles is 6.7 nm[124,164]), the difference in average diameter is not as important as mono-dispersion when considering coating the synthesized Fe_3O_4 with gold. The thickness of the gold is negligible as the core-shell structure of the nanoparticle is the crucial factor for our AuNP SELEX application. TEM/EDS analysis and estimated size distribution display the effects of reaction temperature on the formation of Fe_3O_4 nanoparticles. The synthesis was found to be successful and the synthesized Fe_3O_4 nanoparticles were subsequently coated with gold.

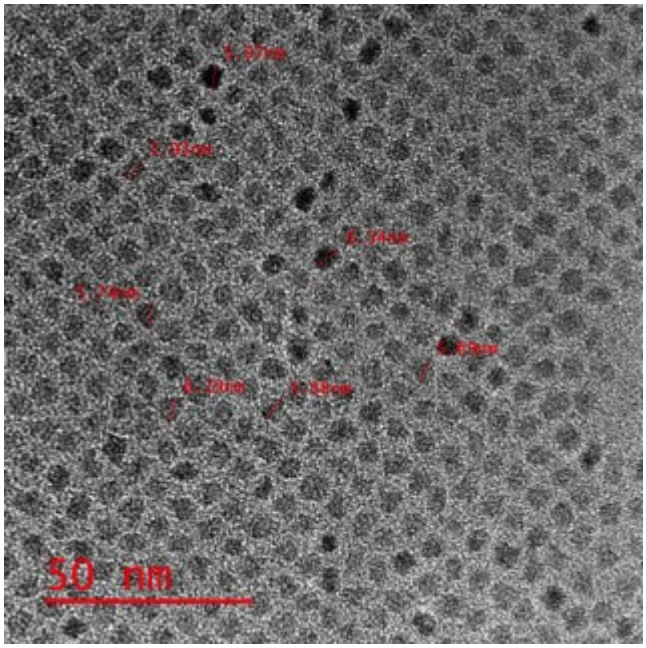

Figure 3.18 TEM image of synthesized Fe_3O_4 nanoparticles (batch 2) with a 50 nm scale bar and representation of the estimated diameter of the synthesized nanoparticles

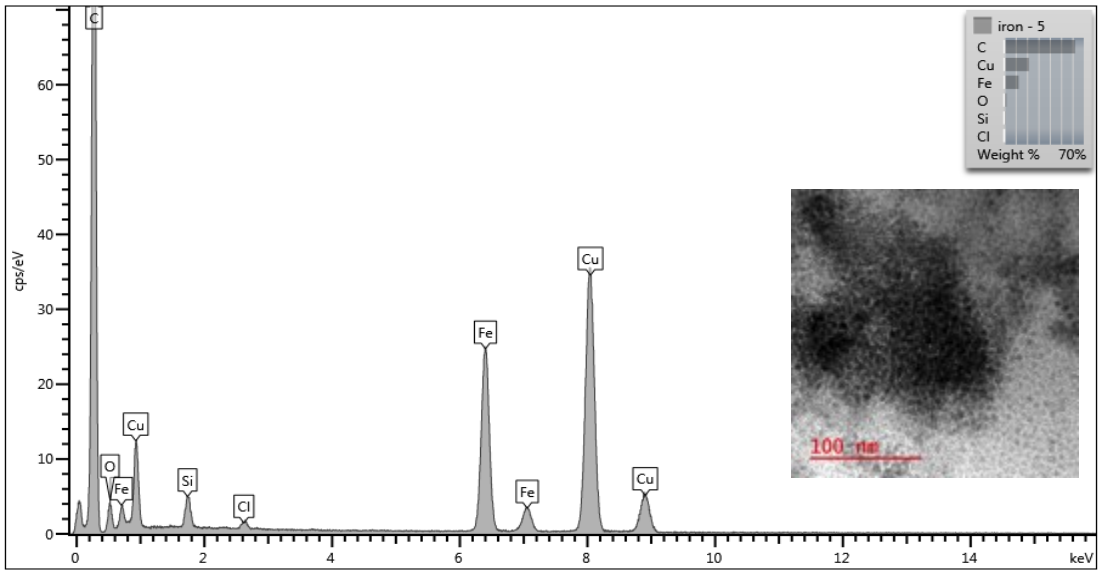

3.19 TEM image with corresponding EDS analysis of synthesized Fe_3O_4 nanoparticles (batch 2) with a 100 nm scale bar

The reported method used to improve the synthesis of Fe_3O_4, outlines specific temperature requirements with respect to time for the synthesis Fe_3O_4 –AuNPs. In this

work by Wang and co-workers, the reaction time for the synthesis of Fe_3O_4 –AuNPs is increased from 1.5 hours to 3 hours. In addition, the solution of Fe_3O_4, $Au(ac)_3$, oleic acid, oleylamine and 1, 2- hexadecanediol is heated to 180-190°C, increasing the temperature by 10°C/min.[124] These two modifications considerably increased the success of Fe_3O_4 –AuNPs synthesis. TEM/EDS analysis displays nanoparticles that are more uniform in composition and size (Figure 3.21). TEM/EDS of the sample and single particle HRTEM/EDS analysis concluded that the Fe_3O_4 nanoparticles are coated with gold (Figure 3.22). The consistency of the nanoparticle size and composition found by TEM/EDS is supportive of the successful synthesis of mono-disperse Fe_3O_4 –AuNPs. Further analysis by measuring the lattice spacing of the synthesized nanoparticles resulting in 0.235 Å suggests that the Fe_3O_4 nanoparticles are coated with gold (Figure 3.20).[164]

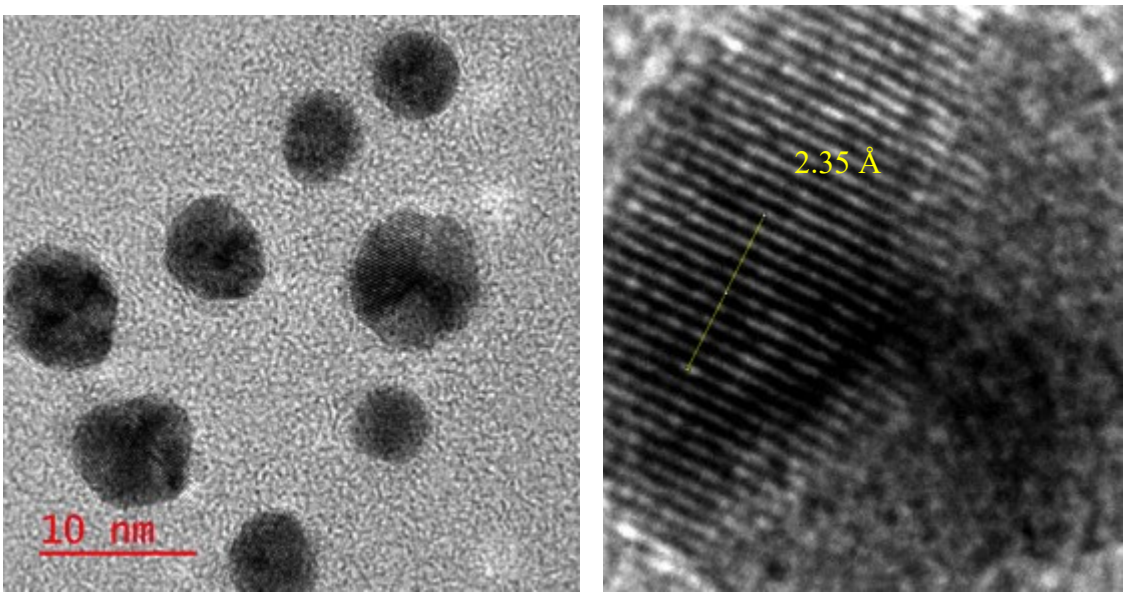

Figure 3.20 TEM image of synthesized Fe_3O_4-AuNPs (batch 3) with a 10 nm scale bar (left) and estimated length surface lattice spacing of the gold shell via ImageJ analysis (right)

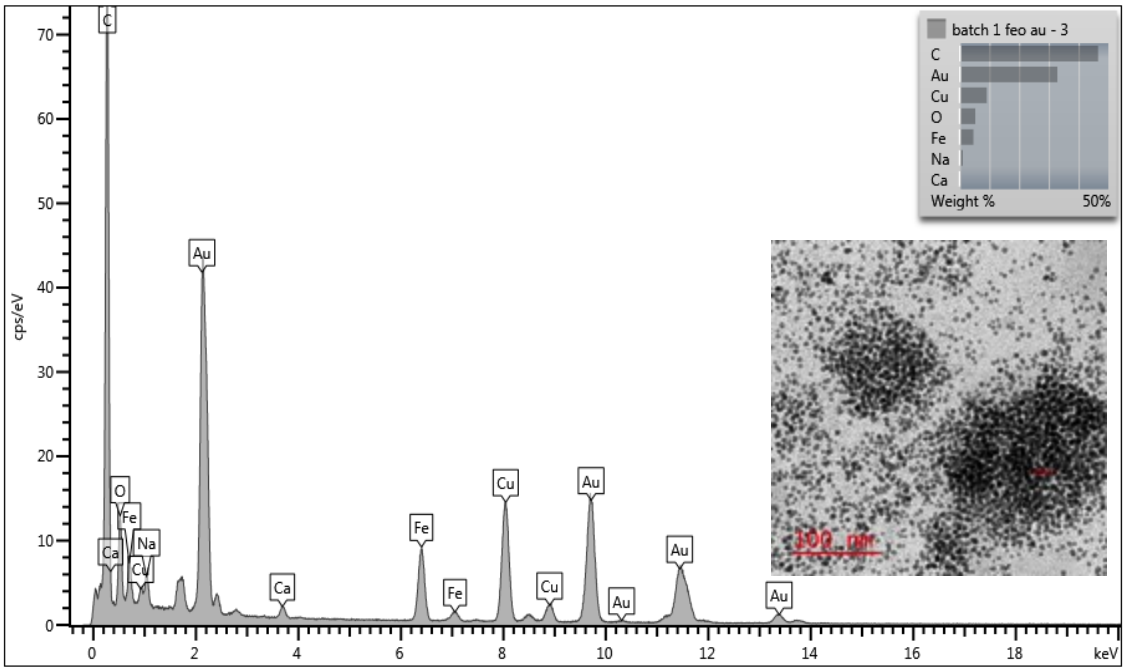

Figure 3.21 TEM image with corresponding EDS analysis of synthesized Fe_3O_4-AuNPs (batch 3) with a 100 nm scale bar

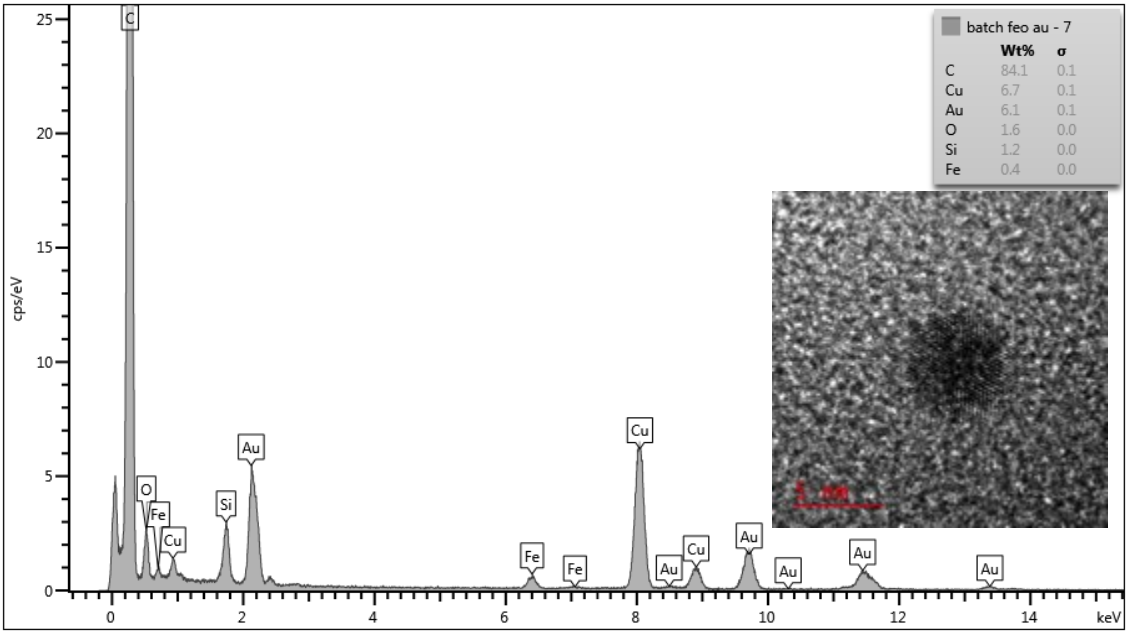

Figure 3.22 TEM image with corresponding EDS analysis of a single synthesized Fe_3O_4-AuNPs (batch 3) with a 5 nm scale bar

The synthesis of Fe_3O_4 –AuNPs was performed again following the same procedure and modifications using the mono-disperse Fe_3O_4 synthesized at 210°C. The TEM/EDS shows that the Fe_3O_4 were successfully coated with gold (Figures 3.24-3.25). At larger magnitudes (500 nm), it appears that there are two types of nanoparticles present in solution. However, TEM/EDS analysis verifies that both areas contain iron and gold (Figures 3.23). In this case, the nanoparticles appear less uniform than the nanoparticles previously synthesized (Figures 3.21).

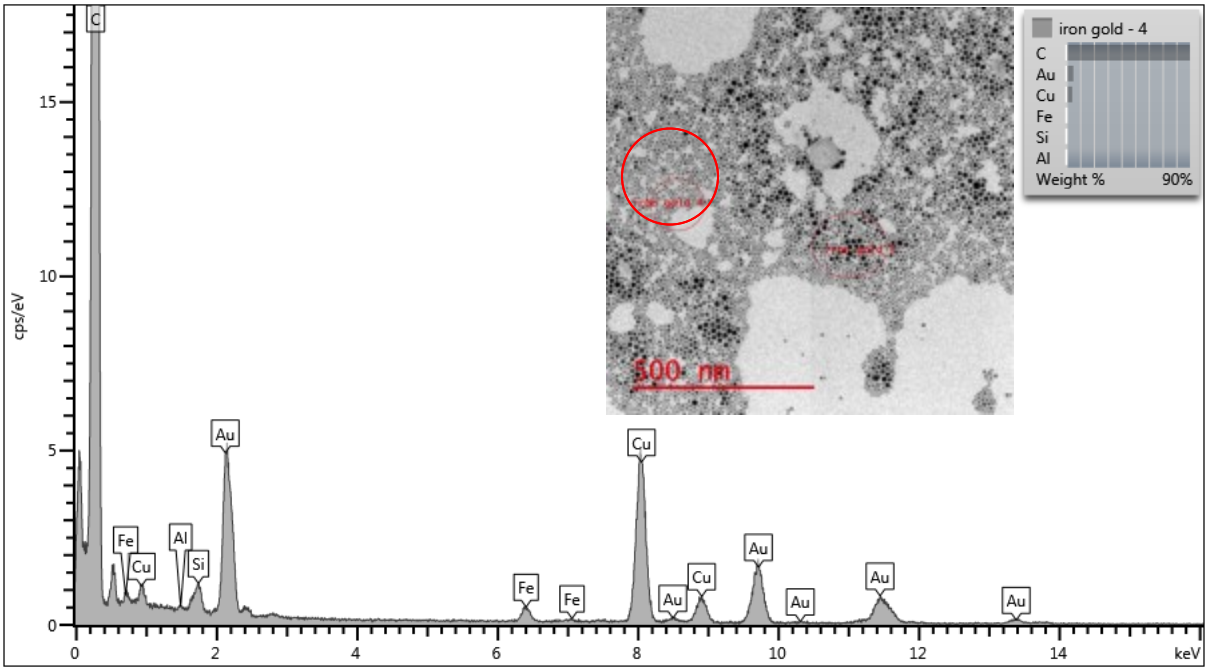

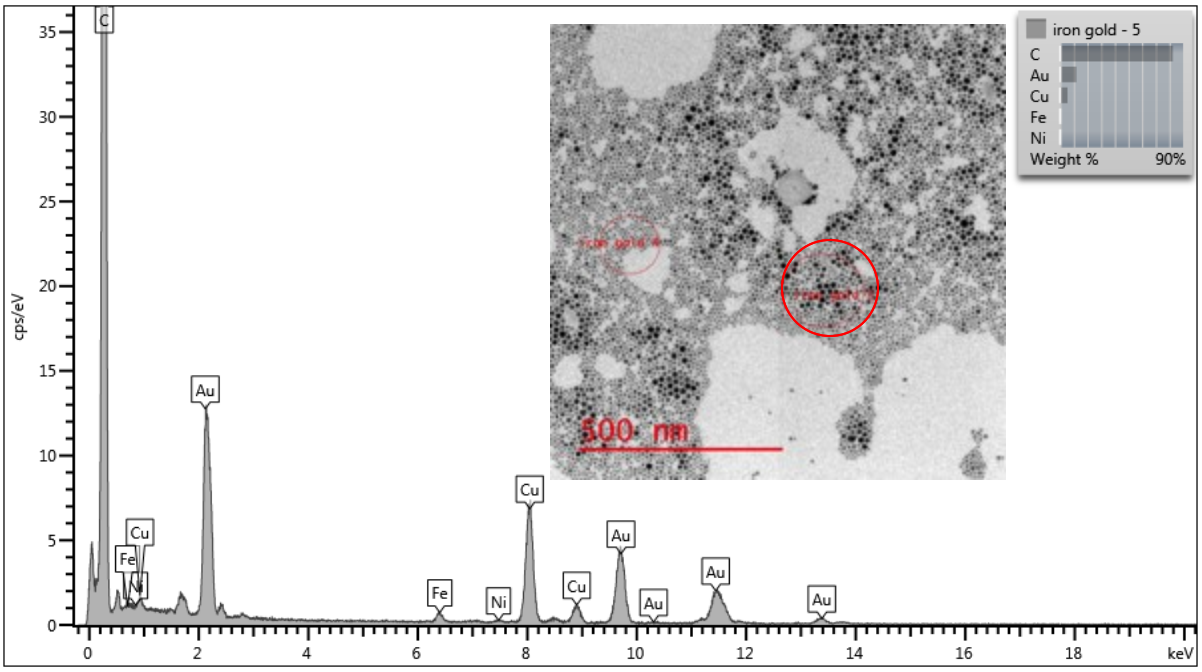

Figure 3.23 TEM image with corresponding EDS analysis of synthesized Fe_3O_4-AuNPs (batch 4) with a 500 nm scale bar. EDS 4 (top) and EDS 5 (bottom) of different areas within the sample.

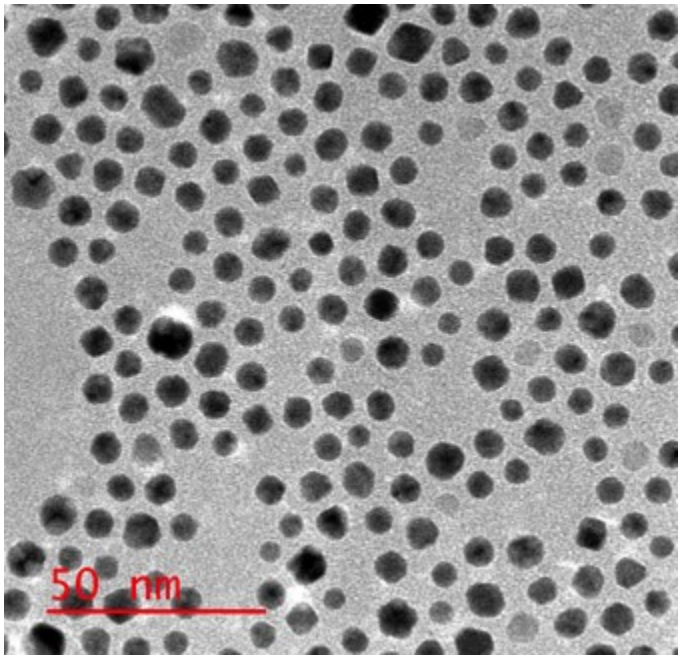

Figure 3.24 TEM image synthesized Fe_3O_4-AuNPs (batch 4) with a 50 nm scale bar

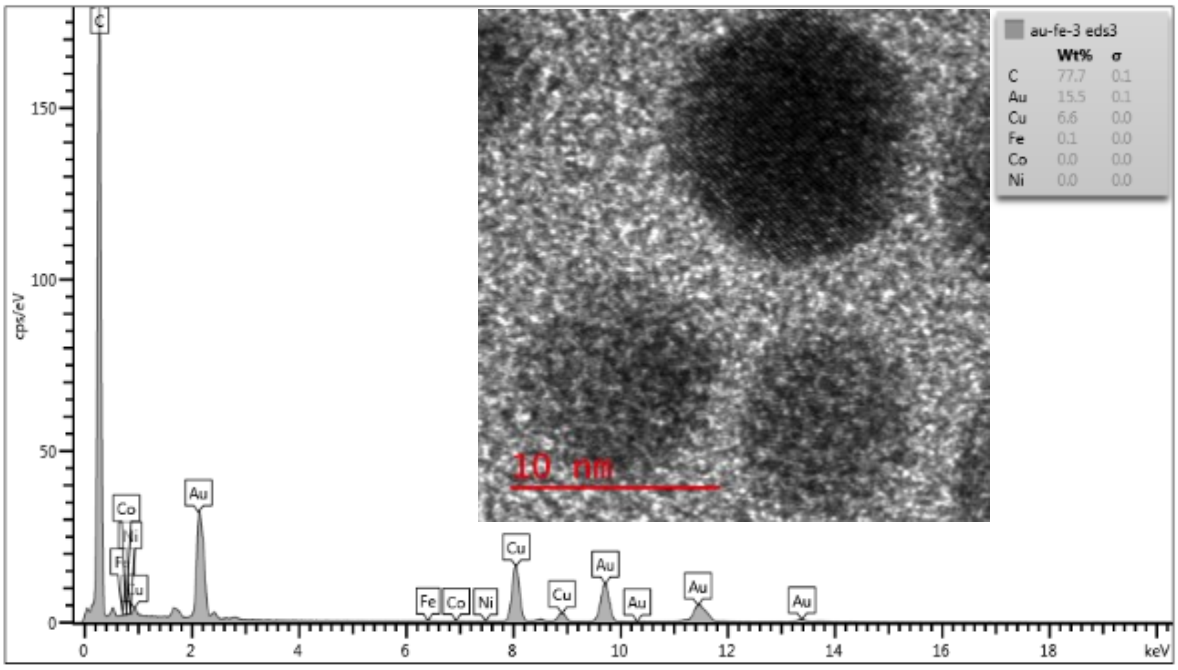

3.25 TEM image with corresponding EDS analysis of synthesized Fe_3O_4-AuNPs (batch 4) with a 10 nm scale bar

By TEM analysis, the average diameter of the Fe_3O_4 –AuNPs was found to be 6.53 nm (σ= 1.18, n= 71) (Figures 3.26-3.27), compared to an average diameter of 8.71 nm (σ= 3.44, n= 620) (Figures 3.28- 3.29). In comparison, the size distribution of the first synthesis is much more mono-disperse. The average diameter of the synthesized Fe3O4-AuNPs is also the most frequent diameter during analysis (Figure 3.27). However, the Fe3O4-AuNPs produced during the second synthesis yield an average particle diameter that is skewed due to a group of larger particles (Figure 3.29).

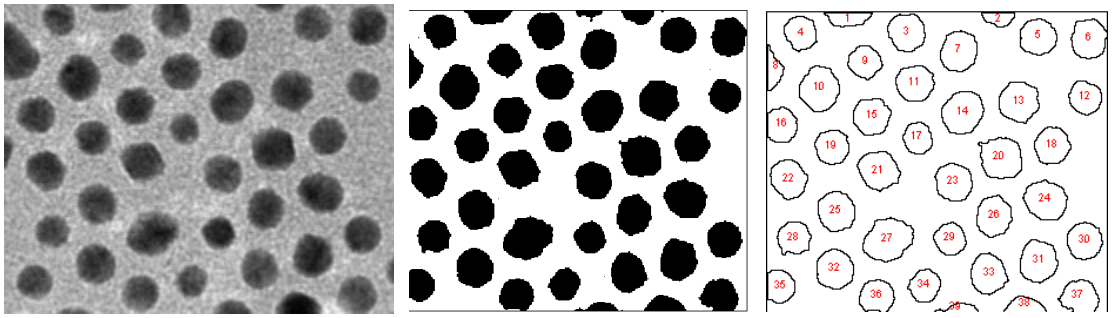

Figure 3.26 TEM image of synthesized Fe_3O_4-AuNPs (batch 3) (A) used for size distribution analysis outline (B) and count (C)

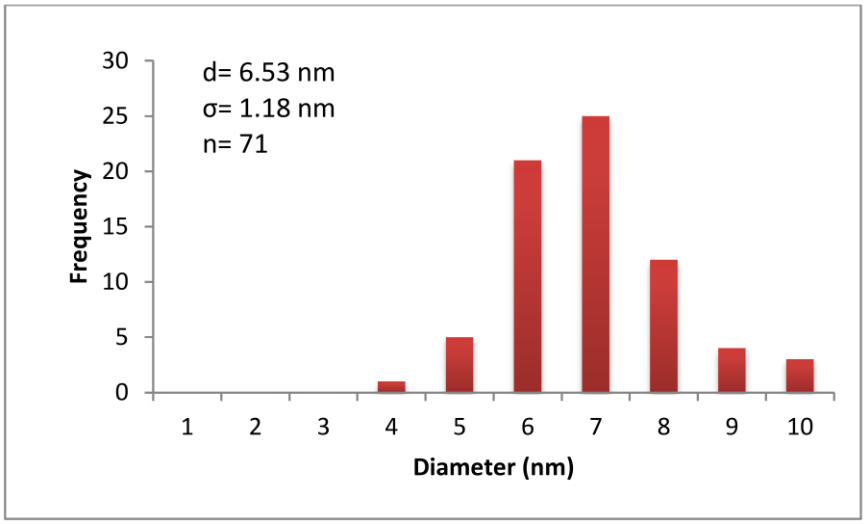

Figure 3.27 Histogram of synthesized Fe_3O_4-AuNPs (batch 3) with associated average diameter of the nanoparticles, standard deviation and number of particles analyzed. TEM image was analyzed with ImageJ software for the area of the nanoparticles.

Figure 3.28 TEM image of synthesized Fe_3O_4-AuNPs (batch 4) (A) used for size distribution analysis outline (B) and count (C)

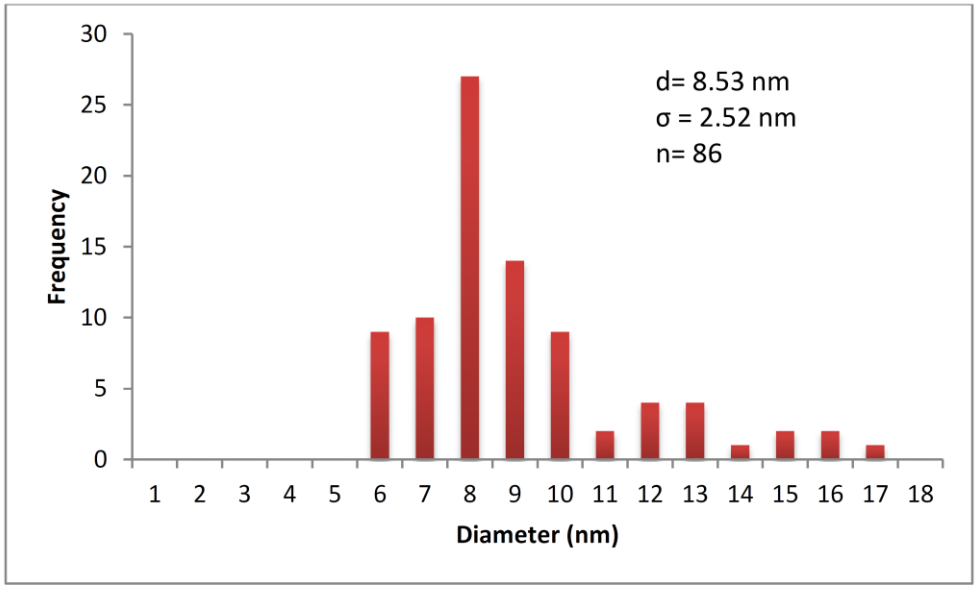

Figure 3.29 Histogram of synthesized Fe_3O_4-AuNPs (batch 4) with associated average diameter of the nanoparticles, standard deviation and number of particles analyzed. TEM image was analyzed with ImageJ software for the area of the nanoparticles.

The difference in size distribution is further supported by the UV-Vis absorption spectra of Fe_3O_4 –AuNPs produced from each synthesis (Figure 3.31). Both samples have the same expected absorption peak of between 535-550 nm, which is consistent with the predicted absorption peak for Fe_3O_4 –AuNPs.[150] Depending on the diameter of Fe_3O_4

nanoparticles and the thickness of the gold coating, the absorption of the core-shell nanoparticles can be more or less red-shifted than the Surface Plasmon resonance (SPR) characteristic of gold (approximately 525 nm for 13 nm AuNPs). The second Fe_3O_4 – AuNPs sample displays a broader peak relative to the first Fe_3O_4 –AuNPs sample (Figure 3.31, blue line). The difference in absorption could be due to size distribution or the thickness of gold coating the Fe_3O_4. Since the same Fe_3O_4 nanoparticles were used for both synthesis methods, the average diameter can be compared to determine a difference in the thickness of the gold shell of the nanoparticle. The first and second Fe_3O_4 –AuNPs synthesis resulted in an average diameter of 6.53 nm (σ= 1.18, n= 71) and 8.53nm (σ= 2.52, n= 86), respectively. With standard deviation and frequency considered, it is determined that UV-Vis absorption spectra are inconsistent due to a notable difference in size distribution between each Fe3O4-AuNP products (Figure 3.30). Both Fe_3O_4 –AuNPs products are found to be consistent with previously reported TEM/EDS and UV-VIS absorption spectra analysis. The first of these two syntheses produced mono-disperse, consistent nanoparticles that were stored until later transferred from organic to aqueous media. As previously mentioned the temperature during the synthesis Fe_3O_4 –AuNP is quite sensitive. During the second synthesis, the temperature reached approximately 200-210°C before it was returned to 180-190°C. The temperature during the previous synthesis never exceed 190-200°C. This further suggests that the temperature during the reaction is important for the formation of a mono-disperse Fe_3O_4 –AuNP product. The second synthesis yielded a thicker gold coating on Fe_3O_4, however the non-uniform size distribution would require centrifugation in order eliminate the larger particles from the sample. This would, in turn, lower the concentration of Fe_3O_4 –AuNPs further in

comparison to the previous Fe_3O_4 –AuNP product. Although centrifugation would be required to further improve the size distribution of the sample, these size distributions were acceptable for our application.

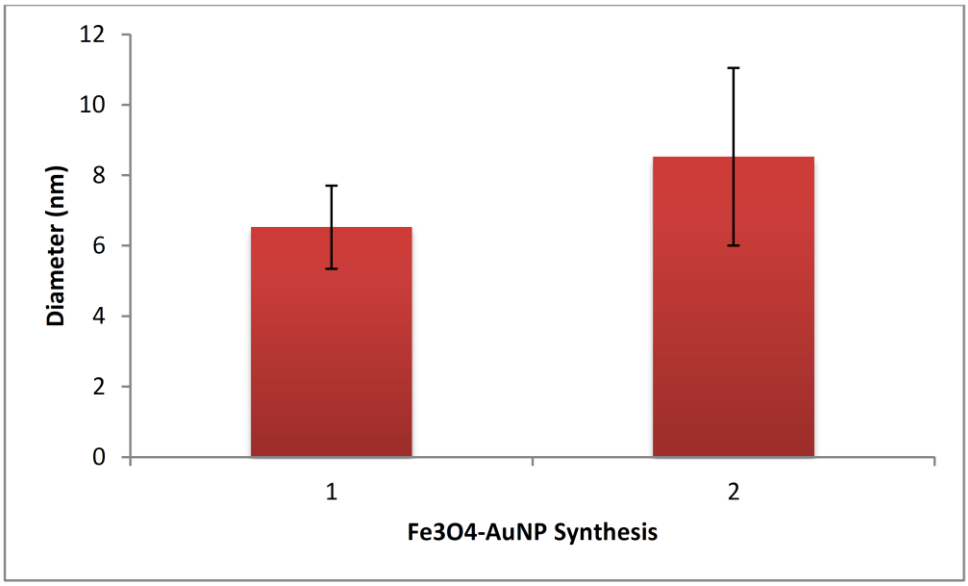

Figure 3.30 Average diameter (nm) of Fe_3O_4-AuNPs (batch 3) (left (1)) and Fe_3O_4-AuNPs (batch 4) (right (2)) with calculated standard deviations

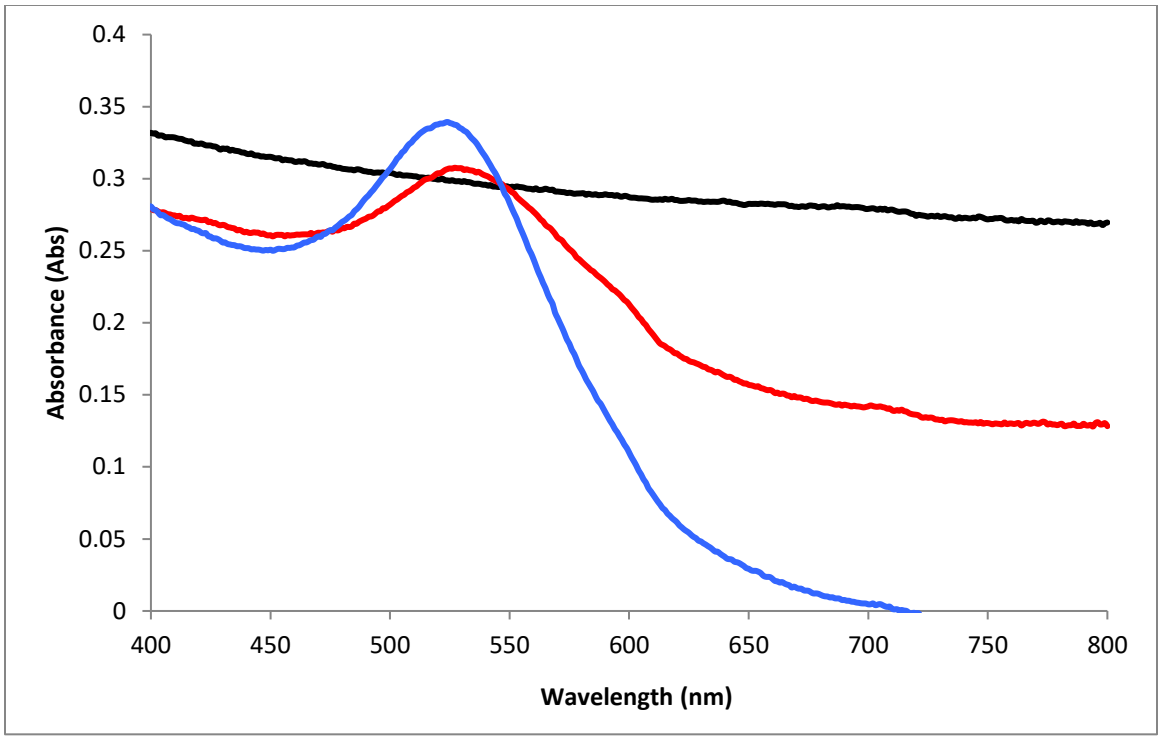

Figure 3.31 UV-Vis absorption spectra of Fe_3O_4 (batch 2) (black line), Fe_3O_4-AuNPs (batch 3) (blue line) and Fe_3O_4-AuNPs (batch 4) (red line)

3.3.3 Challenges and optimization of ligand exchange phase transfer

Although the previously described synthesis successfully coats Fe_3O_4 nanoparticle with Au to yield small, mono-disperse nanoparticles, the reaction solvent is challenging for our application. Transfer of the synthesized Fe_3O_4 –AuNPs from organic to aqueous solution is required for use in biosensor applications, specifically small molecule aptamer SELEX. In order to transfer the Fe_3O_4 –AuNPs from hexanes to water, the capping agent on the surface of the nanoparticles must be exchanged. In this case, the Fe_3O_4 –AuNPs are synthesized with oleic acid, oleylamine and 1, 2- hexadecanediol. These capping agents are soluble in hexanes, which is what the nanoparticles are dispersed and stored in post synthesis. Absolute ethanol causes solvent induced reversible aggregation of the

synthesized particles, as oleylamine and oleic acid are insoluble in this media. Therefore, this solvent can be used to wash the synthesized nanoparticles. However, the polarity of water causes the nanoparticles to experience irreversible aggregation. Polar and non-polar environments offer different advantageous and disadvantageous, depending on the synthesis method and application. The non-polar nature of the synthesized nanoparticles is problematic for our work, as the Fe_3O_4-AuNPs will be used in a bioassay to investigate non-specific aptamer-AuNP interactions. The current environment of the synthesized nanoparticles does not mimic future testing conditions and is not compatible with the bimolecular assay components. Therefore, the synthesized nanoparticle surface modifications must be exchanged to accomplish solubility in water.

Initially, transfer was based on the previously reported synthesis of Fe_3O_4 – AuNPs where the hexane soluble ligands are replaced with sodium citrate.[164] Following this protocol, the nanoparticles were precipitated and washed with ethanol until re-dispersed in tetramethylammonium hydroxide (TMAOH). TMAOH is used to remove the original capping agents from the AuNP surface, allowing for ligand exchange. Sodium citrate was then added to the solution and the solution is sonicated finally being re-dispersed in water at a pH of 6.5. This transferring method proved to be challenging and resulted in aggregation of the Fe_3O_4 –AuNPs. TEM/EDS analysis displays the extensive aggregation of the Fe_3O_4 –AuNPs (Figure 3.32). This aggregation was found to be irreversible as the nanoparticles could not be sonicated or re-dispersed back into solution. Aggregation was observed at the first addition of TMAOH and continues further when re-dispersed in water and during pH adjustments. Optimization of this method was attempted by adding TMOH incrementally over time, adding sodium citrate before or

during the addition of TMAOH and increasing the concentration of sodium citrate. However, these attempts were unsuccessful and produced an aggregated product similar to previous characterization (Figure 3.32-3.33). It is also important to note that this method of transfer results in significant loss of Fe_3O_4–AuNPs. Although visible by TEM, the coloured Fe_3O_4–AuNPs are no longer visible by eye. Since the Fe_3O_4–AuNP product is aimed to serve as a novel separation method during SELEX, the severe loss of product is problematic. This transferring method was found to be unsuccessful due to the low yield and extensive non-reversible aggregation of the Fe_3O_4–AuNPs.

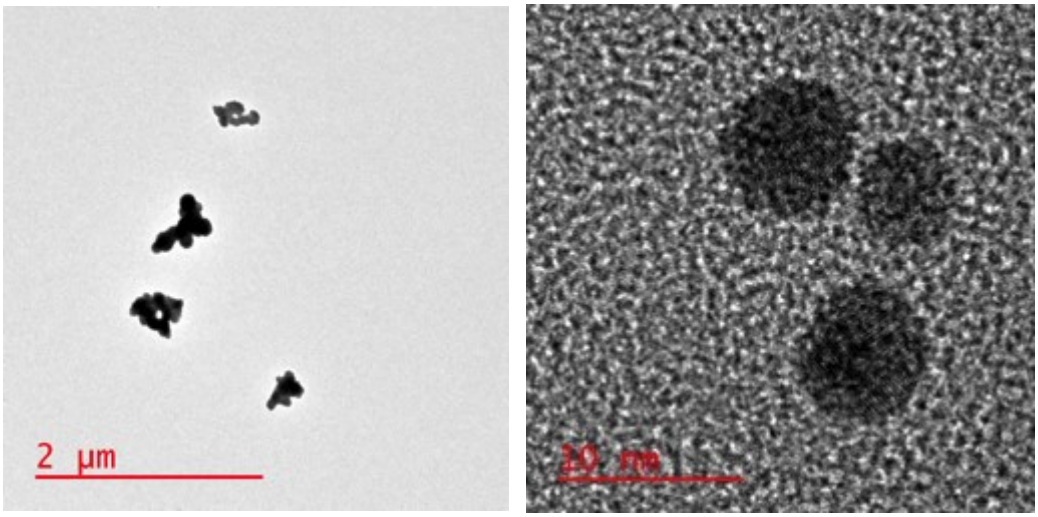

Figure 3.32 TEM images with 2 µm and 10 nm scale bars of synthesized Fe_3O_4-AuNPs (batch 3) after ligand exchange with citrate using TMAOH

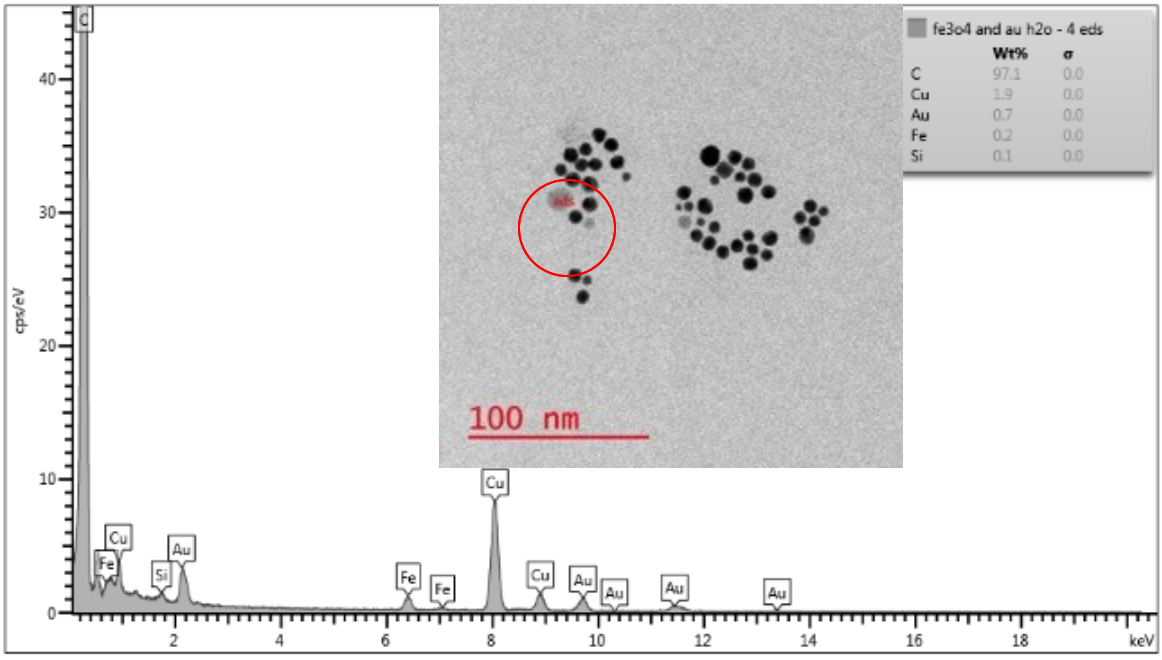

Figure 3.33 TEM image with a 100 nm scale bar of synthesized Fe_3O_4-AuNPs (batch 3) after ligand exchange with citrate using TMAOH

Phase transfer using 4-(Dimethylamino)pyridine (DMAP) as a capping agent for Fe_3O_4 –AuNPs was explored. DMAP has been successfully used as a capping agent for AuNPs and adsorb DNA molecules.[167] Therefore, replacing sodium citrate with DMAP to optimize the transfer of the Fe_3O_4 –AuNPs is reasonable. Previously reported methods successfully transferred AuNPs from organic solvent to aqueous solution with 4-(Dimethylamino)pyridine. Here, it is reported that tetraoctylammonium bromide (TOAB) was replaced with DMAP resulting in a spontaneous phase transfer of AuNPs from toluene to water within 1 hour.[156]

This method was investigated to transfer our synthesized core-shell Fe_3O_4-AuNPs. Capped with oleylamine and oleic acid in hexanes, this transfer aimed to move the synthesized Fe_3O_4-AuNPs nanoparticles into water through a DMAP ligand

exchange. Two notable differences exist between the previously reported transfer and our attempt. The nanoparticles are capped with oleylamine and oleic acid instead of tetraalkylammonium salt. In addition, the Fe_3O_4-AuNPs are being transferred from hexanes not toluene. It is predicted that the transfer will not be as rapid in comparison. Vigorous magnetic stirring and excess DMAP is required to ensure DMAP is available to the nanoparticle surface. This is because, in comparison to toluene, DMAP is not soluble in hexanes. An increase in DMAP concentration, vigorous stirring of the two solvents and an increase in reaction time aim to provide available DMAP in solution to accomplish ligand exchange. When a new ligand is available in solution, ligand exchange depends on the size, concentration and binding strength of the incoming and outgoing ligands. Partial or complete replacement of a ligand can be achieved, but mainly relies on the binding strength of the ligands with the nanoparticle surface.

This was successfully applied to transfer the Fe_3O_4 –AuNPs into aqueous solution. A 1 mL sample of Fe_3O_4 –AuNPs in hexanes was placed on top of 1 mL sample of 0.5 M DMAP solution in water. At this point, the dark purple coloured nanoparticles are seen in the top layer of the phase transfer (Figure 3.34A). Immediately, the nanoparticles began to transfer into the aqueous phase without any agitation (Figure 3.34B). Vigorous stirring for 1 hour encouraged the transfer of nanoparticles, resulting in almost complete transfer of the Fe_3O_4 –AuNP product (Figure 3.34C). The bottom layer could then be removed, purified and washed by magnetic separation and used for bioassay experiments.

Figure 3.34 Images during ligand exchange phase transfer of synthesized Fe_3O_4-AuNPs (batch 3) using DMAP before transfer in hexanes (A), during transfer (B), and after transfer in aqueous solution (C)

TEM/EDS analysis was used to characterize the DMAP transferred Fe_3O_4 –AuNPs and assess the success of the phase transfer. The Fe_3O_4 –AuNPs are much less aggregated than seen with the sodium citrate/TMAOH transfer (Figures 3.35). This is confirmed both by the colour of the solution (wine red vs. blue), the accompanying UV-Vis absorption spectra and the dispersion of particles seen by TEM (Figures 3.43-3.44). The Fe_3O_4 –AuNPs have a mono-disperse size distribution compared to the previous Fe_3O_4 –AuNP product in aqueous solution (Figure 3.35). TEM/EDS analysis displays peaks corresponding to both iron and gold, confirming that the nanoparticle product is core-shell Fe_3O_4 –AuNPs (Figure 3.36). The size distribution is consistent at 6.45 nm (σ= 1.07, n=73) (Figure 3.37-3.38). In comparison to TMAOH with sodium citrate methods, the phase transfer of Fe_3O_4 –AuNPs with DMAP was found to both decrease aggregation of the nanoparticles during transfer and increase the number of transferred particles significantly.

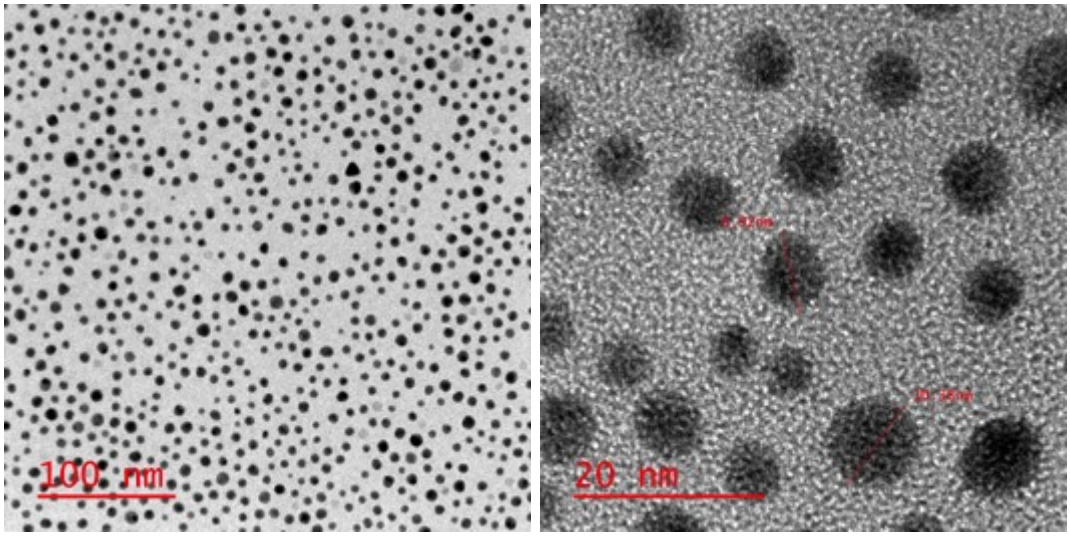

Figure 3.35 TEM images with a 100 nm and 20 nm scale bar of transferred Fe_3O_4-AuNPs (batch 3) after DMAP ligand exchange

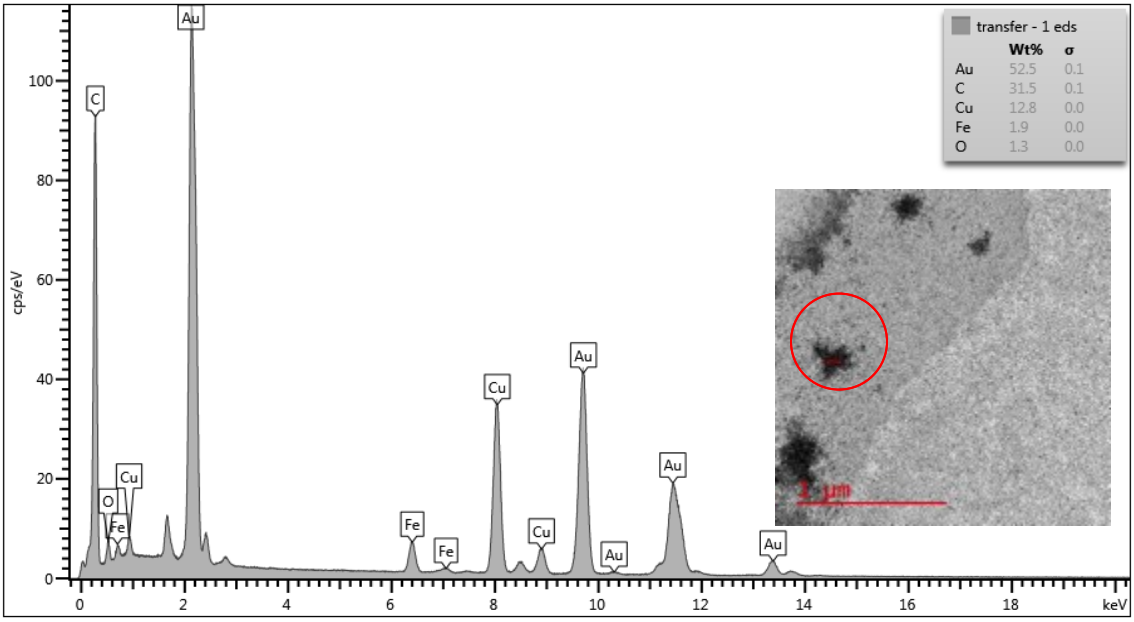

Figure 3.36 TEM image with a 1 µm scale bar of transferred Fe_3O_4-AuNPs (batch 3) after DMAP ligand exchange

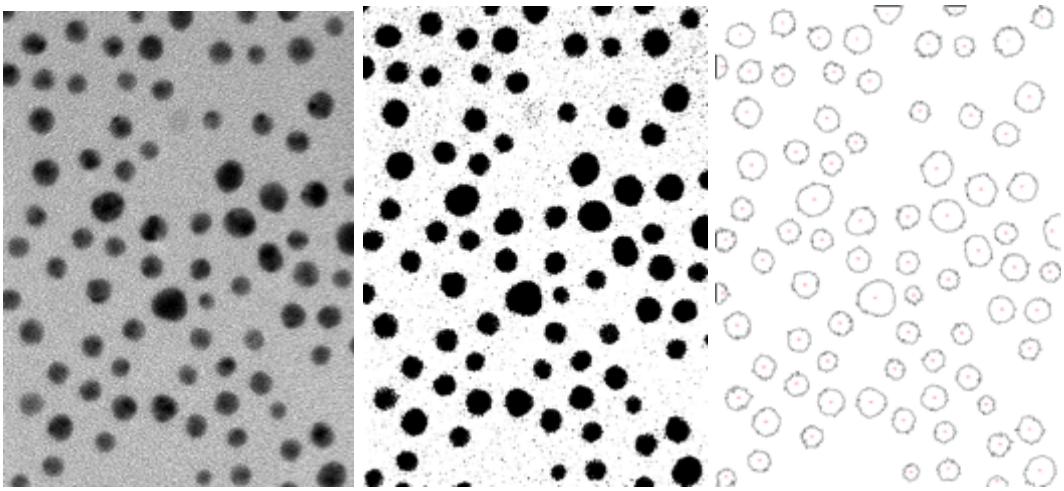

Figure 3.37 TEM image of transferred Fe_3O_4-AuNPs (batch 3) (A) used for size distribution analysis outline (B) and the area of nanoparticles (C)

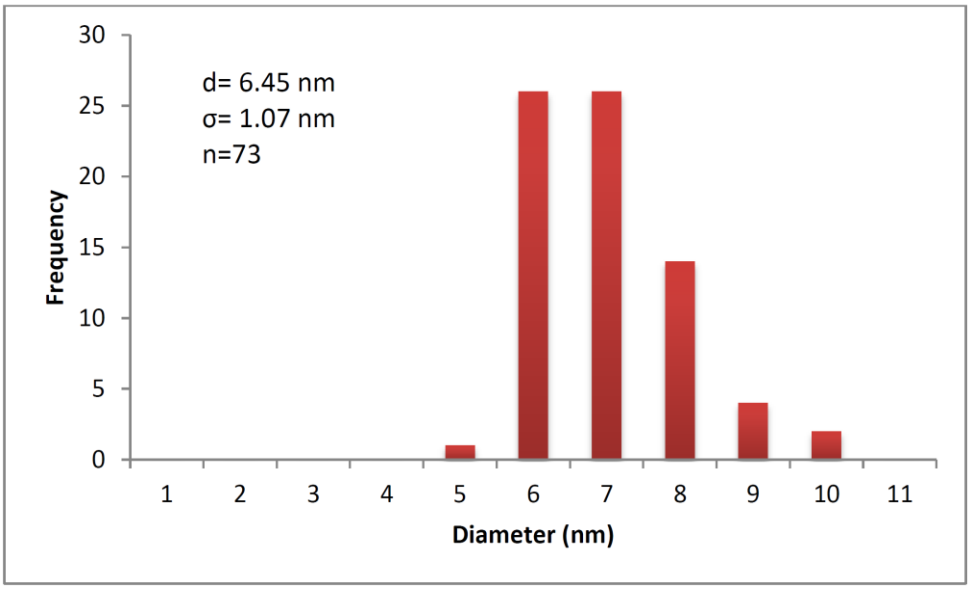

Figure 3.38 Histogram of transferred Fe_3O_4-AuNPs (batch 3) with associated average diameter of the nanoparticles, standard deviation and number of particles analyzed. TEM image was analyzed with ImageJ software for the area of the nanoparticles.

TEM/EDS analysis cannot detect nitrogen on the surface of the Fe_3O_4 –AuNP and therefore, cannot determine if the ligand exchange was successful. Similarly, UV-Vis

spectrometry analysis can not determine the exchange as the absorption spectra overlap each other at approximately 250 nm. Investigating the properties of the Fe_3O_4 –AuNPs before and after the phase transfer can confirm the DMAP ligand exchange. If the Fe_3O_4 –AuNPs are not transferred with DMAP and placed directed into deionized water, the nanoparticles agglomerate (Figure 3.39A and 3.40). Likewise, when transferred Fe_3O_4 –AuNPs are placed in a solution of hexanes, the nanoparticles remain in the water phase (Figure 3.39B). These experimental results are supportive of successful ligand exchange and phase transfer of the Fe_3O_4 –AuNPs using DMAP.

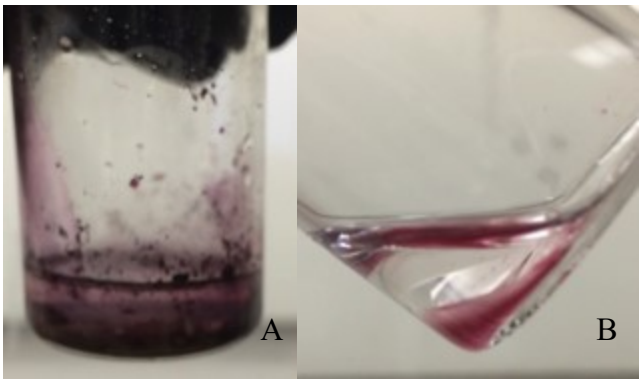

Figure 3.39 Images displaying solvent induced aggregation of the synthesized Fe_3O_4 –AuNPs. A displays Fe_3O_4 –AuNPs capped with oleylamine and oleic acid in deionized water while B displays Fe_3O_4 –AuNPs capped with DMAP in hexanes

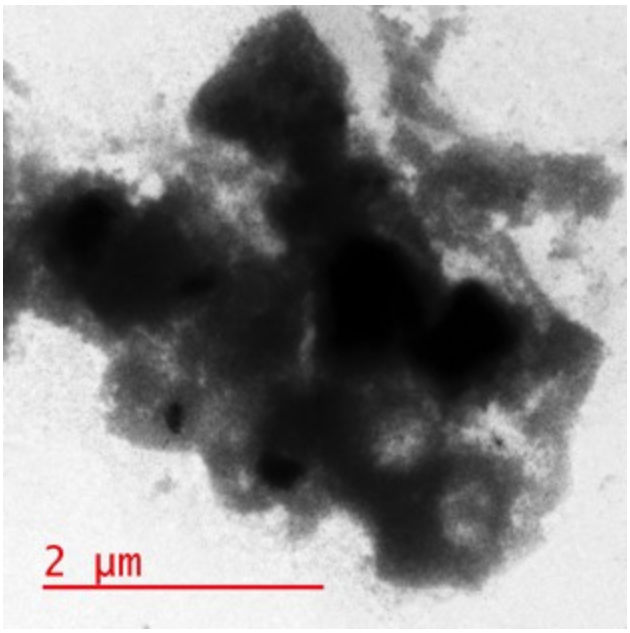

Figure 3.40 TEM image of aggregated Fe_3O_4–AuNPs with 2 µm scale bar. Sample of Fe_3O_4–AuNPs capped with oleylamine and oleic acid re-suspended in deionized water.

Precipitation of nanoparticles with DMAP was also reported.[156] In order to compare these methods, the synthesized Fe_3O_4–AuNPs were precipitated by adding DMAP to a hexane solution nanoparticles at a concentration of 0.5 M. This solution was vortexed and allowed to sit without agitation for 1 hour. At which point, the solvent was removed by decanting. The Fe_3O_4–AuNPs were then purified and washed via magnetic separation and redispersed in deionized water. Precipitation of the particles was found to successfully transfer the Fe_3O_4–AuNPs from organic to aqueous solution. TEM/EDS analysis displays the presence of core-shell Fe_3O_4–AuNPs (Figures 3.41-3.42). However, the size distribution and composition of the transferred Fe_3O_4–AuNPs is slightly better than the precipitated Fe_3O_4–AuNPs. Figures 3.43 show the two samples of Fe_3O_4–AuNPs. When placed on the magnet the transferred sample has clearer separation (Figure 3.43). The precipitated Fe_3O_4–AuNPs could be precipitated and washed with magnetic

separation, however this would only result in a decreased concentration. Comparing the UV-Vis absorption spectra confirms that transferring the Fe_3O_4 –AuNPs is advantageous, as the sample is more concentrated and displays a sharper peak at approximately 530 nm (Figure 3.44).

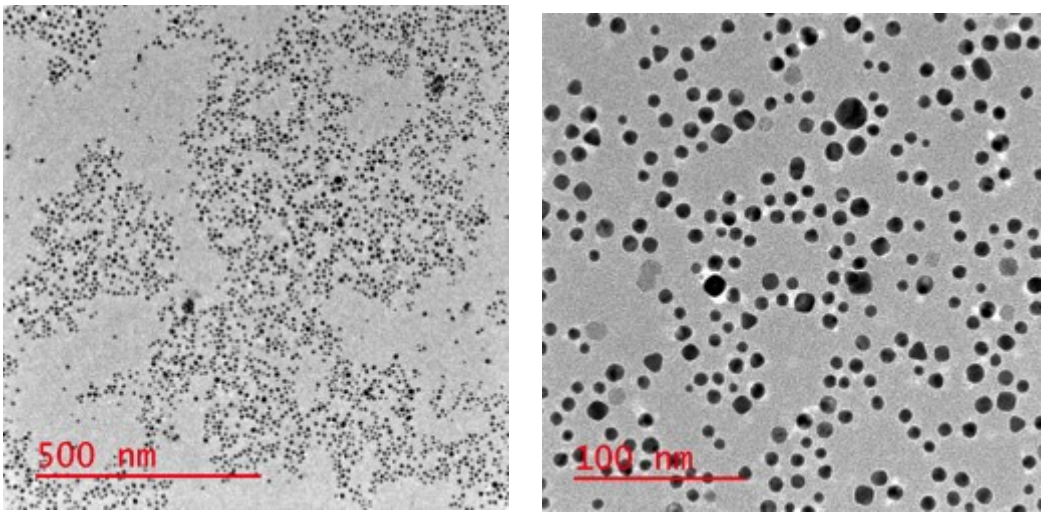

Figure 3.41 TEM images with 500 nm and 100 nm scale bars of precipitated Fe_3O_4-AuNPs (batch 3) after DMAP ligand exchange

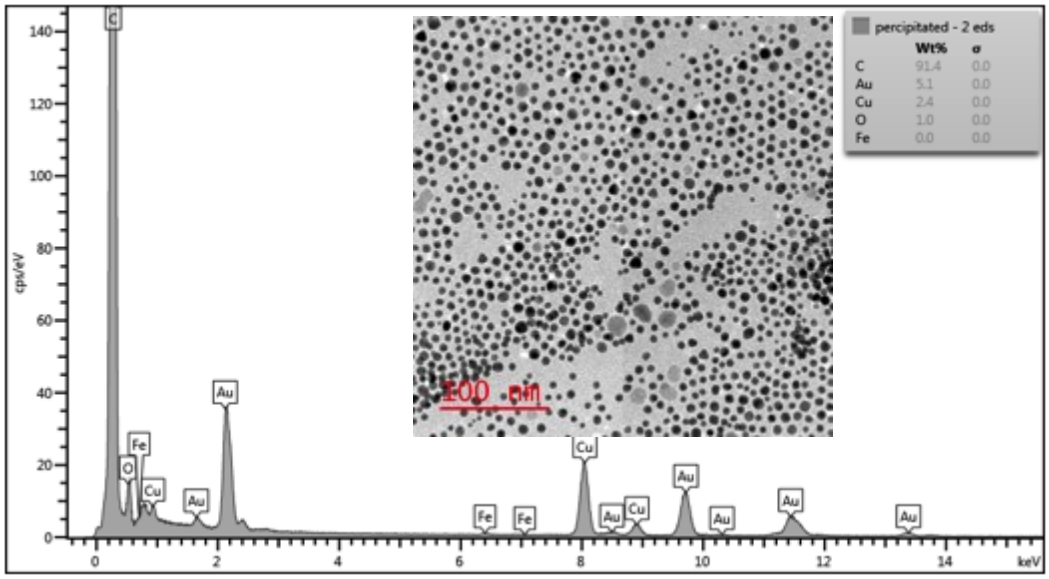

Figure 3.42 TEM image with a 100 nm scale bar and corresponding EDS analysis of precipitated Fe_3O_4-AuNPs (batch 3) after DMAP ligand exchange

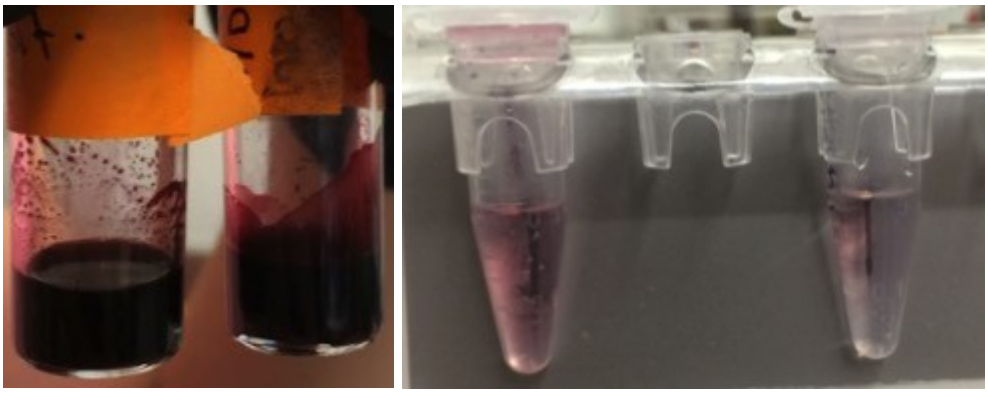

Figure 3.43 Images of DMAP capped Fe_3O_4-AuNPs (3) after precipitation with DMAP in hexanes (left) and ligand exchange transfer with DMAP in aqueous solution (right)

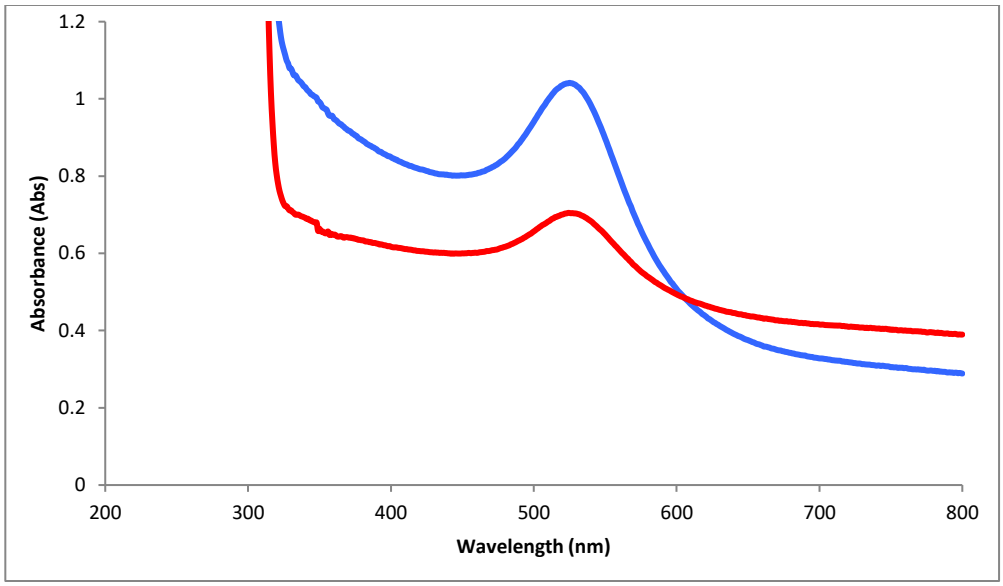

Figure 3.44 UV-Vis absorption spectra of transferred Fe_3O_4-AuNPs (batch 3) (blue line) and precipitated Fe_3O_4-AuNPs (batch 3) (red line)

In conclusion, DMAP was used to successfully transfer the Fe_3O_4–AuNPs via liquid-liquid extraction with vigorous stirring for 1 hour. The Fe_3O_4–AuNPs were stable in aqueous solution for approximately 1-2 months. Transferring the Fe_3O_4–AuNPs within days of using the sample for bioassay and SELEX applications was found to be advantageous due to the increased stability of the Fe_3O_4–AuNPs in hexanes post synthesis. It was noted that the DMAP capped Fe_3O_4–AuNPs seemed to be inhibited by solvent during magnetic separation as high concentrations of nanoparticles required a longer time to separate from solution and a stronger magnetic source.[93]

3.3.4 Investigation and confirmation of synthesized Fe_3O_4-AuNP EDS results

In an attempt to determine if the TEM/EDS analysis of nanoparticle composition is accurate enough to distinguish Fe_3O_4 –AuNPs from separate Fe_3O_4 nanoparticles and AuNPs, a sample of mixed Fe_3O_4 nanoparticles and AuNPs (1:1 ratio) was investigated. Within the sample, there were Fe_3O_4 nanoparticles and AuNPs in close proximity to one another (Figure 3.45). TEM/EDS analysis was used to characterize both nanoparticles in the sample. The Fe_3O_4 nanoparticles did not show any peak for gold, and the AuNPs did not display any more iron that is already found within the grid (Figure 3.46). This supports the characterization of Fe_3O_4-AuNPs by TEM/EDS and confirms that the EDS peaks for iron and gold are coming from within the same core-shell nanoparticle and not from another particle close by.

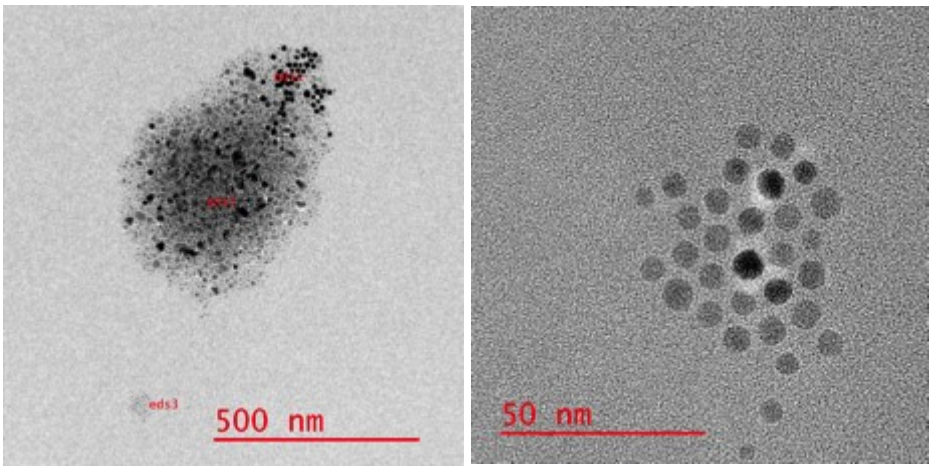

Figure 3.45 TEM images of a sample of Fe_3O_4 and AuNPs in solution with 500 nm and 50 nm scale bars

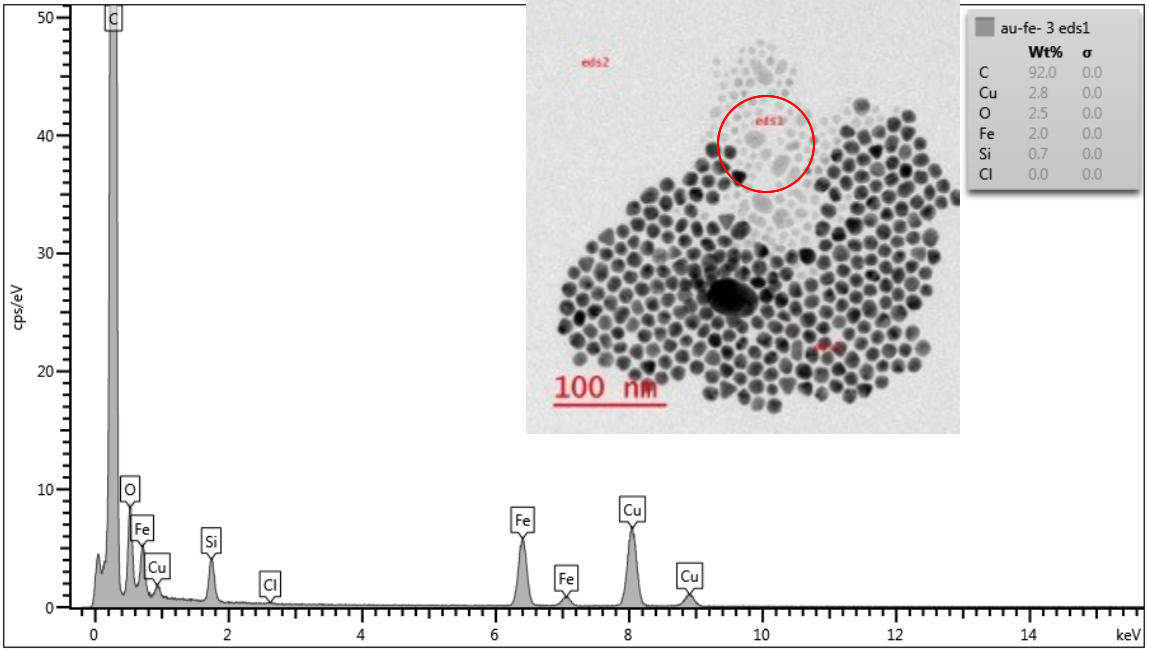
au-fe- 3 eds1
Wt% σ
C 92.0 0.0
Cu 2.8 0.0
O 2.5 0.0
Fe 2.0 0.0
Si 0.7 0.0
Cl 0.0 0.0
100 nm
cps/eV
keV
C
O
Fe
Cu
Si
Cl
Fe
Fe
Cu
Cu

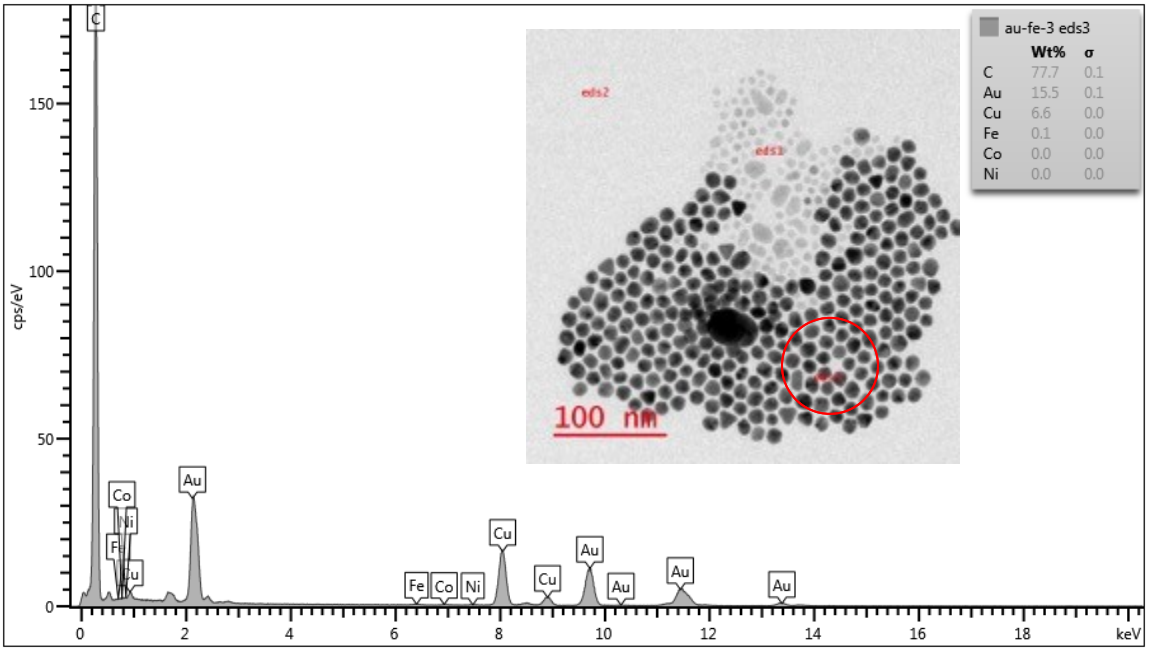
au-fe-3 eds3
Wt% σ
C 77.7 0.1
Au 15.5 0.1
Cu 6.6 0.0
Fe 0.1 0.0
Co 0.0 0.0
Ni 0.0 0.0
100 nm
cps/eV
keV
C
Co
Ni
Fe
Cu
Au
Fe
Co
Ni
Cu
Au
Au
Au
Au

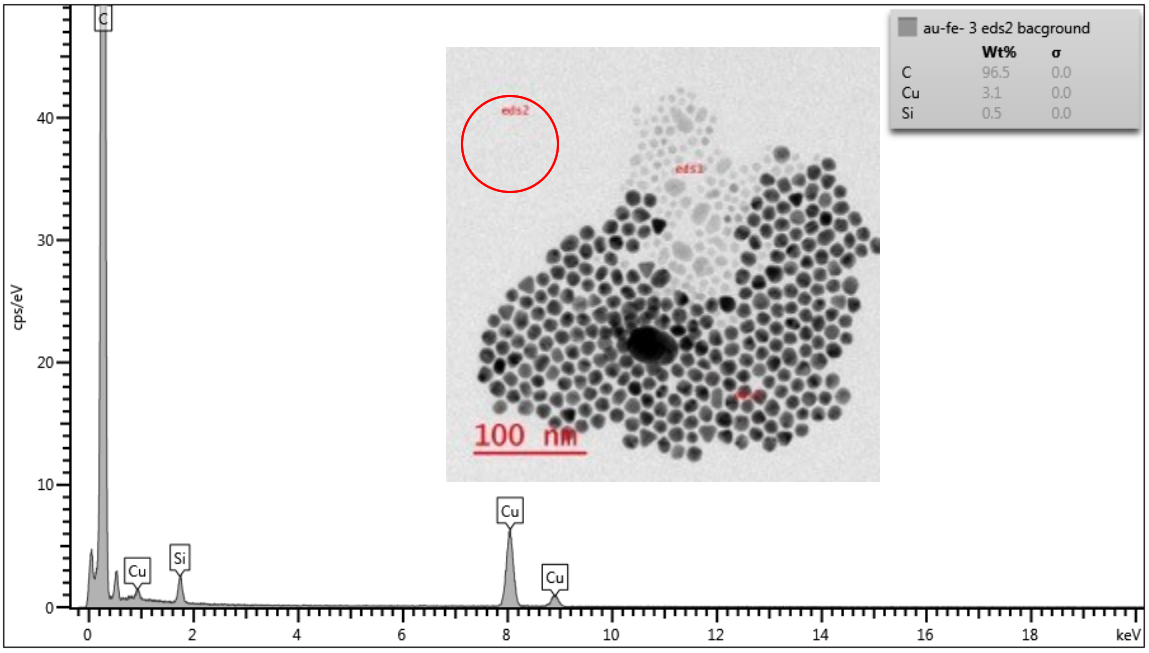

Figure 3.46 TEM image with a 100 nm scale bar and corresponding EDS analysis of various areas on the sample; the Fe_3O_4 nanoparticles (top), the AuNPs (middle) and the background TEM grid (bottom)

The ability for AuNPs without a magnetic core to remain in solution after magnetic separation was questioned. As previously mentioned, a 1:1 sample of Fe_3O_4 nanoparticles and AuNPs was prepared. The solution was placed on the magnet for 30 mins, at which point the supernatant and nanoparticles precipitated on the magnet were separated for analysis. TEM/EDS analysis clearly displays only Fe_3O_4 nanoparticles are present in the solution of nanoparticles precipitated on the magnet (Figures 3.47), and only AuNPs are present in the supernatant solution (Figure 3.48). It is important to note one fundamental difference between this study and the actual synthesis. In this experiment, the Fe_3O_4 nanoparticles and AuNPs are synthesized separately with two different capping agents. However, AuNPs that formed during the synthesis of Fe_3O_4 - AuNPs are in the presence of Fe_3O_4 nanoparticles. Furthermore, the nanoparticles are

coated with capping agents that are insoluble in ethanol and experience solvent induced reversible aggregation (Figure 3.49) to encourage magnet precipitate. Since Fe_3O_4-AuNPs or AuNPs without a magnetic core have the same capping agent, solvent effects could influence the presence of AuNPs in the supernatant solution. Therefore, there are two reasons that AuNPs could remain in solution after post Fe_3O_4-AuNP synthesis magnetic purification. However, it is also important to note that after the nanoparticles are transferred with DMAP into aqueous solution, the nanoparticles no longer experience solvent induced reversible aggregation. Therefore, this bias is removed and hypothetically the AuNPs without a magnetic core should be separated from solution during magnetic separation.

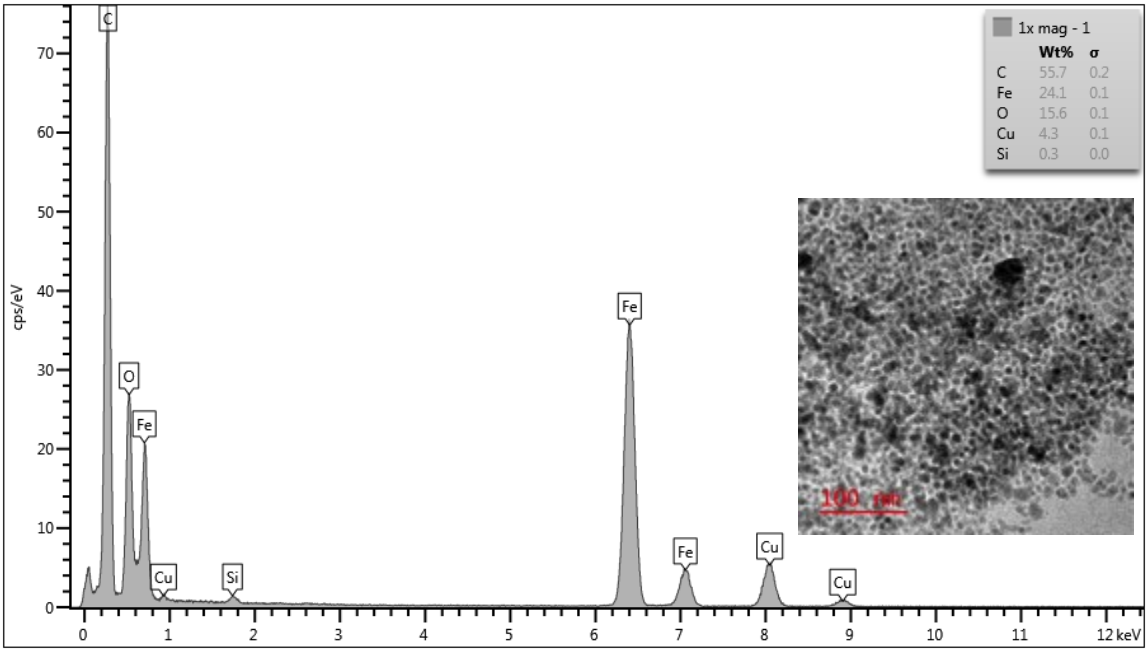

Figure 3.47 TEM image with a 100 nm scale bar and associated EDS analysis of nanoparticles on the magnet after a mix of Fe_3O_4 nanoparticles and AuNPs were separated by magnetic separation

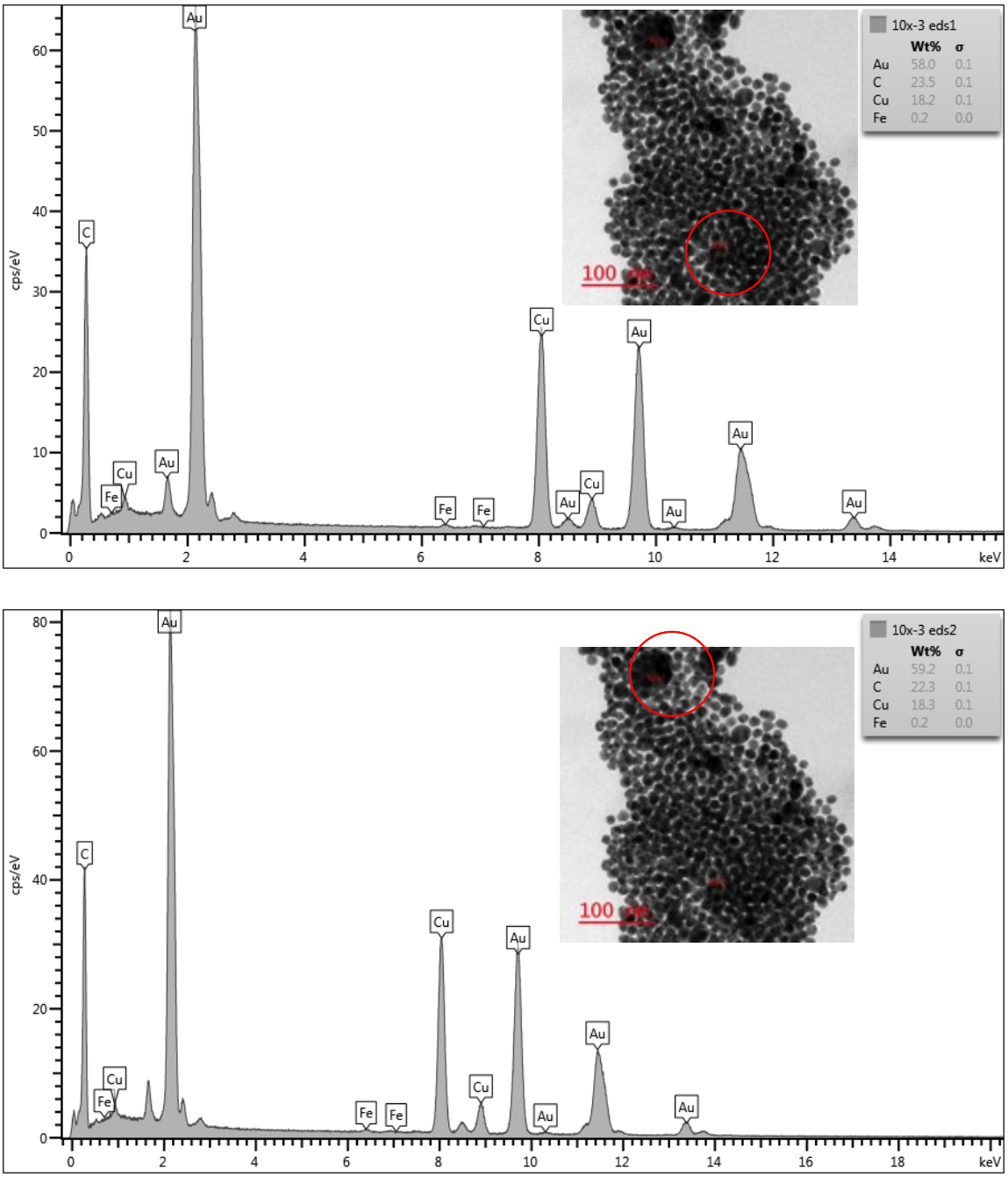

Figure 3.48 TEM image with 100 nm scale bar and associated EDS analysis of nanoparticles in the supernatant after a mix of Fe_3O_4 nanoparticles and AuNPs were separated by magnetic separation

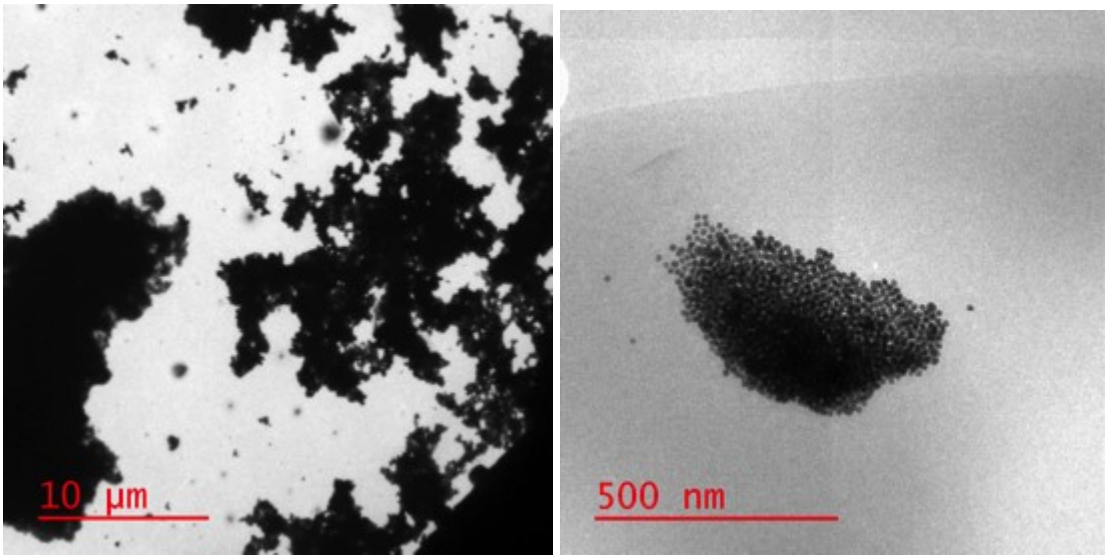

Figure 3.49 TEM images with 10 µm and 500 nm scale bars of aggregated Fe_3O_4-AuNPs after solvent induced aggregation with ethanol

3.4 Conclusions

Based upon previous reported methods by Robinson et al. and Wang et al., this work confirms the importance of temperature during the synthesis of core-shell Fe_3O_4-AuNPs.[124,164] It was found that temperature influences both the size and dispersion of the core Fe_3O_4 nanoparticle and the uniform, successful coating of the Fe_3O_4 with Au. Our studies confirm that precise temperature of 210°C during the synthesis is required; even temperatures of 190°C and 258°C hinder the production of monodisperse particles. Secondly, we determined that the controlled increase in temperature, 180-190°C at a rate of 10°C/ minute, had the largest influence on the final core-shell product.

In this work, we also transferred synthesized Fe_3O_4-AuNPs in hexanes to water via a ligand exchange with DMAP. The transfer of nanoparticles can be seen between the two solvent phases after 2-3 hours with vigorous stirring. We confirmed ligand exchange through solubility experiments and confirmed the transfer of synthesized nanoparticles

with HRTEM. The quick and gentle transfer of Fe_3O_4-AuNPs with DMAP avoided previously encountered aggregation with TMAOH and sodium citrate. This method also increased the yield of Fe_3O_4-AuNPs in the aqueous phase. Both of these improvements were essential in developing an aqueous based AuNP magnetic separation method for the investigation of ssDNA-AuNP interactions, which will be discussed in the following chapter.

3.5 Acknowledgements

Thank you to Jianqun Wang for producing TEM images with EDS data of all the studied nanoparticle samples.

Chapter 4: A novel library partitioning method for small molecule SELEX using magnetic gold nanoparticles

4.1 Introduction

4.1.1 Adsorption of DNA onto DMAP capped AuNPs

The positive surface charge resulting from the position of DMAP on Fe_3O_4-AuNPs is advantageous for biomolecular interactions; namely, the adsorption of negatively charged species such as DNA. As an example, Biver et al. investigated the interaction of calf thymus DNA and whole cells with DMAP capped AuNPs.[167] First, the authors determined that free DMAP and DNA did not interact. Next, the authors studied the interaction between DNA and DMAP capped AuNPs.

$$AuNP + DNA \leftrightharpoons DNA \cdot AuNPs \qquad \textbf{Equation 11}$$

Assuming the above interaction between DNA and DMAP-capped AuNPs, Biver and co-workers[167] derived the following equation to analyze the binding isotherm of DMAP-AuNPs and calf thymus DNA:

$$\frac{\Delta A}{C_{AuNPs}} = \frac{K\Delta\mathcal{E}[S]}{(1 + K[S])} \qquad \textbf{Equation 12}$$

where ΔA is the difference in absorption between the AuNP-DNA complex and the AuNP alone, $\Delta\mathcal{E}$ is the difference between $\mathcal{E}_{ssDNA-AuNPs}$ and $\mathcal{E}_{AuNPs}$, C_{AuNPs} is the concentration of Au, and [S] is the concentration of DNA was derived. A binding isotherm for DMAP capped AuNPs and DNA was plotted, and the equilibrium constant of this interaction was estimated based on this model ($(2.8 \pm 0.8) \times 10^5$ M^{-1}). While this is

a relatively strong interaction, it is important to note that calf thymus DNA is approximate 800 bps of dsDNA, compared to the shorter ssDNA aptamers that are typically adsorbed onto AuNPs.[167]

Most recently, it has been proposed that the main stabilizing force in the adsorption of DNA and citrate capped AuNPs is the interaction between the exposed bases of flexible ssDNA and the AuNP surface.[79,80] However, DMAP capped stabilization results in an overall partially positive surface.[157] Therefore, it is suggested that the negatively charged backbone of dsDNA or ssDNA is able to interact and adsorb to the DMAP capped AuNP surface. This explains why Biver et al. observed adsorption of dsDNA onto the surface of DMAP capped AuNPs.[167] For SELEX purposes, the adsorption of dsDNA and ssDNA is important to consider; therefore, adsorption of ssDNA aptamers (differing in length and structure) onto DMAP capped Fe_3O_4-AuNP must be investigated and tested as a potential platform for AuNP-based SELEX.

4.1.2 Gold nanoparticle-based SELEX using Fe_3O_4-AuNPs for separation

By employing Fe_3O_4-AuNPs for SELEX partitioning, the efficiency of magnetic separation can be applied without the need for immobilizing the small molecule target. The general workflow begins with an initial library of random DNA sequences adsorbed onto the surface of a known volume of Fe_3O_4-AuNPs. Next, a magnet is used to pull the Fe_3O_4-AuNPs to the side of the tube, permitting easy removal of the supernatant containing the non-binding DNA sequences. At this point, the isolated Fe_3O_4-AuNPs with adsorbed putative aptamer sequences can be introduced to the target molecule directly in solution. During this step, the aptamers with affinity for the target molecule

will leave the Fe_3O_4-AuNP surface to bind to the target molecule in solution. Finally, magnetic separation can be used again to partition the aptamer-target complex from the non-binding aptamers that remain on the Fe_3O_4-AuNP surface (Figure 4.1).

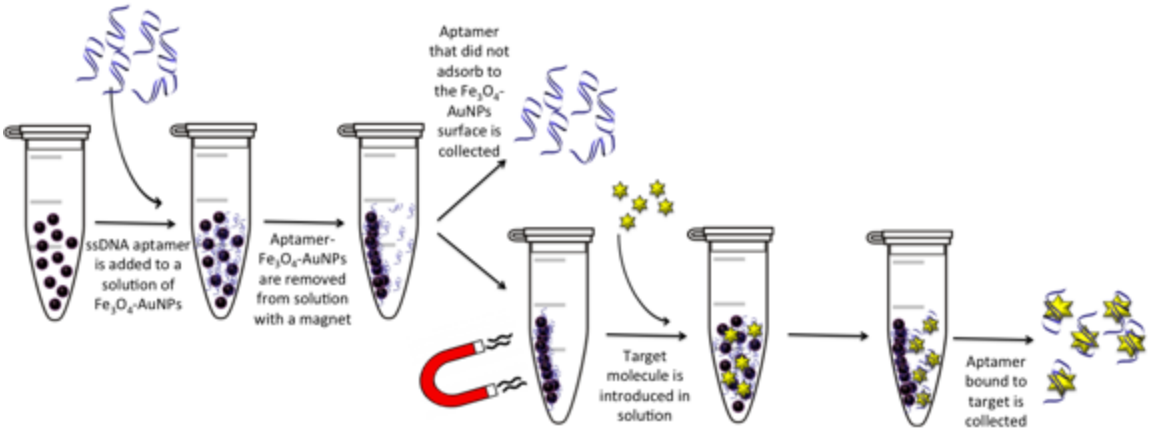

Figure 4.1 Partitioning via magnetic separation for Fe_3O_4-AuNP-based SELEX. After ssDNA (blue ribbons) are adsorbed onto the core-shell Fe_3O_4-AuNP surface (purple circles), the AuNPs can be separated from solution with a magnet. The supernatant containing the sequences not adsorbed to the Fe_3O_4-AuNPs in solution can be removed. Following the target (yellow star) incubation, the non-binding sequences that remain on the Fe_3O_4-AuNP surface can be separated. The binding sequences interact with the target in solution and can be collected.

4.1.3 Chapter Objectives

This chapter describes the assessment and optimization of the previously synthesized DMAP capped Fe_3O_4-AuNPs as an improved separation method for AuNP-based SELEX. First, the adsorption of various DNA aptamer sequences onto DMAP capped Fe_3O_4-AuNPs will be investigated. The adsorption will be compared to citrate capped AuNPs (chapter 2). Next, the adsorption mechanism will be analyzed further by competitively adsorbing various aptamer sequences onto the surface of DMAP capped

Fe_3O_4-AuNPs. Finally, to compare and evaluate the developed partitioning method, we will attempt to selectively remove aptamers with affinity for a specific target molecule. A proof of concept selectivity experiment will be used to gauge the reliability and selectivity of magnetic separation using Fe_3O_4-AuNPs for AuNP based SELEX. This method can also be compared to centrifugation by considering the amount of AuNPs left in solution after separation.

4.2 Experimental

4.2.1 Materials

Phosphoramidites, 1000 Å pore size controlled glass pore (CGP) columns, Glen-Pak DNA purification cartridges, 2 M triethylamine acetate (TEAA) and 2% trifluoroacetic acid (TFA) were purchased from Glen Research (Sterling, VA, USA). Ochratoxin A (OTA) was purchased from Sigma-Aldrich (St. Louis, MO, USA).

4.2.2 DNA aptamer synthesis, purification and quantification

All aptamers and primers were synthesized a BioAutomation Mermade 6 oligonucleotide synthesizer (Plano, Texas). The unmodified aptamer sequences were synthesized through standard phosphoramidite chemistry using 1 μmol controlled glass pore (CGP) columns with a 1000 Å pore size. Forward primers were modified with 5'-fluorescein phosphoramidite (Glen Research) and reverse primers were modified with 5'-spacer phosphoramidite 18 (Glen research). Aptamer sequences and reverse primers were left with DMT-ON during synthesis. To cleave the sequences after synthesis, the beads were placed in a 1.5 mL eppendorf tube with 1 mL of ammonium hydroxide (NH_4OH)

and allowed to incubate overnight at 55 °C. The tubes were removed from heat and allowed to cool for at least 30 mins. The solution was centrifuged to pellet the beads and the supernatant, containing the sequences, was removed and placed in a clean 2 mL eppendorf tube. The beads were washed with 1 mL of a 100 mg/mL sodium chloride (NaCl) solution and centrifuged to pellet the beads. The supernatant was removed and added to the same 2 mL eppendorf tube. Forward primers were washed with 1 mL of deionized water instead of 100 mg/mL sodium chloride (NaCl). The tubes for the forward primers were placed on Savant AES2010 SpeedVac overnight or until dry.

All synthesized sequences (DMT-ON) were purified through Glen-Pak purification methods. The Glen-Pak DNA purification cartridges were placed in the manifold ports and 15 mL collection tubes were placed beneath these ports. The vacuum was attached to the manifold, turned on and adjusted to approximately 7 mm Hg. To wet the cartridges, 0.5 mL of acetonitrile was added to each cartridge and allowed to flow through the ports into the collection tubes. This was followed by 1 mL of 2 M triethylamine acetate (TEAA), which was collected in the same 15 mL tubes. The DNA samples were applied to the cartridges in 1 mL aliquots and collected in the same 15 mL tubes. Each cartridge was then washed twice with 1 mL of a salt wash solution (5% Acetonitrile in 100 mg/mL Sodium Chloride solution), twice with 1 mL of 2% trifluoroacetic acid (TFA) and twice with 1 mL of deionized water. A faint orange band appeared in the cartridge when TFA was added, indicating the removal of DMT. The collection tubes were replaced with new 15 mL tubes before the DNA was eluted from the cartridge. The cartridge was washed twice with 1 mL of 50% acetonitrile in deionized

water with 0.5% ammonium hydroxide, and the eluted DNA was collected. The DNA was quantified using a Cary 300 Bio UV-Vis Spectrometer (Varian, USA) at 260 nm.

Table 4.1 List of synthesized unmodified ssDNA aptamer sequences for a proof of concept Fe_3O_4-AuNP based SELEX study

DNA Aptamer	Sequence	Length	Aptamer mass g/mol
1.12.2	5'- GATCGGGTGTGGGTGGCGTAAAGGGAGCATCGG ACA-3'	36	11311.4
Dop	5'-GTCTCTGTGTGCGCCAGAGAC AGTGGGGCAGATATGGGCCAGCACAGAATGAGGCCC-3'	58	17709.5
FB139	5'-ATACCAGCTTATTCAATTAATCGCATT ACCTT AT ACCAGCTTATTCAATTACGT CT GCACAT ACCAGCTT ATTCA ATT AGATAGTAAGTGC AATCT-3'	96	29340.2

4.2.3 Fe_3O_4-AuNP assay

4.2.3.1 Preparation and washing of DMAP capped Fe_3O_4-AuNPs

Six 1.5 mL Eppendorf tubes were labeled as blank and test samples, then placed on the Dynamag magnet holder . 100 µL of Fe_3O_4-AuNPs were placed in each tube with 900 µL of deionized water. The tubes were left on the magnet for 30 mins and the supernatant was removed. This was repeated twice to wash the Fe_3O_4-AuNPs, and the Fe_3O_4-AuNPs were redispersed in 800 µL. 900 µL of deionized water was placed in 3 1.5 mL Eppendorf tubes and were labelled at control samples.

4.2.3.2 Preparation of aptamer dilutions

1 mL of 10 μM DNA aptamer was prepared and heated to 90 °C for 5 mins and allowed to cool to room temperature for approximately 15-30 mins. When three sequences were added to Fe_3O_4-AuNPs competitively, 1 mL of each sequence was prepared at a concentration of 10 μM. 1 mL of each sequences was mixed together in the same 1.5 mL Eppendorf tube and heated together for 5 mins to 90°C and cooled to room temperature for 15-30 mins.

4.2.3.3 Preparation of target molecule (OTA)

Purchased ochratoxin A (OTA) was dissolved in 1 mL of deionized water and placed on a shaker at room temperature overnight. The solution was filtered through 0.5 mL Corning Costar Spin-X centrifuge filter tubes. The filtrate was collected and quantified by UV-Vis absorption spectroscopy at 330 nm. 10 μM of OTA was prepared in deionized water and stored at room temperature.

4.2.3.4 Introduction of aptamer to Fe_3O_4-AuNPs

100 μL of 10 μM DNA was added to control samples and test sample tubes containing 100 μL of washed Fe_3O_4-AuNPs and 800 μL of deionized water. 100 μL of water was added instead of DNA to the blank sample tubes. The tubes were vortexed quickly and allowed to incubate at room temperature for 30 mins on a shaker at a low setting.

4.2.3.5 Removal of non-binding DNA sequences

After 30 mins, the tubes were placed on a Dynamagnet for 30 mins. The supernatant solution was removed and placed in the new appropriate 1.5 mL tube for analysis.

4.2.3.6 Introduction of target molecule (OTA)

100 µL of 10 µM OTA and 800 µL of deionized water were added to the Fe_3O_4-AuNPs after removal of non-binding DNA sequences. The tubes were once again vortexed quickly and allowed to incubate at room temperature for 30 mins on a shaker at a low setting. After 30 mins, the tubes were placed on a Dynamag magnet for 30 mins. This supernatant solution was removed and collected in the new appropriate 1.5 mL tube for analysis.

4.2.3.7 PAGE analysis of proof–of-concept SELEX study

The collected DNA sequences were mixed with formamide in a 1:1 volume ratio, vortexed quickly and heated to 90 °C for 5 mins. 80 µL of each tube of DNA was loaded into different individual wells and the gel was run at 300 V between 2-3 hours.

4.2.3.8 Imaging and analyzing the PAGE gel

After the gel run was complete, the gel was placed on a 20 cm by 20 cm TLC plate with plastic wrap. The gel was imaged using an Alpha Imager Multi Light Cabinet (Alpha Innotech). The intensity of each UV-Vis absorption band was found and analyzed with Image J software.

4.3 Results and Discussion

4.3.1 Investigating DMAP capped Fe_3O_4-AuNPs as a SELEX separation method

Since previously reported SELEX partitioning methods were unsuitable for our application, core-shell Fe_3O_4-AuNPs were synthesized as a magnetic separation method. An initial library of ssDNA aptamers could be adsorbed onto the surface of Fe_3O_4-AuNPs, as the shell properties are consistent with those of AuNPs. Magnetic separation could provide a more gentle separation method in comparison to centrifugation. Centrifugation has been successfully used to separate ssDNA aptamer-AuNPs from free ssDNA aptamer when the aptamer is bound to the AuNP surface through a specific thiol covalent bond.[168] However, the force required to pellet the AuNPs out of solution by centrifugation may disrupt the relatively weak interaction between ssDNA aptamers and AuNPs. The magnetic core of the synthesized Fe_3O_4-AuNPs allows for the nanoparticles to be separated from solution in the same way, but removes the physical force required when separating by centrifugation. Therefore, the quick and gentle separation of AuNPs with a magnetic core is investigated as a partitioning method for AuNP SELEX.

First, the capacity of the synthesized Fe_3O_4-AuNPs was examined. The capacity of the Fe_3O_4-AuNPs was compared to the experimentally-estimated capacity of AuNPs for ssDNA via separation by centrifugation. This capacity must be estimated to ensure it is compatible with the large libraries required for SELEX. As an example, if the required volume of synthesized Fe_3O_4-AuNPs to adsorb an entire 1000 pmol initial library of ssDNA aptamers was over 10 mL, manipulation would be difficult and would not be compatible with the following PCR step required in SELEX.

One limiting factor for separation with magnetic nanoparticles is the size and solubility of the nanoparticle surface in solution: the synthesized Fe_3O_4-AuNPs are relatively small in size and the capping agent used to transfer the Fe_3O_4-AuNPs into aqueous media is soluble in water. Both the relatively small size and solubility of the nanoparticles increase the applied magnetic force required to separate the particles from solution. Thus, to achieve quick and complete separation, the Fe_3O_4-AuNPs were diluted 10 times in water.

To assess capacity, a known individual or combination of ssDNA aptamer sequences were introduced to a solution of Fe_3O_4-AuNPs and allowed to incubate at room temperature. After incubation, the Fe_3O_4-AuNPs were separated from solution and the aptamers that did not adsorb to the Fe_3O_4-AuNP surface remained in solution. These sequences left in the supernatant were collected and analyzed by gel electrophoresis. The capacity (or amount of aptamer adsorbed onto the Fe_3O_4-AuNPs surface) was determined by comparing the band intensity of the amount of aptamer added (control) and the amount of aptamer in the supernatant (Figure 4.2).

We next examined the effect of aptamer lengths and structure on the separation via Fe_3O_4-AuNPs magnetic separation. We included a variety of aptamers to elucidate any bias in the separation of these sequences. Previously, using the centrifugation method, there appeared to be a bias during separation that resulted from aptamer length. It was suggested through the salt aggregation test, that the interaction between longer aptamer sequences and AuNPs were not disturbed when centrifuged. However, the salt aggregation assay varied with centrifugation for the shorter aptamer sequences. This bias is problematic when analyzing the adsorption and desorption of aptamers on an AuNP

surface for SELEX applications. Therefore, the sequences used for proof-of-concept SELEX analysis need to be compared with this method. The adsorption and desorption of each sequence when incubated individually or competitively can provide insight into any potential bias between the tested sequences.

Finally, as a SELEX platform, the specific removal of aptamers with affinity for a target molecule should be evaluated for Fe_3O_4-AuNPs. Previously, separation through centrifugation resulted in the non-specific removal of aptamer sequences from the AuNP surface. Not only were sequences with and without affinity for the target molecule removed when target was introduced, but the same amount of each sequence was removed when a negative control or blank solution was added. The extensive non-specific nature of the AuNP platform in this method would not provide a reliable separation of aptamers for a target molecule under AuNP sensor conditions. Therefore, the specificity of the developed Fe_3O_4-AuNPs partitioning method was investigated through a proof of concept SELEX experiment. The previously mentioned assay was developed and used to adsorb ssDNA aptamer on the surface of Fe_3O_4-AuNPs and remove the sequences that did not adsorb and remained in solution. Once the aptamer-Fe_3O_4-AuNPs complex was isolated from unbound sequences, a target molecule could be introduced in solution. Hypothetically, the addition of a target molecule would remove aptamers with affinity for the target from the surface of the Fe_3O_4-AuNPs into solution. The Fe_3O_4-AuNPs with aptamers that remain on the nanoparticle surface can be separated from sequences that were removed to preferentially bind the target molecule. Again, the sequences removed from the Fe_3O_4-AuNP surface with target are now in the supernatant solution. This supernatant can be collected and analyzed by PAGE to determine the

amount of each sequence removed from the Fe_3O_4-AuNP surface with target. If an aptamer for the target molecule is compared to aptamers without affinity for the target, the specificity of the method can be evaluated. Similarly, if a blank sample without target is examined, the amount of aptamer removed from the surface due to a change in equilibrium can be compared and subtracted from the amount of each sequence removed when the target is introduced.

4.3.2 Adsorption of ssDNA aptamers on DMAP capped Fe_3O_4-AuNP

To understand the interaction between various DNA aptamers and synthesized DMAP capped Fe_3O_4-AuNPs, the adsorption capacity was first tested. First, 3 aptamers of various lengths were examined individually. The aptamers chosen for this study were 1.12.2 (36), Dop (58) and FB139 (96) (Table 4.1). The difference in aptamer length allows for analysis by gel electrophoresis, and insight into how aptamer length may affect DNA adsorption to the DMAP capped Fe_3O_4-AuNP surface. A known concentration of DMAP capped Fe_3O_4-AuNPs and aptamer were allowed to incubate at room temperature for 30 mins. A blank sample of DMAP capped Fe_3O_4-AuNPs without any DNA and a control sample of DNA without any DMAP capped Fe_3O_4-AuNPs were prepared and incubated simultaneously. After incubation, the samples were placed on a magnet for 30 mins. At this point, the Fe_3O_4-AuNPs were separated from solution and the clear supernatant solution was removed and collected for analysis.

By PAGE analysis, the concentration of DNA in the supernatant was estimated using Image J software. For each experiment, three blank samples, three test samples and three control samples were analyzed. As an example, the PAGE gel for the capacity of

1.12.2 with DMAP capped Fe_3O_4-AuNPs is shown below (Figure 4.2). As expected, the three blank samples did not show any bands suggesting the absence of 1.12.2 in the supernatant of the blank samples. The next three lanes (Figure 4.2) are the test samples, which were expected to display a band for the 1.12.2 in the supernatant that did not adsorb onto the Fe_3O_4-AuNP surface. Hypothetically, the final 3 lanes (Figure 4.2) for the control samples should display the UV-Vis absorption of the concentration of 1.12.2 added, as no Fe_3O_4-AuNPs were present to adsorb any DNA. The test sample bands in the gel were predicted to display more UV-Vis absorption in comparison to the blank samples, but less UV-Vis absorption than the control samples. This difference was found for all three aptamers, which suggests that some percentage of the concentration of aptamer added does adsorb onto the surface of Fe_3O_4-AuNPs. The intensity of the bands in the gel resulting from UV-Vis absorption of a certain concentration of DNA present was analyzed. Using Image J, the band intensities were represented numerically and compared to the control sample. This provided an estimated concentration of DNA in the supernatant of the test samples, and therefore, an estimated concentration of DNA that adsorbed onto the Fe_3O_4-AuNP surface. Hypothetically the entire amount of DNA added to the control sample should be present in the supernatant solution analyzed by PAGE. The band intensity for the control sample was set to 100% or the amount of DNA originally added at the concentration of the assay (1 nmol). With this, the amount of 1.12.2, Dop and FB139 in the test samples was found to be approximately 68.8% (0.69 ± 0.01 nmol), 58.4% (0.58 ± 0.08 nmol) and 68.3% (0.68 ± 0.08 nmol) of the control sample, respectively. Therefore, by difference, the amount of 1.12.2, Dop and FB139 adsorbed onto the sample of Fe_3O_4-AuNPs is estimated to be 34.2% (0.34 nmol), 41.6%

(0.42 nmol) and 31.7% (0.32 nmol) of the DNA originally added, respectively (Figure 4.3-4.6). An adsorption of aptamer onto DMAP capped Fe_3O_4-AuNPs was supported by the consistent and unbiased difference in aptamer concentration between the test and control samples. The difference in aptamer length did not appear to affect adsorption, as approximately 30-40% of each sequence adsorbed onto the synthesized DMAP capped Fe_3O_4-AuNPs. However, it is important to notice there is an adsorption capacity difference between DMAP capped Fe_3O_4-AuNPs and citrate capped AuNPs. These differences found during preliminary testing could be attributed to a number of factors; such as the separation technique (magnetic separation vs centrifugation), size of the nanoparticles (7 nm vs 13 nm), but more importantly a difference in the capping agent (DMAP vs citrate). This concern compels additional comparison of DMAP and citrate as capping agent with respect to the adsorption of ssDNA aptamers.

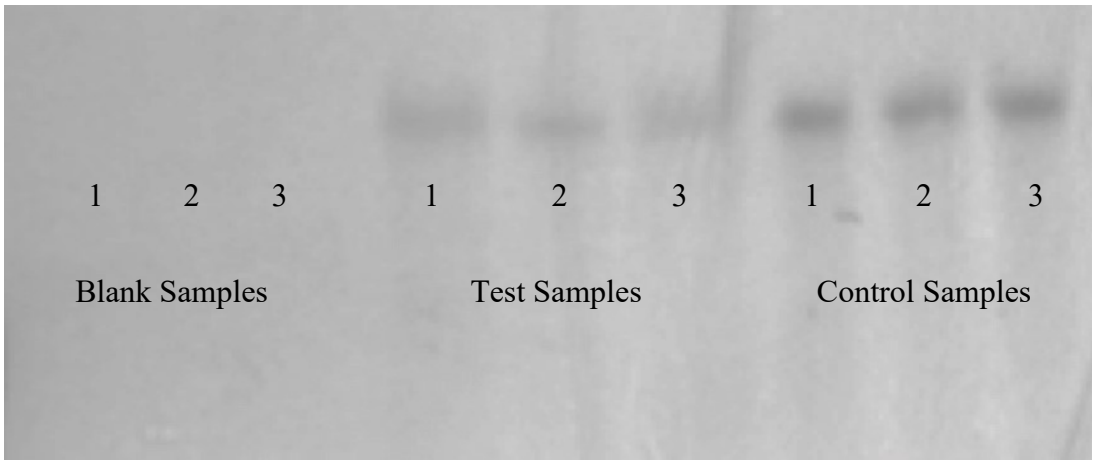

Figure 4.2 Representative PAGE gel image used analyzed through ImageJ software to determine the amount of ssDNA aptamer in the supernatant solution after magnetic partitioning with Fe_3O_4-AuNPs

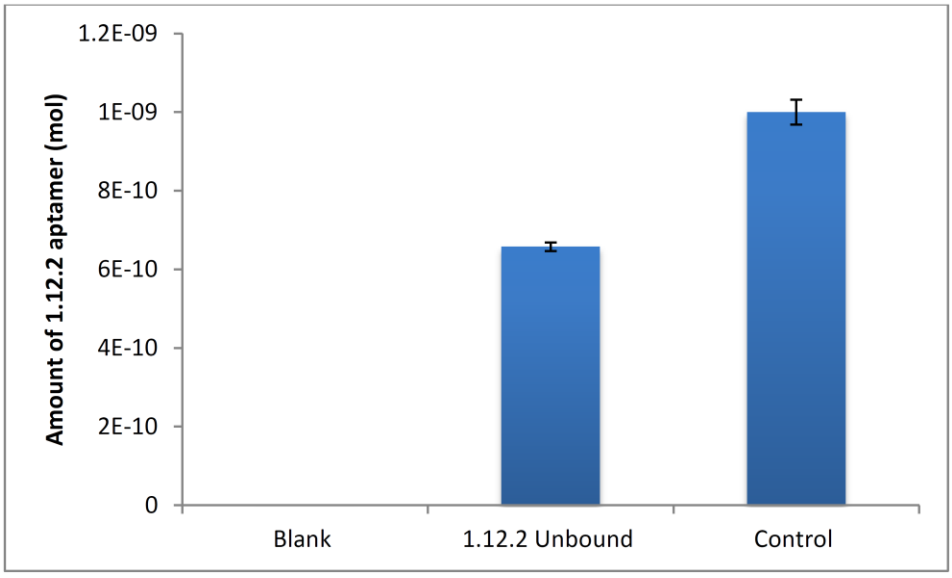

Figure 4.3 Amount of 1.12.2 aptamer in the supernatant solution after incubation with Fe_3O_4-AuNPs and magnetic separation. Using PAGE, the amount of 1.12.2 is determined via Image J software analysis and represented as a percentage of a control sample

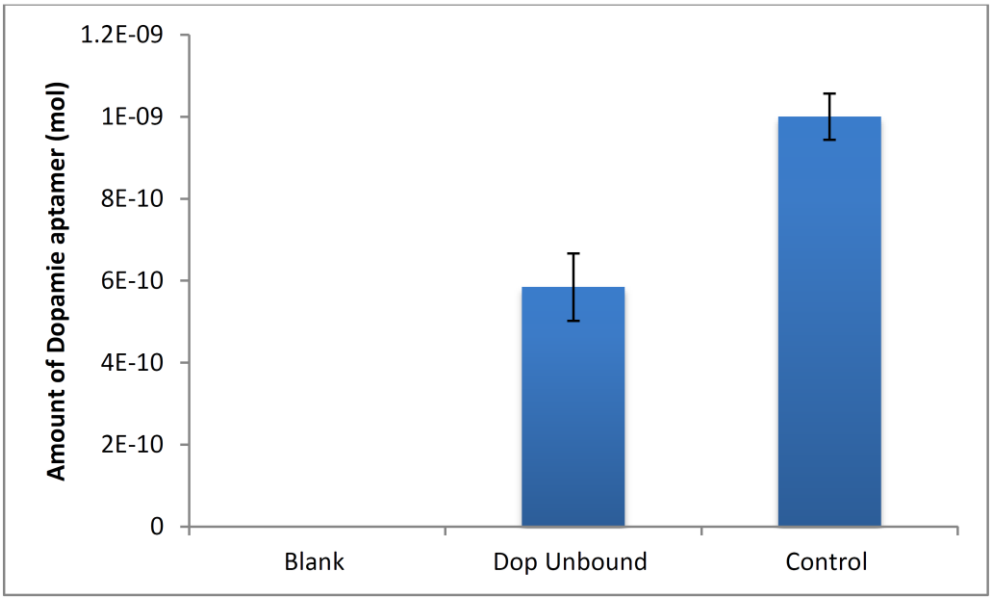

Figure 4.4 Amount of dopamine aptamer in the supernatant solution after incubation with Fe_3O_4-AuNPs and magnetic separation. Using PAGE, the amount of dopamine aptamer is determined via Image J software analysis and represented as a percentage of a control sample

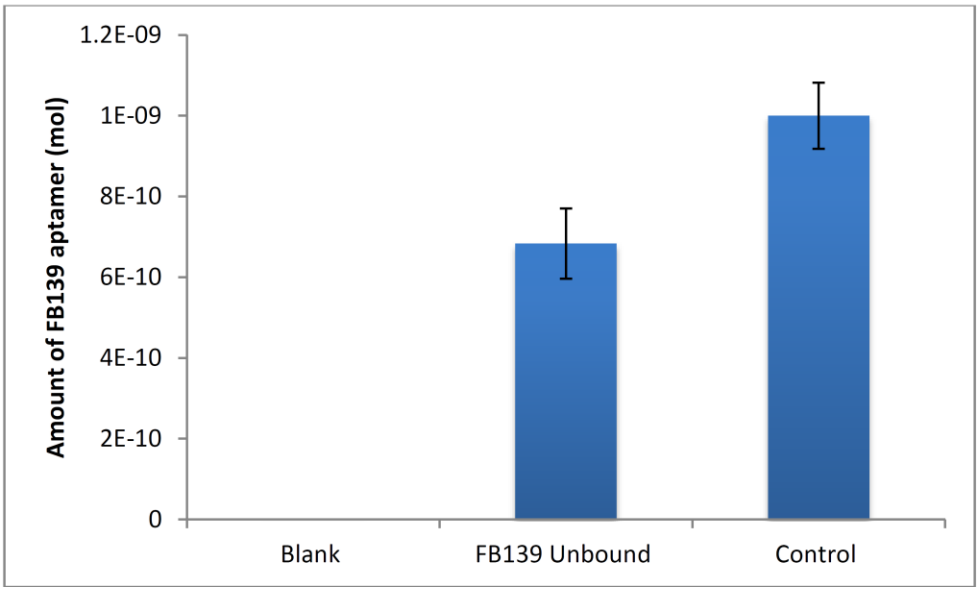

Figure 4.5 Amount of FB139 aptamer in the supernatant solution after incubation with Fe_3O_4-AuNPs and magnetic separation. Using PAGE, the amount of FB139 is determined via Image J software analysis and represented as a percentage of a control sample

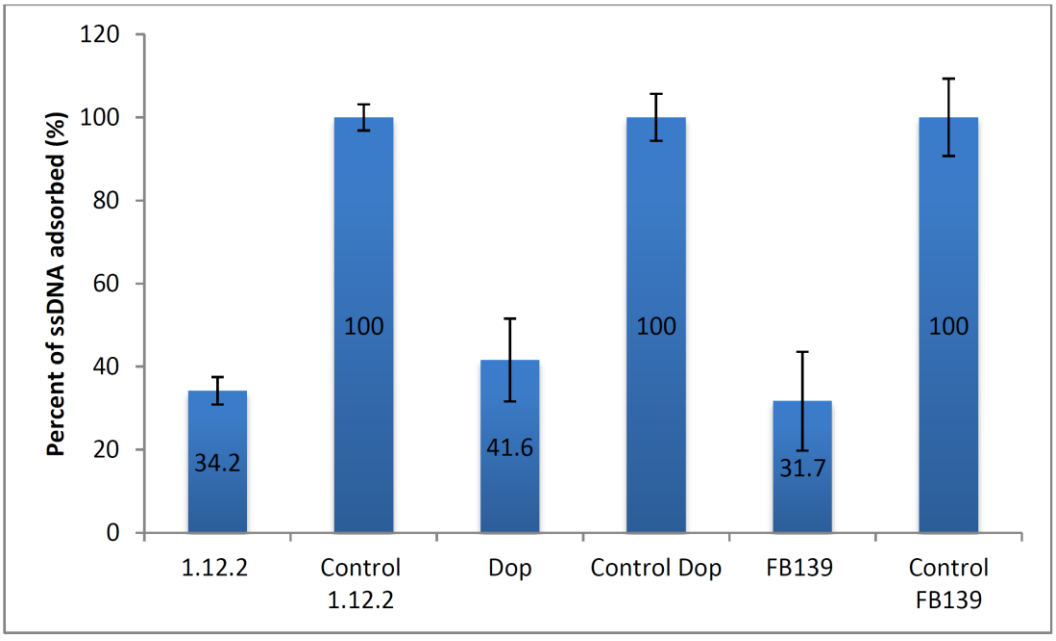

Figure 4.6 Amount of 1.12.2, Dop and FB139 aptamers adsorbed separately onto the surface of synthesized Fe_3O_4-AuNPs after magnetic separation. Using PAGE, the amount of each sequence is determined via Image J software analysis and, by difference, represented as a percentage of a control sample

4.3.3 Competitive assay analysis of aptamer dependent adsorption

In order to test how these three aptamer sequences competitively interact with the DMAP capped Fe_3O_4-AuNP surface, all three sequences were mixed together in a 1:1:1 ratio with a concentration totaling the concentration used when investigating each aptamer individually. This mixture was then introduced to the same concentration of Fe_3O_4-AuNPs and allowed to incubate at room temperature for 30 mins. The supernatant of the blank, test and control samples were removed after magnetic separation and analyzed by PAGE. As previously mentioned, the band(s) for each sample were denoted numerically using Image J software. Using this method, the amount or percentage of each test sample was compared to the control samples. This was done to estimate the amount of each aptamer sequences adsorbed onto the Fe_3O_4-AuNP surface, and compare the possible difference in adsorption between these three sequences.

In this competitive assay, there was a slight difference in the band intensity for the test samples compared to the control samples. Analysis determined that there was approximately a 10-20% reduction in the band intensity between the test and control samples for each sequence. The amount of 1.12.2, Dop and FB139 in the test samples was found to be approximately 75.3% (0.25 ± 0.02 nmol), 79.7% (0.27 ± 0.02 nmol) and 85.4% (0.28 ± 0.01 nmol) of the control sample, respectively (Figure 4.7). Therefore, by difference, the amount of 1.12.2, Dop and FB139 adsorbed onto the sample of Fe_3O_4-AuNPs is estimated to be 24.7% (0.08 nmol), 20.3% (0.07 nmol) and 14.6% (0.05 nmol) of the DNA originally added, respectively.

Previously, it was found that an average of approximately 0.35 ± 0.11 nmol of the control sample was adsorbed onto the surface of Fe_3O_4-AuNPs when incubated

individually. The results of this competitive assay are in agreement with this estimation, as it is assumed that approximately 0.07 ± 0.02 nmol of each sequence was adsorbed onto the surface of Fe_3O_4-AuNPs. Adding all three sequences together results in a total of approximately 0.21 ± 0.03 nmol of DNA.

Since each of the aptamer sequences differed in length and structure, the relationship between these differences and the adsorption of DNA to Fe_3O_4-AuNPs should be investigated. The results of this experiment suggest that there may be a slight difference in adsorption when comparing the length of the sequences. 1.12.2 appeared to result in a larger difference in band intensity, compared to FB139. This suggests that 1.12.2, the shorted DNA sequence, preferentially adsorbed to the surface of Fe_3O_4-AuNPs. There is a slight trend between the amount of DNA adsorbed and the length of the aptamer sequence (Figure 4.8). However, when relative error and kinetics are considered, this difference is found to be negligible. This experiment provides important insight into the potential utility and challenges of Fe_3O_4-AuNPs as a platform for SELEX. Considering the amount of Fe_3O_4-AuNPs needed for selection could determine if this product and method is realistic as a SELEX platform. In this work, it is estimated that approximately 20-30 nmol of DNA aptamer is adsorbed onto 100 μL of Fe_3O_4-AuNPs. Therefore, approximately 4 mL of Fe_3O_4-AuNPs would be required to adsorb 1000 pmol of DNA library. The estimated volume of Fe_3O_4-AuNPs required is reasonable, especially for later selection rounds containing less than 1000 pmol of DNA (typically 200 pmol).

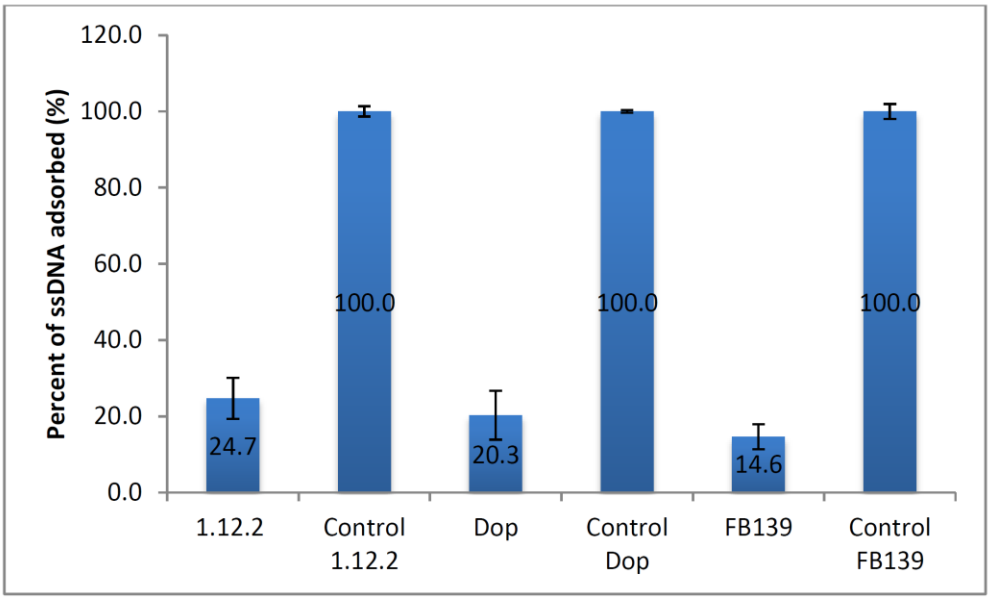

Figure 4.7 Amount of 1.12.2, Dop and FB139 aptamers adsorbed competitively onto the surface of synthesized Fe_3O_4-AuNPs after magnetic separation. Using PAGE, the amount of each sequence is determined via Image J software analysis and, by difference, represented as a percentage of a control sample

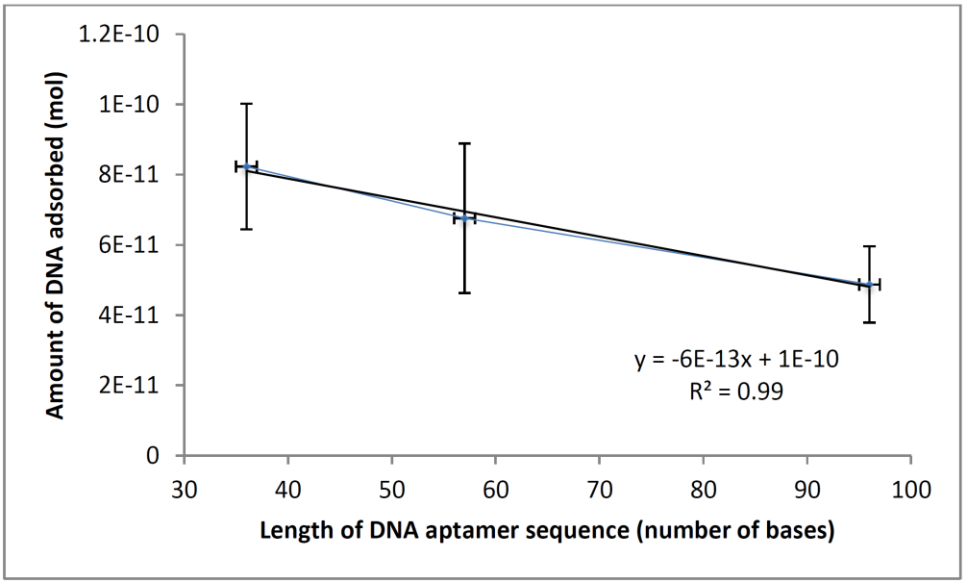

Figure 4.8 Amount of ssDNA absorbed with respect to the number of bases in the ssDNA sequence. After being adsorbed competitively onto the surface of synthesized Fe_3O_4-AuNPs and partitioned via magnetic separation, the PAGE image was analyzed with ImageJ software to determine the percent difference.

4.3.4 Removal of adsorbed 1.12.2 aptamer with target molecule (OTA)

Having established successful adsorption of three ssDNA aptamers onto synthesized Fe_3O_4-AuNPs, we next examined the removal of the adsorbed aptamers with a specific target molecule. Aptamer 1.12.2 was selected for the small molecule mycotoxin target molecule, ochratoxin A (OTA). To test this, a known amount of 1.12.2 was incubated with Fe_3O_4-AuNPs for 30 mins. The sequences that did not adsorb onto the surface of the Fe_3O_4-AuNPs were removed and estimated (as above). Next, the target molecule (OTA) was introduced, and the amount of 1.12.2 that was released from the surface of the Fe_3O_4-AuNPs was approximated using gel electrophoresis. However, it is expected that when the aptamers that do not adsorb to the surface of the Fe_3O_4-AuNPs are removed, there will be a shift in the equilibrium between 1.12.2 and Fe_3O_4-AuNPs. In order to determine the amount of 1.12.2 that was removed when target is introduced, the amount of 1.12.2 that is found in the supernatant of a blank sample should be compared. As the amount of ssDNA removed after adsorption was not concentrated enough to analyze by PAGE, a fluorescein-modified sequence was employed. Preliminary work displays that after 1.12.2F adsorbed on the surface of Fe_3O_4-AuNPs are isolated; 1.12.2F can be removed from the surface with target incubation. However, the amount of 1.12.2F removed with target is not significantly greater than the amount removed with water (Figure 4.9). Alternatively, DMAP as a capping agent differs from the studied citrate capped AuNPs with respect to DNA adsorption, which results in the adsorbed sequence being easily removed (with water). As previously mentioned, it is possible that the non-specific interaction of ssDNA and AuNPs is affected by the removal of the individual

ssDNA sequence in solution. In turn, it is likely that the equilibrium between the ssDNA-AuNP complex and the individual components is shifted which results in the non-specific removal of ssDNA sequences from the AuNP surface.

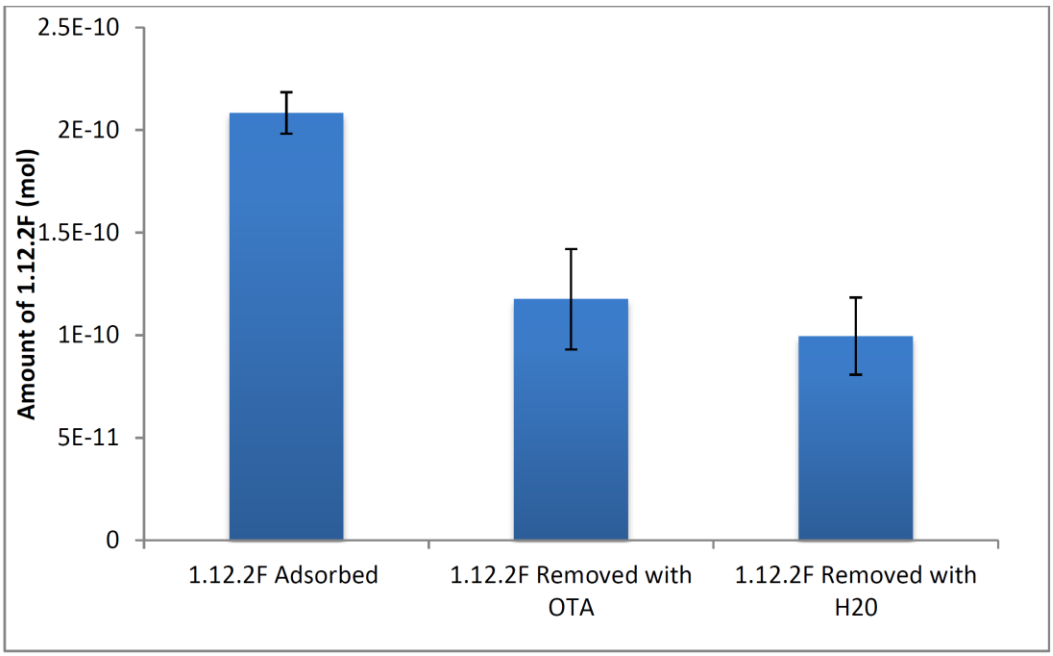

Figure 4.9 Amount of 1.12.2F aptamer adsorbed onto the surface of synthesized Fe_3O_4-AuNPs after magnetic separation and the amount of 1.12.2F removed with OTA and a blank sample was represented as an estimated amount of 1.12.2F (mol) compared to a control sample

To test whether or not Fe_3O_4-AuNP would be a viable platform for SELEX, a proof of concept selectivity assay was designed. In this experiment, the selectivity of aptamers removed from the Fe_3O_4-AuNP surface for a specific target molecule would be investigated. The assay utilizes one aptamer for the target molecule, 1.12.2, and two aptamers without affinity for the same target molecule, Dop and FB139. These sequences are mixed in a 1:1:1 ratio and allowed to incubate with Fe_3O_4-AuNPs for 30 mins. After the sequences that did not adsorb onto the surface of the Fe_3O_4-AuNPs are removed, the

target molecule (OTA) is introduced. Hypothetically, only the aptamer for the target molecule should leave the surface of the Fe_3O_4-AuNPs to preferentially bind its target. As previously mentioned, it is expected that when the aptamers that do not adsorb to the surface of the Fe_3O_4-AuNPs are removed, there will be a shift in the equilibrium between DNA aptamers and Fe_3O_4-AuNPs. In order to determine the actual amount of each sequence that was removed when the target is introduced, the amount of each sequence that is found in the supernatant of a blank sample is subtracted. Compared to adsorption and removal of one aptamer sequence, three aptamer sequences resulted in a third of the concentration of each sequence being added. Analyzing the percentage of each sequence adsorbed was possible (section 4.3.3). However, as previously discussed with the removal of 1.12.2, the amount of ssDNA removed was not visible by UV-Vis analysis of the PAGE gel and required modification of the sequence. Optimization of this procedure to assess the specificity of this POC study would require amplification of the sequences by PCR before PAGE analysis or modification of the ssDNA sequences.

Comparing centrifugation with magnetic separation via Fe_3O_4-AuNPs, it is suggested that both methods result in the non-specific removal of ssDNA aptamers. Although magnetic separation appeared to slightly increase specificity, this improvement is not significant when considering the error associated with these results (Figure 4.9).

4.3.5 Comparing Fe_3O_4-AuNP to centrifugation for SELEX separation

There were two main problems with centrifugation as a separation method for AuNP SELEX. Both, the presence of AuNP in the supernatant solution after centrifugation and the difference in salt induced AuNP aggregation before and after

centrifugation were a concern. This section aims to demonstrate that magnetic separation with synthesized Fe_3O_4-AuNPs is superior to centrifugation as a partitioning method for AuNP SELEX and that the previously mentioned concerns with separation have been addressed. First, the presence of nanoparticles in the supernatant solutions were analyzed by TEM and these local concentrations were qualitatively compared to one another. The UV-Vis absorption spectra of these samples could not be used as a method of comparison due to the low concentrations of nanoparticles found within these samples. Figure 4.10 displays the AuNPs present in solution after centrifugation at 14,000 g for 30 mins. In comparison, the Fe_3O_4-AuNPs present in solution after magnetic separation for 30 mins are displayed (Figure 4.10). TEM analysis suggests that there are less Fe_3O_4-AuNPs in solution after magnetic separation than AuNPs in solution after centrifugation. In addition, the speed that is required to separate this amount of AuNPs from solution by centrifugation results in a tendency to undergo unexpected salt induced aggregation. With this considered, magnetic separation for AuNP SELEX is advantageous in comparison. Next, salt induced aggregation of AuNPs after separation by centrifugation and Fe_3O_4-AuNPs after magnetic separation was investigated. As previously discussed in section 2.3.4, centrifugation influences salt-induced AuNP aggregation. Specifically, high centrifuge speeds and shorter aptamer sequences are found to affect aggregation results. More importantly, it is crucial to note that the adsorption of DNA aptamers has been reported to protect AuNP from salt induced aggregation. Assuming salt induced aggregation can predict the presence or absence of DNA aptamers on the surface of AuNPs, the change in aggregation results with separation via centrifugation is concerning. To assess magnetic separation as an improved separation method, salt

induced aggregation of nanoparticles before and after separation was examined. However, AuNPs capped with sodium citrate and Fe_3O_4-AuNPs capped with DMAP were found to behave differently with respect to salt induced aggregation. Various nanoparticle-capping agents can withstand different concentrations of sodium chloride (NaCl). It has been reported that the stronger the interaction of the capping agent with the nanoparticle surface, the more resistance the nanoparticles are to salt induced aggregation. Both concentration of salt and the time required to observe aggregation have been shown to fluctuate depending on the capping agent used.[169] Therefore, a higher concentration of salt could be required to prompt salt-induced aggregation of the DMAP capped Fe_3O_4-AuNPs in comparison to the citrate capped AuNPs (0.25 M).

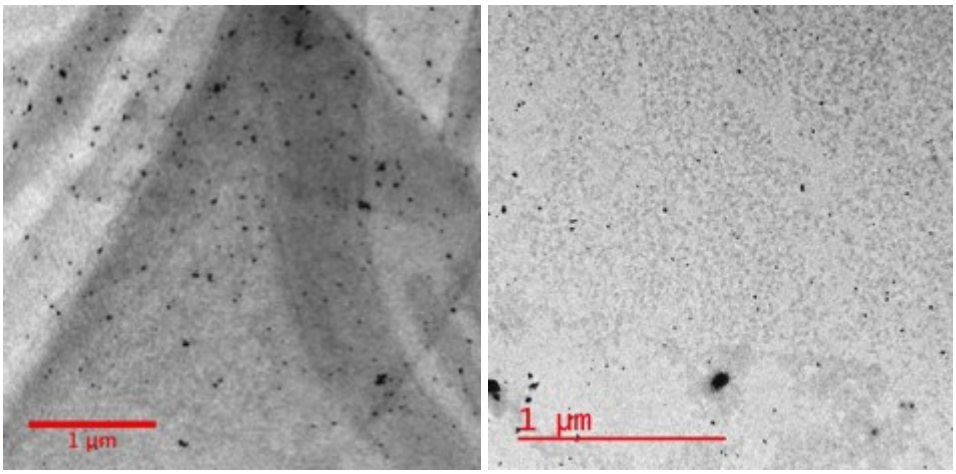

Figure 4.10 TEM images at 1 µm of AuNPs (11 nM) in supernatant after separation with centrifugation at 13,000g for 30 mins (left) and of Fe_3O_4-AuNPs (~ 10 nM) in supernatant after magnetic separation (right).

In order to further compare these two separation methods, the AuNP bioassay was employed. Previously, the interaction between ssDNA and AuNPs was tested with the

AuNP bioassay before and after AuNPs were separated from solution by centrifugation. It was suggested, with 1.12.2, that the interaction between this ssDNA aptamer and the AuNPs in solution was disrupted during separation. Magnetic separation with Fe_3O_4-AuNPs was compared to centrifugation by investigating the results the AuNP bioassay. It appeared that magnetic separation did not have an effect on the interaction between AuNPs and 1.12.2 (Figure 4.10). However, with no salt-induced aggregation of the AuNP control, this result was not a reliable method of assessing the separation platform. This difference in salt induced aggregation is attributed to the difference in capping agents between AuNPs and Fe_3O_4-AuNPs. DMAP capped Fe_3O_4-AuNPs can withstand a much higher concentration against salt-induced aggregation. The addition of 0.5 M, 1.0 M and 1.5 M NaCl to a control sample did not induce aggregation of DMAP capped Fe_3O_4-AuNPs solution. Therefore, the AuNP bioassay was not a possible method for comparing the integrity of these separation methods for AuNP-based SELEX.

4.4 Conclusions

Although previous studies have shown the adsorption of dsDNA onto DMAP capped AuNPs, no studies have investigated the adsorption of ssDNA aptamers onto DMAP capped Fe_3O_4-AuNPs. Optimization of Fe_3O_4-AuNPs as a platform for ssDNA adsorption is of particular interest as this could provide a quick and reliable separation method for AuNP-based SELEX and other aptamer applications. Adsorption of ssDNA onto Fe_3O_4-AuNPs and removal of these adsorbed sequences was attempted through a proof-of-concept study. Three different aptamers were successfully adsorbed onto the surface of Fe_3O_4-AuNPs and separated from solution via magnetic separation. All three

sequences were adsorbed individually and competitively at relatively similar quantities. However, the detection limits of UV-Vis via PAGE analysis prevented the quantification of removed aptamer when introduced to target. To quantify and compare the amount of each aptamer sequence removed with the addition of OTA, the removed sequences could be amplified by PCR amplification. This would increase the amount of each sequence sufficiently to estimate the relative amounts of each aptamer sequence by PAGE analysis. These amounts could be compared to assess the specificity of the developed AuNP-based SELEX platform. 1.12.2 modified with fluorescein was used to assess the specificity and reliability of Fe_3O_4-AuNPs as a partitioning method. Since the removal of sequences is found to be non-specific, regardless of the separation method, it is proposed that the equilibrium between ssDNA and AuNPs is the main challenge with this SELEX design. To overcome this, the manner in which the AuNPs are incorporated as a SELEX platform should be revisited. With the optimization of Fe_3O_4-AuNPs as a quick, reliable separation method, the core-shell NP could be used as a negative selection during SELEX. Proposed as further studies in chapter 5, adding a negative selection round would eliminate multiple AuNP based separations. After an initial library of DNA sequences is incubated with Fe_3O_4-AuNPs, the sequences that adsorbed onto the Fe_3O_4-AuNP surface could be separated, amplified and identified. These sequences would continue in the selection process. Once the target molecule of interest and this reduced DNA library are incubated, Fe_3O_4-AuNPs can be introduced as a negative selection. The sequences without affinity for the target molecule will be available to adsorb onto the surface of Fe_3O_4-AuNPs. The magnetic core will allow for these non-binding sequences on the surface of the nanoparticle to be removed from solution, and from the DNA library

(Figure 4.11). In addition, it is not forgotten that the synthesized Fe_3O_4-AuNPs are capped with DMAP in comparison to citrate. This difference is important to consider, and should be tested further. Either determining if the AuNP assay is feasible with DMAP as a capping agent, or capping Fe_3O_4-AuNPs with citrate is an important next step in the development of this platform.

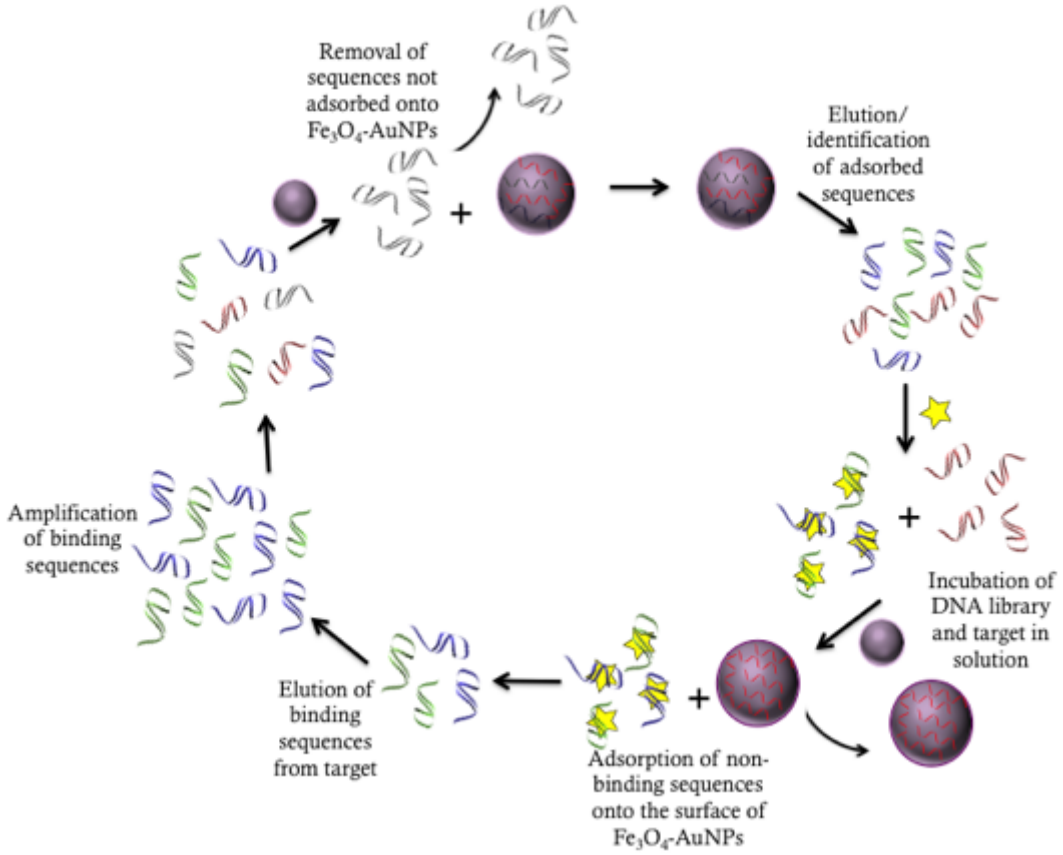

Figure 4.11 Proposed two-step AuNP-based SELEX process. Adsorbed sequences are separated (with Fe_3O_4-AuNP magnetic separation). The adsorbed sequences are identified and used as the library that is incubated with the target molecule. Sequences of this library without affinity for the target, are available and adsorbed onto the Fe_3O_4-AuNP surface to be removed via magnetic separation. The sequences with an affinity for the target molecule that is greater than the adsorption of those sequences to the AuNP surface are isolated through two steps of selection. These sequences can be eluted from the target, amplified via PCR amplification and used for the next round of selection.

Chapter 5: Contributions to knowledge and further studies

This research presented the challenges and opportunities associated with a novel AuNP-based SELEX design. Optimizing a reliable separation method for selection through AuNP-based SELEX was the focus of this work. Limitations of previously reported SELEX partitioning methods lead to the synthesis, optimization, and transfer of DMAP capped Fe_3O_4-AuNPs. The adsorption of various ssDNA aptamers onto DMAP capped Fe_3O_4-AuNPs is a promising result that leaves opportunities for DMAP capped Fe_3O_4-AuNPs as a selection or bioassay platform. The amount of DMAP capped Fe_3O_4-AuNPs required as a selection platform was estimated and determined as a realistic working volume for the novel selection method. However, the specificity of the developed SELEX platform was unresolved due to difficulties encountered during initial partitioning and optimization. Despite these challenges, AuNP-based SELEX is beneficial for improving selected aptamers for AuNP biosensor working conditions. If not by incorporating AuNPs into SELEX as the selection platform, the optimized DMAP capped Fe_3O_4-AuNPs could be used as a two step selection method including a negative selection round to improve the specificity of aptamers used in AuNP- based sensors. In addition, aptamers could be adsorbed or covalently bound to Fe_3O_4-AuNPs for various other biosensor and biomedical applications.

Although this preliminary work displays the promise of AuNPs as a platform for small molecule SELEX, a number of key experiments are required to confirm the potential of Fe_3O_4-AuNPs as a partitioning platform. The Fe_3O_4-AuNPs were capped with DMAP for phase transfer of the synthesized core-shell nanoparticles into aqueous

solution. However, this differs from the citrate capped AuNPs used for both the AuNP bioassay and LFD. Therefore, it is of importance to investigate if this alteration is capable of mimicking adsorption of ssDNA onto citrate capped AuNPs and future testing conditions. To test this, the AuNP bioassay with DMAP capped AuNPs should be compared to the results of the assay with citrate capped AuNPs. Furthermore, transfer and capping Fe_3O_4-AuNPs with citrate instead of DMAP should be investigated and optimized for further opportunities and consistency.

It is suggested that both the partitioning method and the equilibrium between the adsorbed sequences and the AuNP platform can determine the success of this SELEX design. Therefore, the specificity and reliability of DMAP capped Fe_3O_4-AuNPs should be confirmed. Difficulty with assessing the amount of each sequence removed from the DMAP capped Fe_3O_4-AuNP surface after target incubation was associated with the limitations of PAGE as an analysis method. Therefore, amplification of the sequences with PCR should be employed to visualize the amount of each sequence removed. Tests should be completed to demonstrate that the removal of sequences from the AuNP surface is due to specific binding events. By comparing the amount and identity of each sequence removed when a similar molecule or blank solution is introduced, the specificity of the developed platform can be confirmed.

As previously discussed, investigation of the specificity of the developed SELEX platform via two different separation methods resulted in the non-specific removal of ssDNA aptamers from the AuNP surface. These results suggest that the main contributing factor is not the separation technique but the non-covalent interaction between the ssDNA and AuNPs. This design requires two partitioning steps; isolating ssDNA-AuNP

complexes from free ssDNA in solution, and separating the sequences removed with target from sequences remaining on the AuNP surface. It is suggested that the sequences removed with target cannot be accurately determined as the first separation causes a shift in the equilibrium between the ssDNA-AuNP complex and the individual components (ssDNA and AuNPs). An alternative possibility is that the optimized Fe_3O_4-AuNPs could act as a negative selection platform after identifying, which sequences adsorb onto the surface of Fe_3O_4-AuNPs. For this method, the order of incubation that is outlined in the original design of the AuNP-based SELEX would be reversed (Figure 4.11). To test this, a proof-of-concept type analysis could be used to show that sequences without affinity for the target can be removed from solution while sequences with affinity for the target remain in the supernatant after magnetic separation. This would eliminate the challenges faced during multi-step separations, while improving the specificity of DNA aptamers selected under AuNP-based sensor conditions.

Appendices

Appendix A

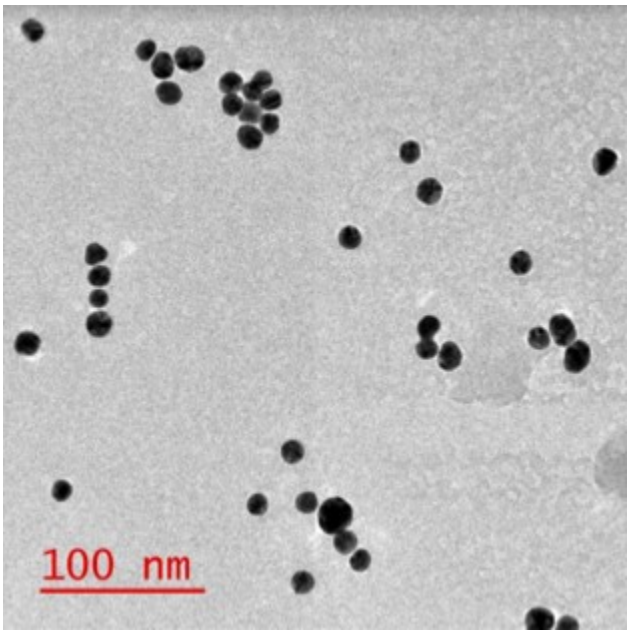

Figure 5.1 TEM image with a 100 nm scale bar of synthesized citrate capped gold nanoparticles (AuNPs)

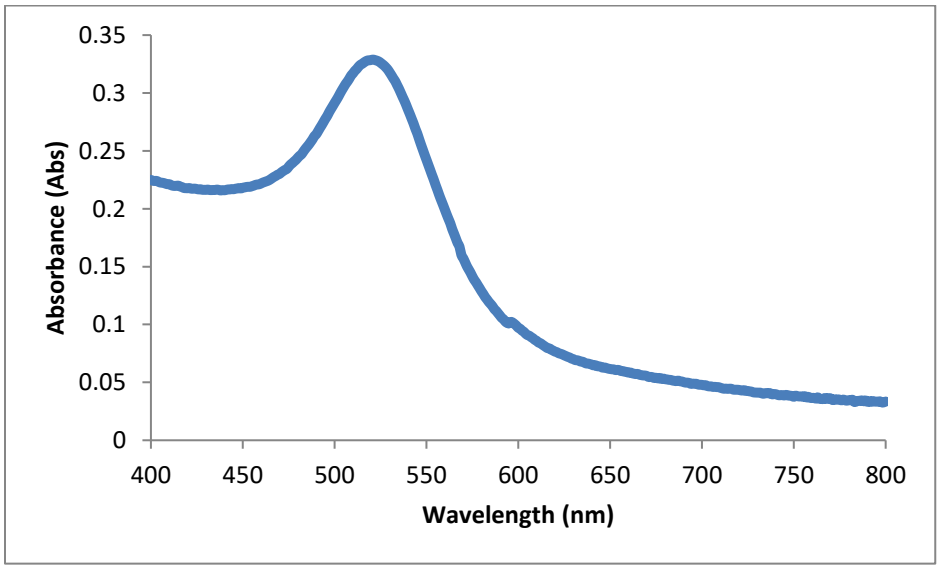

Figure 5.2 UV-Vis spectrum of synthesized citrate capped gold nanoparticles (AuNPs)

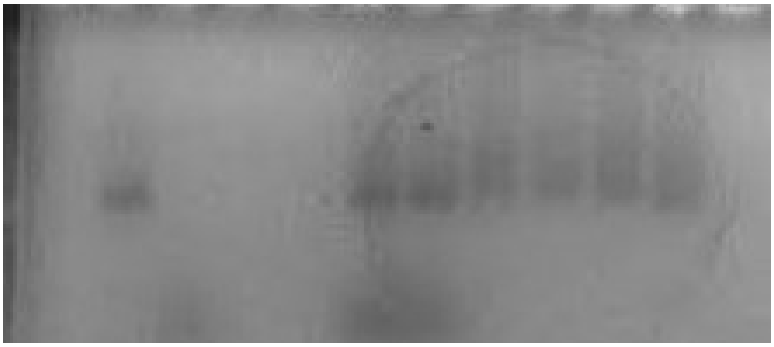

Figure 5.3 Example UV-Vis absorption of agarose gel image after ssDNA-AuNP conjugates and free ssDNA aptamer/AuNPs migration (3h at 200V)

References

(1) Ruscito, A.; DeRosa, M. C. Small-Molecule Binding Aptamers: Selection Strategies, Characterization, and Applications. *Front. Chem.* **2016**, *4* DOI: 10.3389/fchem.2016.00014.

(2) McKeague, M.; Derosa, M. C. Challenges and opportunities for small molecule aptamer development. *J. Nucleic Acids* **2012**, *2012* DOI: 10.1155/2012/748913.

(3) Cho, M. J.; Juliano, R. Macromolecular versus smallmolecule therapeutics: drug discovery, development and clinical considerations. *Trends Biotechnol.* **1996**, *14* (5), 153–158 DOI: 10.1016/0167-7799(96)10024-X.

(4) Walsh, T. A. The emerging field of chemical genetics: potential applications for pesticide discovery. *Pest Manag. Sci.* **2007**, *63* (12), 1165–1171 DOI: 10.1002/ps.1452.

(5) Marin, S.; Ramos, a J.; Cano-Sancho, G.; Sanchis, V. Mycotoxins: occurrence, toxicology, and exposure assessment. *Food Chem. Toxicol.* **2013**, *60*, 218–237 DOI: 10.1016/j.fct.2013.07.047.

(6) Edite Bezerra da Rocha, M.; Freire, F. D. C. O.; Erlan Feitosa Maia, F.; Izabel Florindo Guedes, M.; Rondina, D. Mycotoxins and their effects on human and animal health. *Food Control* **2014**, *36* (1), 159–165 DOI: 10.1016/j.foodcont.2013.08.021.

(7) Pereira, V. L.; Fernandes, J. O.; Cunha, S. C. Mycotoxins in cereals and related foodstuffs: A review on occurrence and recent methods of analysis. *Trends Food Sci. Technol.* **2014**, *36* (2), 96–136 DOI: 10.1016/j.tifs.2014.01.005.

(8) Ruscito, A.; Smith, M.; Goudreau, D. N.; Derosa, M. C. Current status and future prospects for aptamer-based mycotoxin detection. *J. AOAC Int.* **2016**, *99* (4), 865–877 DOI: 10.5740/jaoacint.16-0114.

(9) Reddy, K.; Salleh, B.; Saad, B.; Abbas, H.; Abel, C.; Shier, W. An overview of mycotoxin contamination in foods and its implications for human health. *Toxin Rev.* **2010**, *29* (1), 3–26 DOI: 10.3109/15569541003598553.

(10) Smith, M. C.; Madec, S.; Coton, E.; Hymery, N. Natural Co-occurrence of mycotoxins in foods and feeds and their in vitro combined toxicological effects. *Toxins (Basel).* **2016**, *8* (4) DOI: 10.3390/toxins8040094.

(11) Wood, G. E. Mycotoxins in foods and feeds in the United States. *J. Anim. Sci.* **1992**, *70* (12), 3941 DOI: 10.2527/1992.70123941x.

(12) Union, I.; Pure, O. F.; Chemistry, A. International Union of Pure Commission on Food Chemistry- Ochratoxin : A Review (Technical Report). **1992**, *64* (7), 1029–1046.

(13) Anklam E., Stroka J., B. A. (2002). Acceptance of analytical methods for implementation of EU legislation with a focus on mycotoxins. *Food Control.* **2002**, *13* (3), 173–183.

(14) von Holst, C.; Stroka, J. Performance criteria for rapid screening methods to detect mycotoxins. *World Mycotoxin J.* **2014**, *7* (4), 439–447 DOI: 10.3920/WMJ2014.1710.

(15) Terato, K.; Do, C. T.; Cutler, D.; Waritani, T.; Shionoya, H. Preventing intense false positive and negative reactions attributed to the principle of ELISA to re-investigate antibody studies in autoimmune diseases. *J. Immunol. Methods* **2014**, *407*, 15–25 DOI: 10.1016/j.jim.2014.03.013.

(16) Tuerk, C.; Gold, L. Systematic evolution of ligands by exponential enrichment: RNA ligands to bacteriophage T4 DNA polymerase. *Science* **1990**, *249* (4968), 505–510.

(17) Balogh, Z.; Lautner, G.; Bardoczy, V.; Komorowska, B.; Gyurcsanyi, R. E.; Meszaros, T. Selection and versatile application of virus-specific aptamers. *FASEB J.* **2010**, *24* (11), 4187–4195 DOI: 10.1096/fj.09-144246.

(18) Burke, D. H. Expressing RNA aptamers inside cells to reveal proteome and ribonome function. *Briefings Funct. Genomics Proteomics* **2002**, *1* (2), 169–188 DOI: 10.1093/bfgp/1.2.169.

(19) McKeague, M.; Bradley, C. R.; de Girolamo, A.; Visconti, A.; David Miller, J.; de Rosa, M. C. Screening and initial binding assessment of fumonisin B 1 aptamers. *Int. J. Mol. Sci.* **2010**, *11* (12), 4864–4881 DOI: 10.3390/ijms11124864.

(20) Okazawa, a; Maeda, H.; Fukusaki, E.; Katakura, Y.; Kobayashi, a. In vitro selection of hematoporphyrin binding DNA aptamers. *Bioorg. Med. Chem. Lett.* **2000**, *10* (23), 2653–2656 DOI: 10.1016/S0960-894X(00)00540-0.

(21) De Soultrait, V. R.; Lozach, P. Y.; Altmeyer, R.; Tarrago-Litvak, L.; Litvak, S.; Androla, M. L. DNA aptamers derived from HIV-1 RNase H inhibitors are strong anti-integrase agents. *J. Mol. Biol.* **2002**, *324* (2), 195–203 DOI: 10.1016/S0022-2836(02)01064-1.

(22) Paborsky, L. R.; McCurdy, S. N.; Griffin, L. C.; Toole, J. J.; Leung, L. L. K. the Single-Stranded-Dna Aptamer-Binding Site of Human Thrombin. *J. Biol. Chem.* **1993**, *268*, 20808–20811.

(23) Jayasena, S. D. Aptamers: An emerging class of molecules that rival antibodies in diagnostics. *Clin. Chem.* **1999**, *45* (9), 1628–1650 DOI: 10.1038/mtna.2014.74.

(24) Cruz-Toledo, J.; McKeague, M.; Zhang, X.; Giamberardino, A.; McConnell, E.; Francis, T.; DeRosa, M. C.; Dumontier, M. Aptamer base: a collaborative knowledge base to describe aptamers and SELEX experiments. *Database* **2012**, *2012*, bas006–bas006 DOI: 10.1093/database/bas006.

(25) McKeague, M.; DeRosa, M. C. Aptamers and SELEX: Tools for the Development of Transformative Molecular Recognition Technology. *Aptamers Synth. Antibodies* **2014**, *1* (1), 12–16.

(26) D. R. Mills, R. L. Peterson, and S. S. An extracellular Darwinian experiment with a self-duplicating nucleic acid molecule,. *Proc. Natl. Acad. Sci. U. S. A.* **1967**, *58* (1), 217–224.

(27) Wilson, D. S.; Szostak, J. W. In Vitro Selection of Functional Nucleic Acids. *Annu. Rev. Biochem.* **1999**, *68* (1), 611–647 DOI: 10.1146/annurev.biochem.68.1.611.

(28) Ellington, A. D.; Szostak, J. W. In vitro selection of RNA molecules that bind specific ligands. *Nature* **1990**, *346* (6287), 818–822 DOI: 10.1038/346818a0.

(29) Gold, L.; Janjic, N.; Jarvis, T.; Schneider, D.; Walker, J. J.; Wilcox, S. K.; Zichi, D. Aptamers and the RNA World, Past and Present. *Cold Spring Harb. Perspect. Biol.* **2012**, *4* (3), a003582–a003582 DOI: 10.1101/cshperspect.a003582.

(30) *Functional Nucleic Acids for Analytical Applications*; Yingfu, L., Yi, L., Eds.; Springer New York: New York, NY, 2009.

(31) Ulrich, H.; Wrenger, C. Identification of Aptamers as Specific Binders and Modulators of Cell-Surface Receptor Activity; 2013; pp 17–39.

(32) Stoltenburg, R.; Reinemann, C.; Strehlitz, B. SELEX-A (r)evolutionary method to generate high-affinity nucleic acid ligands. *Biomol. Eng.* **2007**, *24* (4), 381–403 DOI: 10.1016/j.bioeng.2007.06.001.

(33) Ellington, A. D.; Szostak, J. W. Selection in vitro of single-stranded DNA molecules that fold into specific ligand-binding structures. *Nature* **1992**, *355* (6363), 850–852 DOI: 10.1038/355850a0.

(34) Robertson, D. L.; Joyce, G. F. Selection in vitro of an RNA enzyme that specifically cleaves single-stranded DNA. *Nature* **1990**, *344* (6265), 467–468 DOI: 10.1038/344467a0.

(35) Gold, L.; Ayers, D.; Bertino, J.; Bock, C.; Bock, A.; Brody, E. N.; Carter, J.; Dalby, A. B.; Eaton, B. E.; Fitzwater, T.; et al. Aptamer-Based Multiplexed Proteomic Technology for Biomarker Discovery. *PLoS One* **2010**, *5* (12), e15004 DOI: 10.1371/journal.pone.0015004.

(36) Luo, X.; McKeague, M.; Pitre, S.; Dumontier, M.; Green, J.; Golshani, A.; Derosa, M. C.; Dehne, F. Computational approaches toward the design of pools for the in vitro selection of complex aptamers. *RNA* **2010**, *16* (11), 2252–2262 DOI: 10.1261/rna.2102210.

(37) Ruff, K. M.; Snyder, T. M.; Liu, D. R. Enhanced Functional Potential of Nucleic Acid Aptamer Libraries Patterned to Increase Secondary Structure. *J. Am. Chem. Soc.* **2010**, *132* (27), 9453–9464 DOI: 10.1021/ja103023m.

(38) Marshall, K. A.; Ellington, A. D. In vitro selection of RNA aptamers. *Methods Enzymol.* **2000**, *318*, 193–214.

(39) Murphy, M. B.; Fuller, S. T.; Richardson, P. M.; Doyle, S. A. An improved method for the in vitro evolution of aptamers and applications in protein detection and purification. *Nucleic Acids Res.* **2003**, *31* (18), e110.

(40) Stoltenburg, R.; Reinemann, C.; Strehlitz, B. FluMag-SELEX as an advantageous method for DNA aptamer selection. *Anal. Bioanal. Chem.* **2005**, *383* (1), 83–91 DOI: 10.1007/s00216-005-3388-9.

(41) Cox, J. C.; Rudolph, P.; Ellington, A. D. Automated RNA Selection. *Biotechnol. Prog.* **1998**, *14* (6), 845–850 DOI: 10.1021/bp980097h.

(42) Goertz, P. Automated selection of aminoglycoside aptamers. *J. Assoc. Lab. Autom.* **2004**, *9* (3), 150–154 DOI: 10.1016/j.jala.2004.04.008.

(43) Wochner, A.; Cech, B.; Menger, M.; Erdmann, V.; Glökler, J. Semi-automated selection of DNA aptamers using magnetic particle handling. *Biotechniques* **2007**, *43* (3), 344–353 DOI: 10.2144/000112532.

(44) Stoltenburg, R.; Nikolaus, N.; Strehlitz, B. Capture-SELEX: Selection of DNA Aptamers for Aminoglycoside Antibiotics. *J. Anal. Methods Chem.* **2012**, *2012*, 1–14 DOI: 10.1155/2012/415697.

(45) McKeague, M.; McConnell, E. M.; Cruz-Toledo, J.; Bernard, E. D.; Pach, A.; Mastronardi, E.; Zhang, X.; Beking, M.; Francis, T.; Giamberardino, A.; et al. Analysis of In Vitro Aptamer Selection Parameters. *J. Mol. Evol.* **2015**, *81* (5-6), 150–161 DOI: 10.1007/s00239-015-9708-6.

(46) Carothers, J. Selecting RNA aptamers for synthetic biology: investigating magnesium dependence and predicting binding affinity. *Nucleic Acids Res.* **2010**, *38* (8), 2736–2747.

(47) Pfeffer, P.; Gohlke, H. DrugScore RNA Knowledge-Based Scoring Function To Predict RNA−Ligand Interactions. *J. Chem. Inf. Model.* **2007**, *47* (5), 1868–1876 DOI: 10.1021/ci700134p.

(48) Jo, M.; Ahn, J.-Y.; Lee, J.; Lee, S.; Hong, S. W.; Yoo, J.-W.; Kang, J.; Dua, P.; Lee, D.-K.; Hong, S.; et al. Development of Single-Stranded DNA Aptamers for Specific Bisphenol A Detection. *Oligonucleotides* **2011**, *21* (2), 85–91 DOI: 10.1089/oli.2010.0267.

(49) Frost, N. R.; McKeague, M.; Falcioni, D.; DeRosa, M. C. An in solution assay for interrogation of affinity and rational minimer design for small molecule-binding aptamers. *Analyst* **2015**, *140* (19), 6643–6651 DOI: 10.1039/C5AN01075F.

(50) McKeague, M.; De Girolamo, A.; Valenzano, S.; Pascale, M.; Ruscito, A.; Velu, R.; Frost, N. R.; Hill, K.; Smith, M. K.; McConnell, E. M.; et al. Comprehensive Analytical Comparison of Strategies Used for Small Molecule Aptamer Evaluation. *Anal. Chem.* **2015**, *87* (17), 8608–8612 DOI: 10.1021/acs.analchem.5b02102.

(51) McKeague, M.; Velu, R.; De Girolamo, A.; Valenzano, S.; Pascale, M.; Smith, M.; Derosa, M. C. Comparison of in-solution biorecognition properties of aptamers against ochratoxin A. *Toxins (Basel).* **2016**, *8* (11) DOI: 10.3390/toxins8110336.

(52) Daniel, M. C. M.; Astruc, D. Gold Nanoparticles: Assembly, Supramolecular Chemistry, Quantum-Size Related Properties and Applications toward Biology, Catalysis and Nanotechnology,. *Chem. Rev.* **2004**, *104* (1), 293–346 DOI: 10.1021/cr030698.

(53) Saha, K.; Agasti, S. S.; Kim, C.; Li, X.; Rotello, V. M. Gold nanoparticles in chemical and biological sensing. *Chem. Rev.* **2012**, *112* (5), 2739–2779 DOI: 10.1021/cr2001178.

(54) Jain, P. K.; Lee, K. S.; El-Sayed, I. H.; El-Sayed, M. A. Calculated absorption and scattering properties of gold nanoparticles of different size, shape, and composition: Applications in biological imaging and biomedicine. *J. Phys. Chem. B* **2006**, *110*, 7238–7248 DOI: 10.1021/jp057170o.

(55) Guo, S.; Wang, E. Synthesis and electrochemical applications of gold nanoparticles. *Anal. Chim. Acta* **2007**, *598* (2), 181–192 DOI: 10.1016/j.aca.2007.07.054.

(56) Zhao, Y.; Luo, Y.; Li, T.; Song, Q. Au NPs driven electrochemiluminescence aptasensors for sensitive detection of fumonisin B1. *RSC Adv.* **2014**, *4*, 57709–57714 DOI: 10.1039/C4RA10350E.

(57) Lv, X.; Zhang, Y.; Liu, G.; Du, L.; Wang, S. Aptamer-based fluorescent detection of ochratoxin A by quenching of gold nanoparticles. *RSC Adv.* **2017**, *7* (27), 16290–16294 DOI: 10.1039/C7RA01474K.

(58) Wu, S.; Duan, N.; Li, X.; Tan, G.; Ma, X.; Xia, Y.; Wang, Z.; Wang, H. Homogenous detection of fumonisin B1 with a molecular beacon based on fluorescence resonance energy transfer between NaYF4: Yb, Ho upconversion nanoparticles and gold nanoparticles. *Talanta* **2013**, *116*, 611–618 DOI: 10.1016/j.talanta.2013.07.016.

(59) Li, H.; Rothberg, L. Colorimetric detection of DNA sequences based on electrostatic interactions with unmodified gold nanoparticles. *Proc. Natl. Acad. Sci. U. S. A.* **2004**, *101* (39), 14036–14039 DOI: 10.1073/pnas.0406115101.

(60) Dreaden, E. C.; Alkilany, A. M.; Huang, X.; Murphy, C. J.; El-Sayed, M. A. The golden age: gold nanoparticles for biomedicine. *Chem. Soc. Rev.* **2012**, *41* (7), 2740–2779 DOI: 10.1039/C1CS15237H.

(61) Sato, K.; Hosokawa, K.; Maeda, M. Colorimetric biosensors based on DNA-nanoparticle conjugates. *Anal. Sci.* **2007**, *23* (1), 17–20 DOI: 10.2116/analsci.23.17.

(62) Zhang, J.; Liu, B.; Liu, H.; Zhang, X.; Tan, W. Aptamer-conjugated gold nanoparticles for bioanalysis. *Nanomedicine* **2013**, *8* (6), 983–993 DOI: 10.2217/nnm.13.80.

(63) Wang, L.; Ma, W.; Chen, W.; Liu, L.; Ma, W.; Zhu, Y.; Xu, L.; Kuang, H.; Xu, C. An aptamer-based chromatographic strip assay for sensitive toxin semi-quantitative detection. *Biosens. Bioelectron.* **2011**, *26* (6), 3059–3062 DOI: 10.1016/j.bios.2010.11.040.

(64) Zheng, Y.; Wang, Y.; Yang, X. Aptamer-based colorimetric biosensing of dopamine using unmodified gold nanoparticles. *Sensors Actuators, B Chem.* **2011**, *156* (1), 95–99 DOI: 10.1016/j.snb.2011.03.077.

(65) Yang, C.; Wang, Y.; Marty, J.-L.; Yang, X. Aptamer-based colorimetric biosensing of Ochratoxin A using unmodified gold nanoparticles indicator. *Biosens. Bioelectron.* **2011**, *26* (5), 2724–2727 DOI: 10.1016/j.bios.2010.09.032.

(66) Bai, W.; Zhu, C.; Liu, J.; Yan, M.; Yang, S.; Chen, A. Gold nanoparticle-based colorimetric aptasensor for rapid detection of six organophosphorous pesticides. *Environ. Toxicol. Chem.* **2015**, *34* (10), 2244–2249 DOI: 10.1002/etc.3088.

(67) Luan, Y.; Chen, J.; Xie, G.; Li, C.; Ping, H.; Ma, Z.; Lu, A. Visual and microplate detection of aflatoxin B2 based on NaCl-induced aggregation of aptamer-modified gold nanoparticles. *Microchim. Acta* **2015**, *182* (5-6), 995–1001 DOI: 10.1007/s00604-014-1420-5.

(68) Tan, L.; Chen, Z.; Zhao, Y.; Wei, X.; Li, Y.; Zhang, C.; Wei, X.; Hu, X. Dual channel sensor for detection and discrimination of heavy metal ions based on colorimetric and fluorescence response of the AuNPs-DNA conjugates. *Biosens. Bioelectron.* **2016**, *85*, 414–421 DOI: 10.1016/j.bios.2016.05.038.

(69) Liu, Y.; Yu, J.; Wang, Y.; Liu, Z.; Lu, Z. An ultrasensitive aptasensor for detection of Ochratoxin A based on shielding effect-induced inhibition of fluorescence resonance energy transfer. *Sensors Actuators, B Chem.* **2016**, *222*, 797–803 DOI: 10.1016/j.snb.2015.09.007.

(70) Evtugyn, G.; Porfireva, A.; Stepanova, V.; Kutyreva, M.; Gataulina, A.; Ulakhovich, N.; Evtugyn, V.; Hianik, T. Impedimetric aptasensor for ochratoxin A determination based on Au nanoparticles stabilized with hyper-branched polymer. *Sensors (Basel).* **2013**, *13* (12), 16129–16145 DOI: 10.3390/s131216129.

(71) Jiang, L.; Qian, J.; Yang, X.; Yan, Y.; Liu, Q.; Wang, K.; Wang, K. Amplified impedimetric aptasensor based on gold nanoparticles covalently bound graphene sheet for the picomolar detection of ochratoxin A. *Anal. Chim. Acta* **2014**, *806*, 128–135 DOI: 10.1016/j.aca.2013.11.003.

(72) Chen, X.; Huang, Y.; Ma, X.; Jia, F.; Guo, X.; Wang, Z. Impedimetric aptamer-based determination of the mold toxin fumonisin B1. *Microchim. Acta* **2015**, *182* (9-10), 1709–1714 DOI: 10.1007/s00604-015-1492-x.

(73) Chen, Z.; Li, L.; Mu, X.; Zhao, H.; Guo, L. Electrochemical aptasensor for detection of copper based on a reagentless signal-on architecture and amplification by gold nanoparticles. *Talanta* **2011**, *85* (1), 730–735 DOI: 10.1016/j.talanta.2011.04.056.

(74) Wang, B.; Chen, Y.; Wu, Y.; Weng, B.; Liu, Y.; Lu, Z.; Li, C. M.; Yu, C. Aptamer induced assembly of fluorescent nitrogen-doped carbon dots on gold nanoparticles for sensitive detection of AFB1. *Biosens. Bioelectron.* **2016**, *78*, 23–30 DOI: 10.1016/j.bios.2015.11.015.

(75) Chen, A.; Yang, S. Replacing antibodies with aptamers in lateral flow immunoassay. *Biosens. Bioelectron.* **2015**, *71*, 230–242 DOI: 10.1016/j.bios.2015.04.041.

(76) Shim, W.; Jin, M.; Mun, H.; Kim, M. An aptamer-based dipstick assay for the rapid and simple detection of aflatoxin B1. *Biosens. Bioelectron.* **2014**, *62*, 288–294 DOI: 10.1016/j.bios.2014.06.059.

(77) Wang, L.; Ma, W.; Chen, W.; Liu, L.; Ma, W.; Zhu, Y.; Xu, L.; Kuang, H.; Xu, C. An aptamer-based chromatographic strip assay for sensitive toxin semi-quantitative detection. *Biosens. Bioelectron.* **2011**, *26* (6), 3059–3062 DOI: 10.1016/j.bios.2010.11.040.

(78) Nelson, E. M.; Rothberg, L. J. Kinetics and mechanism of single-stranded DNA adsorption onto citrate-stabilized gold nanoparticles in colloidal solution. *Langmuir* **2011**, *27* (5), 1770–1777 DOI: 10.1021/la102613f.

(79) Zhang, X.; Servos, M. R.; Liu, J. Surface science of DNA adsorption onto citrate-capped gold nanoparticles. *Langmuir* **2012**, *28* (8), 3896–3902 DOI: 10.1021/la205036p.

(80) Farkhari, N.; Abbasian, S.; Moshaii, A.; Nikkhah, M. Mechanism of adsorption of single and double stranded DNA on gold and silver nanoparticles: Investigating some important parameters in bio-sensing applications. *Colloids Surfaces B Biointerfaces* **2016**, *148*, 657–664 DOI: 10.1016/j.colsurfb.2016.09.022.

(81) Pong, B.-K.; Lee, J. Y.; Trout, B. L. A Computational Study to Understand the Surface Reactivity of Gold Nanoparticles with Amines and DNA. **2006**.

(82) Akhlaghi, Y.; Kompany-Zareh, M.; Ebrahimi, S. Model-based approaches to investigate the interactions between unmodified gold nanoparticles and DNA strands. *Sensors Actuators, B Chem.* **2015**, *221*, 45–54 DOI: 10.1016/j.snb.2015.06.102.

(83) Pellegrino, T.; Sperling, R. A.; Alivisatos, A. P.; Parak, W. J. Gel Electrophoresis of Gold-DNA Nanoconjugates. *J. Biomed. Biotechnol.* **2007**, *2007*, 1–9 DOI: 10.1155/2007/26796.

(84) Cruz-Aguado, J. a; Penner, G. Determination of ochratoxin a with a DNA aptamer. *J. Agric. Food Chem.* **2008**, *56* (22), 10456–10461 DOI: 10.1021/jf801957h.

(85) Mally, a; Hard, G. C.; Dekant, W. Ochratoxin A as a potential etiologic factor in endemic nephropathy: lessons from toxicity studies in rats. *Food Chem. Toxicol.* **2007**, *45* (11), 2254–2260 DOI: 10.1016/j.fct.2007.05.021.

(86) Malir, F.; Ostry, V.; Pfohl-Leszkowicz, A.; Novotna, E. Ochratoxin A: developmental and reproductive toxicity-an overview. *Birth Defects Res. B. Dev. Reprod. Toxicol.* **2013**, *98* (6), 493–502 DOI: 10.1002/bdrb.21091.

(87) Amézqueta, S.; González-Peñas, E.; Murillo-Arbizu, M.; López de Cerain, A. Ochratoxin A decontamination: A review. *Food Control* **2009**, *20* (4), 326–333 DOI: 10.1016/j.foodcont.2008.05.017.

(88) Barthelmebs, L.; Jonca, J.; Hayat, A.; Prieto-Simon, B.; Marty, J.-L. Enzyme-Linked Aptamer Assays (ELAAs), based on a competition format for a rapid and sensitive detection of Ochratoxin A in wine. *Food Control* **2011**, *22* (5), 737–743 DOI: 10.1016/j.foodcont.2010.11.005.

(89) McKeague, M.; Velu, R.; Hill, K.; Bardóczy, V.; Mészáros, T.; DeRosa, M. Selection and Characterization of a Novel DNA Aptamer for Label-Free Fluorescence Biosensing of Ochratoxin A. *Toxins (Basel).* **2014**, *6* (8), 2435–2452 DOI: 10.3390/toxins6082435.

(90) Hill, K. Screening the structure and binding affinity of ochratoxin A aptamers by A thesis submitted to the Faculty of Graduate and Postdoctoral Affairs in partial fulfillment of the requirements for the degree of Master of Science in. **2014**.

(91) Frost, N. Fumonisin B 1 aptamer optimization and progress towards mycotoxin nanoaptasensors by Affairs in partial fulfillment of the requirements for the degree of. **2015**.

(92) Walsh, R.; DeRosa, M. C. Retention of function in the DNA homolog of the RNA dopamine aptamer. *Biochem. Biophys. Res. Commun.* **2009**, *388* (4), 732–735 DOI: 10.1016/j.bbrc.2009.08.084.

(93) Borlido, L.; Azevedo, A. M.; Roque, A. C. A.; Aires-Barros, M. R. Magnetic separations in biotechnology. *Biotechnol. Adv.* **2013**, *31* (8), 1374–1385 DOI: 10.1016/j.biotechadv.2013.05.009.

(94) Nishio, K.; Gokon, N.; Hasegawa, M.; Ogura, Y.; Ikeda, M.; Narimatsu, H.; Tada, M.; Yamaguchi, Y.; Sakamoto, S.; Abe, M.; et al. Identification of a chemical substructure that is immobilized to ferrite nanoparticles (FP). *Colloids Surfaces B Biointerfaces* **2007**, *54* (2), 249–253 DOI: 10.1016/j.colsurfb.2006.10.039.

(95) Sahoo, Y.; Pizem, H.; Fried, T.; Golodnitsky, D.; Burstein, L.; Sukenik, C. N.; Markovich, G. Alkyl phosphonate/phosphate coating on magnetite nanoparticles: A comparison with fatty acids. *Langmuir* **2001**, *17* (25), 7907–7911 DOI: 10.1021/la010703+.

(96) Kalska-Szostko, B.; Wykowska, U.; Satuła, D. Magnetic nanoparticles of core-shell structure. *Colloids Surfaces A Physicochem. Eng. Asp.* **2015**, *481*, 527–536 DOI: 10.1016/j.colsurfa.2015.05.040.

(97) Chaudhuri, R. G.; Paria, S. Core / Shell Nanoparticles : Classes , Properties , Synthesis Mechanisms , Characterization , and Applications. **2012**, 2373–2433 DOI: 10.1021/cr100449n.

(98) McKeague, M.; Foster, A.; Miguel, Y.; Giamberardino, A.; Verdin, C.; Chan, J. Y. S.; DeRosa, M. C. Development of a DNA aptamer for direct and selective homocysteine detection in human serum. *RSC Adv.* **2013**, *3* (46), 24415 DOI: 10.1039/c3ra43893g.

(99) Balakrishnan S, Bonder MJ, H. G. Particle size effect on phase and magnetic properties of polymer-coated magnetic nanoparticles. *J Magn Magn Mater* **2009**, *321*, 117–122.

(100) Laurent, S.; Forge, D.; Port, M.; Roch, A.; Robic, C.; Vander Elst, L.; Muller, R. N. Magnetic Iron Oxide Nanoparticles: Synthesis, Stabilization, Vectorization, Physicochemical Characterizations, and Biological Applications. *Chem. Rev.* **2008**, *108* (6), 2064–2110 DOI: 10.1021/cr068445e.

(101) Caruso, F. Nanoengineering of Particle Surfaces. *Adv. Mater.* **2001**, *13* (1), 11–22 DOI: 10.1002/1521-4095(200101)13:1.

(102) Gawande, M. B.; Goswami, A.; Asefa, T.; Guo, H.; Biradar, A. V.; Peng, D.-L.; Zboril, R.; Varma, R. S. Core–shell nanoparticles: synthesis and applications in catalysis and electrocatalysis. *Chem. Soc. Rev.* **2015**, *44* (21), 7540–7590 DOI: 10.1039/C5CS00343A.

(103) Taghian, F.; Rad, M. Y.; Ahmadi, V. Plamonic behavior of metallic and core-shell nanostructures. In *2013 21st Iranian Conference on Electrical Engineering (ICEE)*; IEEE, 2013; pp 1–4.

(104) Qi, L.; Ma, J.; Cheng, H.; Zhao, Z. Synthesis and characterization of mixed CdS-ZnS nanoparticles in reverse micelles. *Colloids Surfaces A Physicochem. Eng. Asp.* **1996**, *111* (3), 195–202 DOI: 10.1016/0927-7757(96)03545-5.

(105) Ma, G. H.; He, J.; Rajiv, K.; Tang, S. H.; Yang, Y.; Nogami, M. Observation of resonant energy transfer in Au:CdS nanocomposite. *Appl. Phys. Lett.* **2004**, *84* (23), 4684–4686 DOI: 10.1063/1.1760220.

(106) Nasr, C.; Hotchandani, S.; Kim, W. Y.; Schmehl, R. H.; Kamat, P. V. Photoelectrochemistry of Composite Semiconductor Thin Films. Photosensitization of SnO 2 /CdS Coupled Nanocrystallites with a Ruthenium Polypyridyl Complex. *J. Phys. Chem. B* **1997**, *101* (38), 7480–7487 DOI: 10.1021/jp970833k.

(107) Fang, D. F.; Zhang, Z. M.; Wang, Z. P.; Ding, Z. J. Study of Photoluminescence of CdS/ZnS Core/Shell Quantum Dots. *Phys. Procedia* **2012**, *32*, 920–925 DOI: 10.1016/j.phpro.2012.03.657.

(108) Chan, J. M.; Zhang, L.; Yuet, K. P.; Liao, G.; Rhee, J.-W.; Langer, R.; Farokhzad, O. C. PLGA–lecithin–PEG core–shell nanoparticles for controlled drug delivery. *Biomaterials* **2009**, *30* (8), 1627–1634 DOI: 10.1016/j.biomaterials.2008.12.013.

(109) Yan, E.; Ding, Y.; Chen, C.; Li, R.; Hu, Y.; Jiang, X. Polymer/silica hybrid hollow nanospheres with pH-sensitive drug release in physiological and intracellular environments. *Chem. Commun.* **2009**, No. 19, 2718 DOI: 10.1039/b900751b.

(110) Zimmer, J. P.; Kim, S.-W.; Ohnishi, S.; Tanaka, E.; Frangioni, J. V; Bawendi, M. G. Size series of small indium arsenide-zinc selenide core-shell nanocrystals and their application to in vivo imaging. *J. Am. Chem. Soc.* **2006**, *128* (8), 2526–2527 DOI: 10.1021/ja0579816.

(111) Lu, Y.; He, B.; Shen, J.; Li, J.; Yang, W.; Yin, M. Multifunctional magnetic and fluorescent core–shell nanoparticles for bioimaging. *Nanoscale* **2015**, *7* (5), 1606–1609 DOI: 10.1039/C4NR06104G.

(112) Dzudzevic Cancar, H.; Soylemez, S.; Akpinar, Y.; Kesik, M.; Göker, S.; Gunbas, G.; Volkan, M.; Toppare, L. A Novel Acetylcholinesterase Biosensor: Core–Shell Magnetic Nanoparticles Incorporating a Conjugated Polymer for the Detection of Organophosphorus Pesticides. *ACS Appl. Mater. Interfaces* **2016**, *8* (12), 8058–8067 DOI: 10.1021/acsami.5b12383.

(113) LUO, J.; ZENG, G.-M.; TANG, L.; YIN, J.; LI, Y.-P. Study Progress on Biosensing Core/shell Nanoparticles. *Chinese J. Anal. Chem.* **2009**, *37* (12), 1847–1852 DOI: 10.1016/S1872-2040(08)60152-8.

(114) Markides, H.; Rotherham, M.; El Haj, A. J. Biocompatibility and Toxicity of Magnetic Nanoparticles in Regenerative Medicine. *J. Nanomater.* **2012**, *2012*, 1–11 DOI: 10.1155/2012/614094.

(115) Walling, M. A.; Novak, J. A.; Shepard, J. R. E. Quantum Dots for Live Cell and In Vivo Imaging. *Int. J. Mol. Sci.* **2009**, *10* (2), 441–491 DOI: 10.3390/ijms10020441.

(116) Kim, J.; Kim, H. S.; Lee, N.; Kim, T.; Kim, H.; Yu, T.; Song, I. C.; Moon, W. K.; Hyeon, T. Multifunctional Uniform Nanoparticles Composed of a Magnetite Nanocrystal Core and a Mesoporous Silica Shell for Magnetic Resonance and Fluorescence Imaging and for Drug Delivery. *Angew. Chemie Int. Ed.* **2008**, *47* (44), 8438–8441 DOI: 10.1002/anie.200802469.

(117) Kocevski, V.; Rusz, J.; Eriksson, O.; Sarma, D. D. First-principles study of the influence of different interfaces and core types on the properties of CdSe/CdS core-shell nanocrystals. *Sci. Rep.* **2015**, *5*, 10865 DOI: 10.1038/srep10865.

(118) Oldenburg, S. J.; Averitt, R. D.; Westcott, S. L.; Halas, N. J. Nanoengineering of optical resonances. *Chem. Phys. Lett.* **1998**, *288* (2-4), 243–247 DOI: 10.1016/S0009-2614(98)00277-2.

(119) El-Sayed, M. A. Small Is Different: Shape-, Size-, and Composition-Dependent Properties of Some Colloidal Semiconductor Nanocrystals. *Acc. Chem. Res.* **2004**, *37* (5), 326–333 DOI: 10.1021/ar020204f.

(120) Blasiak, B.; van Veggel, F. C. J. M.; Tomanek, B. Applications of Nanoparticles for MRI Cancer Diagnosis and Therapy. *J. Nanomater.* **2013**, *2013*, 1–12 DOI: 10.1155/2013/148578.

(121) Liz-Marzán, L. M.; Giersig, M.; Mulvaney, P. Synthesis of Nanosized Gold−Silica Core−Shell Particles. *Langmuir* **1996**, *12* (18), 4329–4335 DOI: 10.1021/la9601871.

(122) Poovarodom, S.; Bass, J. D.; Hwang, S.-J.; Katz, A. Investigation of the Core−Shell Interface in Gold@Silica Nanoparticles: A Silica Imprinting Approach. *Langmuir* **2005**, *21* (26), 12348–12356 DOI: 10.1021/la052006d.

(123) Hota, G.; Jain, S.; Khilar, K. C. Synthesis of CdS–Ag2S core-shell/composite nanoparticles using AOT/n-heptane/water microemulsions. *Colloids Surfaces A Physicochem. Eng. Asp.* **2004**, *232* (2-3), 119–127 DOI: 10.1016/j.colsurfa.2003.10.021.

(124) Wang; Luo, J.; Fan, Q.; Suzuki, M.; Suzuki, I. S.; Engelhard, M. H.; Lin, Y.; Kim, N.; Wang, J. Q.; Zhong, C.-J. Monodispersed Core−Shell Fe 3 O 4 @Au Nanoparticles. *J. Phys. Chem. B* **2005**, *109* (46), 21593–21601 DOI: 10.1021/jp0543429.

(125) Xuan, S.; Wang, Y.-X. J.; Yu, J. C.; Leung, K. C.-F. Preparation, Characterization, and Catalytic Activity of Core/Shell Fe 3 O 4 @Polyaniline@Au Nanocomposites. *Langmuir* **2009**, *25* (19), 11835–11843 DOI: 10.1021/la901462t.

(126) Zhang, S.; Niu, H.; Hu, Z.; Cai, Y.; Shi, Y. Preparation of carbon coated Fe3O4 nanoparticles and their application for solid-phase extraction of polycyclic aromatic hydrocarbons from environmental water samples. *J. Chromatogr. A* **2010**, *1217* (29), 4757–4764 DOI: 10.1016/j.chroma.2010.05.035.

(127) Imhof, A. Preparation and Characterization of Titania-Coated Polystyrene Spheres and Hollow Titania Shells. *Langmuir* **2001**, *17* (12), 3579–3585 DOI: 10.1021/la001604j.

(128) Gerion, D.; Pinaud, F.; Williams, S. C.; Parak, W. J.; Zanchet, D.; Weiss, S.; Alivisatos, A. P. Synthesis and Properties of Biocompatible Water-Soluble Silica-Coated CdSe/ZnS Semiconductor Quantum Dots †. *J. Phys. Chem. B* **2001**, *105* (37), 8861–8871 DOI: 10.1021/jp0105488.

(129) Gupta, A. K.; Gupta, M. Synthesis and surface engineering of iron oxide nanoparticles for biomedical applications. *Biomaterials* **2005**, *26* (18), 3995–4021 DOI: 10.1016/j.biomaterials.2004.10.012.

(130) Moraes Silva, S.; Tavallaie, R.; Sandiford, L.; Tilley, R.; Gooding, J. J. Gold Coated Magnetic Nanoparticles: Preparation, Surface Modification for Analytical and Biomedical Applications. *Chem. Commun.* **2016**, *52*, 7528–7540 DOI: 10.1039/C6CC03225G.

(131) de Souza, K. C.; Andrade, G. F.; Vasconcelos, I.; de Oliveira Viana, I. M.; Fernandes, C.; de Sousa, E. M. B. Magnetic solid-phase extraction based on mesoporous silica-coated magnetic nanoparticles for analysis of oral antidiabetic drugs in human plasma. *Mater. Sci. Eng. C* **2014**, *40*, 275–280 DOI: 10.1016/j.msec.2014.04.004.

(132) Gooding, J. J.; Ciampi, S. The molecular level modification of surfaces: from self-assembled monolayers to complex molecular assemblies. *Chem. Soc. Rev.* **2011**, *40* (5), 2704 DOI: 10.1039/c0cs00139b.

(133) Cui, Y.-R.; Hong, C.; Zhou, Y.-L.; Li, Y.; Gao, X.-M.; Zhang, X.-X. Synthesis of orientedly bioconjugated core/shell Fe3O4@Au magnetic nanoparticles for cell separation. *Talanta* **2011**, *85* (3), 1246–1252 DOI: 10.1016/j.talanta.2011.05.010.

(134) Park, H.-Y.; Schadt, M. J.; Wang; Lim, I.-I. S.; Njoki, P. N.; Kim, S. H.; Jang, M.-Y.; Luo, J.; Zhong, C.-J. Fabrication of Magnetic Core@Shell Fe Oxide@Au Nanoparticles for Interfacial Bioactivity and Bio-separation. *Langmuir* **2007**, *23* (17), 9050–9056 DOI: 10.1021/la701305f.

(135) Lyon, J. L.; Fleming, D. A.; Stone, M. B.; Schiffer, P.; Williams, M. E. Synthesis of Fe Oxide Core/Au Shell Nanoparticles by Iterative Hydroxylamine Seeding. *Nano Lett.* **2004**, *4* (4), 719–723 DOI: 10.1021/nl035253f.

(136) Yang, D.; Pang, X.; He, Y.; Wang, Y.; Chen, G.; Wang, W.; Lin, Z. Precisely Size-Tunable Magnetic/Plasmonic Core/Shell Nanoparticles with Controlled Optical Properties. *Angew. Chemie Int. Ed.* **2015**, *54* (41), 12091–12096 DOI: 10.1002/anie.201504676.

(137) Goon, I. Y.; Lai, L. M. H.; Lim, M.; Munroe, P.; Gooding, J. J.; Amal, R. Fabrication and Dispersion of Gold-Shell-Protected Magnetite Nanoparticles: Systematic Control Using Polyethyleneimine. *Chem. Mater.* **2009**, *21* (4), 673–681 DOI: 10.1021/cm8025329.

(138) Koenig, S. H.; Kellar, K. E. Theory of 1/T1 and 1/T2 NMRD profiles of solutions of magnetic nanoparticles. *Magn. Reson. Med.* **1995**, *34* (2), 227–233 DOI: 10.1002/mrm.1910340214.

(139) Rawal, R.; Chawla, S.; Pundir, C. S. An electrochemical sulfite biosensor based on gold coated magnetic nanoparticles modified gold electrode. *Biosens. Bioelectron.* **2012**, *31* (1), 144–150 DOI: 10.1016/j.bios.2011.10.007.

(140) Kumagai, M.; Sarma, T. K.; Cabral, H.; Kaida, S.; Sekino, M.; Herlambang, N.; Osada, K.; Kano, M. R.; Nishiyama, N.; Kataoka, K. Enhanced in vivo Magnetic Resonance Imaging of Tumors by PEGylated Iron-Oxide-Gold Core-Shell Nanoparticles with Prolonged Blood Circulation Properties. *Macromol. Rapid Commun.* **2010**, *31* (17), 1521–1528 DOI: 10.1002/marc.201000341.

(141) Kayal, S.; Ramanujan, R. V. Anti-Cancer Drug Loaded Iron–Gold Core–Shell Nanoparticles (Fe@Au) for Magnetic Drug Targeting. *J. Nanosci. Nanotechnol.* **2010**, *10* (9), 5527–5539 DOI: 10.1166/jnn.2010.2461.

(142) Caruntu, D.; Cushing, B. L.; Caruntu, G.; O'Connor, C. J. Attachment of Gold Nanograins onto Colloidal Magnetite Nanocrystals. *Chem. Mater.* **2005**, *17* (13), 3398–3402 DOI: 10.1021/cm050280n.

(143) Seino, S.; Kinoshita, T.; Otome, Y.; Nakagawa, T.; Okitsu, K.; Mizukoshi, Y.; Nakayama, T.; Sekino, T.; Niihara, K.; Yamamoto, T. A. Gamma-ray synthesis of magnetic nanocarrier composed of gold and magnetic iron oxide. *J. Magn. Magn. Mater.* **2005**, *293* (1), 144–150 DOI: 10.1016/j.jmmm.2005.01.054.

(144) Kawaguchi, K.; Jaworski, J.; Ishikawa, Y.; Sasaki, T.; Koshizaki, N. Preparation of gold/iron-oxide composite nanoparticles by a unique laser process in water. *J. Magn. Magn. Mater.* **2007**, *310* (2), 2369–2371 DOI: 10.1016/j.jmmm.2006.11.109.

(145) Wu, W.; He, Q.; Chen, H.; Tang, J.; Nie, L. Sonochemical synthesis, structure and magnetic properties of air-stable Fe 3 O 4 / Au nanoparticles. *Nanotechnology* **2007**, *18* (14), 145609 DOI: 10.1088/0957-4484/18/14/145609.

(146) Lo, C. K.; Xiao, D.; Choi, M. M. F. Homocysteine-protected gold-coated magnetic nanoparticles: synthesis and characterisation. *J. Mater. Chem.* **2007**, *17* (23), 2418 DOI: 10.1039/b617500g.

(147) Spasova, M.; Salgueiriño-Maceira, V.; Schlachter, A.; Hilgendorff, M.; Giersig, M.; Liz-Marzán, L. M.; Farle, M. Magnetic and optical tunable microspheres with a magnetite/gold nanoparticle shell. *J. Mater. Chem.* **2005**, *15* (21), 2095 DOI: 10.1039/b502065d.

(148) Oliva, B. L.; Pradhan, A.; Caruntu, D.; O'Connor, C. J.; Tarr, M. A. Formation of gold-coated magnetic nanoparticles using TiO2 as a bridging material. *J. Mater. Res.* **2006**, *21* (05), 1312–1316 DOI: 10.1557/jmr.2006.0163.

(149) Wang, L.; Park, H.-Y.; Lim, S. I.-I.; Schadt, M. J.; Mott, D.; Luo, J.; Wang, X.; Zhong, C.-J. Core@shell nanomaterials: gold-coated magnetic oxide nanoparticles. *J. Mater. Chem.* **2008**, *18* (23), 2629 DOI: 10.1039/b719096d.

(150) Wang, L.; Park, H.-Y.; Lim, S. I.-I.; Schadt, M. J.; Mott, D.; Luo, J.; Wang, X.; Zhong, C.-J. Core@shell nanomaterials: gold-coated magnetic oxide nanoparticles. *J. Mater. Chem.* **2008**, *18* (23), 2629 DOI: 10.1039/b719096d.

(151) Yang, J.; Lee, J. Y.; Ying, J. Y. Phase transfer and its applications in nanotechnology. *Chem. Soc. Rev.* **2011**, *40* (3), 1672–1696 DOI: 10.1039/B916790K.

(152) Yu, W. W.; Chang, E.; Sayes, C. M.; Drezek, R.; Colvin, V. L. Aqueous dispersion of monodisperse magnetic iron oxide nanocrystals through phase transfer. *Nanotechnology* **2006**, *17* (17), 4483–4487 DOI: 10.1088/0957-4484/17/17/033.

(153) Wilson, O. M.; Scott, R. W. J.; Garcia-Martinez, J. C.; Crooks, R. M. Separation of Dendrimer-Encapsulated Au and Ag Nanoparticles by Selective Extraction. *Chem. Mater.* **2004**, *16* (22), 4202–4204 DOI: 10.1021/cm048699l.

(154) Mayya, K. S.; Caruso, F. Phase Transfer of Gold Nanoparticles by Hydrophobization with Alkylamines. *Langmuir* **2003**, *19* (17), 6987–6993 DOI: 10.1021/la034018+.

(155) Simard, J.; Briggs, C.; Boal, A. K.; Rotello, V. M. Formation and pH-controlled assembly of amphiphilic gold nanoparticles. *Chem. Commun.* **2000**, No. 19, 1943–1944 DOI: 10.1039/b004162i.

(156) Gittins, D. I.; Caruso, F. Spontaneous phase transfer of nanoparticulate metals from organic to aqueous media. *Angew. Chemie - Int. Ed.* **2001**, *40* (16), 3001–3004 DOI: 10.1002/1521-3773(20010817)40:16.

(157) Gandubert, V.; Lennox, R. Assessment of 4-(dimethylamino) pyridine as a capping agent for gold nanoparticles. *Langmuir* **2005**, *21* (14), 6532–6539 DOI: 10.1021/la050195u.

(158) Toma, H. E.; Zamarion, V. M.; Toma, S. H.; Araki, K. The Coordination Chemistry at Gold Nanoparticles. *J. Braz. Chem. Soc* **2010**, *21* (7), 1158–1176 DOI: 10.1590/S0103-50532010000700003.

(159) Boisselier, E.; Astruc, D. Gold nanoparticles in nanomedicine: preparations, imaging, diagnostics, therapies and toxicity. *Chem. Soc. Rev.* **2009**, *38* (6), 1759–1782 DOI: 10.1039/b806051g.

(160) Campisi, S.; Schiavoni, M.; Chan-Thaw, C.; Villa, A. Untangling the Role of the Capping Agent in Nanocatalysis: Recent Advances and Perspectives. *Catalysts* **2016**, *6* (12), 185 DOI: 10.3390/catal6120185.

(161) Brown, R. by P. D. Transmission Electron Microscopy-A Textbook for Materials Science, by David B. Williams and C. Barry Carter. *Microsc. Microanal.* **1999**, *5* (06), 452–453 DOI: 10.1017/S1431927699990529.

(162) Elton, L. R. B.; Jackson, D. F. X-Ray Diffraction and the Bragg Law. *Am. J. Phys.* **1966**, *34* (11), 1036–1038 DOI: 10.1119/1.1972439.

(163) Anker, J. N.; Hall, W. P.; Lyandres, O.; Shah, N. C.; Zhao, J.; Van Duyne, R. P. Biosensing with plasmonic nanosensors. *Nat. Mater.* **2008**, *7* (6), 442–453 DOI: 10.1038/nmat2162.

(164) Robinson, I.; Tung, L. D.; Maenosono, S.; Wälti, C.; Thanh, N. T. K. Synthesis of core-shell gold coated magnetic nanoparticles and their interaction with thiolated DNA. *Nanoscale* **2010**, *2*, 2624–2630 DOI: 10.1039/c0nr00621a.

(165) Nitimmunotech. Nitmagold Cit 50 nm http://www.nitparticles.com/index.php/en/nitmagold-cit-50nm.

(166) Hergert, W.; Wriedt, T. The Mie Theory. *Mie Theory Basics Appl.* **2012**, 53–71 DOI: 10.1007/978-3-642-28738-1.

(167) Biver, T.; Corti, A.; Eltugral, N.; Lorenzini, E.; Masini, M.; Paolicchi, A.; Pucci, A.; Ruggeri, G.; Secco, F.; Venturini, M. Analysis of 4-dimethylaminopyridine (DMAP)-gold nanoparticles behaviour in solution and of their interaction with calf thymus DNA and living cells. *J. Nanoparticle Res.* **2012**, *14* (2) DOI: 10.1007/s11051-011-0681-8.

(168) Kim, E.-Y. A real-time PCR-based method for determining the surface coverage of thiol-capped oligonucleotides bound onto gold nanoparticles. *Nucleic Acids Res.* **2006**, *34* (7), e54–e54 DOI: 10.1093/nar/gkl147.

(169) Li, X.; Shantz, D. F. Specific Ion Effects on Nanoparticle Stability and Organocation−Particle Interactions in Tetraalkylammonium−Silica Mixtures. *Langmuir* **2010**, *26* (23), 18459–18467 DOI: 10.1021/la1035129.